DESIGN AND ANALYSIS OF A MASK PROJECTION MICRO-STEREOLITHOGRAPHY SYSTEM

A Thesis
Presented to
The Academic Faculty

by

Ameya Shankar Limaye

In Partial Fulfillment
of the requirements for the Degree of
Master of Science in Mechanical Engineering

Georgia Institute of Technology
November 2004

DESIGN AND ANALYSIS OF A MASK PROJECTION MICRO STEREOLITHOGRAPHY SYSTEM

Approved by:

Dr. David W. Rosen, Chair
School of Mechanical Engineering
Georgia Institute of Technology

Dr. Ali Adibi
School of Electrical and Computer Engineering
Georgia Institute of Technology

Dr. Peter J. Hesketh
School of Mechanical Engineering
Georgia Institute of Technology

Date Approved: November 2004

To the memory of my grandmother
Late Mrs. Sudha Shridhar Sathe

ACKNOWLEDGEMENTS

Today, as I enjoy a sense of achievement upon completing my Master's thesis, I look back at my past two years as a graduate student. I realize that the work presented in this thesis was possible only because of the encouragement and guidance of a number of people.

First, I would like to thank my advisor Dr. David W. Rosen for his inspiration, guidance, and confidence in my abilities. His insights have guided me to a level of understanding far higher than what I thought was possible. I was introduced to the thrilling and dynamic world of Stereolithography in his course "Fundamentals of Rapid Prototyping". This course motivated me to work in the field of Rapid Prototyping and contribute my two cents to the knowledge in the field.

I was fortunate to be a part of the intellectually stimulating environment of the Systems Realization Laboratory at Georgia Institute of Technology. I would specifically like to thank Dr. Farrokh Mistree. His course "Engineering Design" helped me develop a research-oriented mindset. The learning from this course will last me for a lifetime. I have no words to express the profound respect that I have for Dr. Mistree and Dr. Janet Allen, not just as professors, but also as wonderful people.

I thank Dr. Donald O'Shea from the Physics department of Georgia Institute of Technology for helping me develop strong fundamentals regarding Optics. I found his course "Optical Design" very useful in the course of my research.

I thank my friends in Systems Realization Laboratory for their camaraderie. I especially cherish the friendship of Vincent, Jae, Austina, Benay, Yanyan, Sunji, Jamal, Jitesh, Angela and Chris.

Finally, I would like to express my gratitude towards my parents without whose guidance, I would not have been where I am today. In my parents, I have found wise friends who have guided me all throughout.

TABLE OF CONTENTS

LIST OF TABLES

LIST OF FIGURES

SUMMARY

Mask Projection Microstereolithography (MPμSLA) is an additive manufacturing process capable for fabricating true three-dimensional microparts and hence, holds promise as a potential micro-fabrication process for micro-machine components. With only a few MPμSLA systems developed and studied so far, the research in this field is inchoate and experimental in nature. The process of curing a micropart using an MPμSLA system has not been analytically modeled and no literature on process planning for MPμSLA is available. In order to employ the MPμSLA technology for microfabrication, it is necessary to model its part building process and formulate a process planning method to cure dimensionally accurate microparts.

As a part of this thesis, an MPμSLA system is designed and assembled. The process of curing a single layer using this system is analytically modeled as the "Layer cure model". The Layer cure model is formulated in two steps. First, the irradiance received by the resin surface is modeled as a function of the system parameters (Irradiance model). Then, the resin used in the system is characterized to experimentally determine its working curve. The Irradiance model and the resin characterization enable us to compute the dimensions of any layer cured using our MPμSLA system in terms of the process parameters. The Layer cure model has been validated by curing test layers on our system.

Finally, the Layer cure model has been inverted to formulate a process planning method to cure layers of the required dimensions. Using this process planning method, it is possible to cure layers within a dimensional error of 3%.

CHAPTER 1

MOTIVATION FOR DESIGNING AND MODELING A MASK PROJECTION MICRO-STEREOLITHOGRAPHY SYSTEM

Interest in manufacturing micro-objects stemmed from the enormous potential of the Micro-Electro Mechanical Systems (MEMS). MEMS are systems that combine computers with tiny mechanical devices such as sensors, valves, gears, mirrors, and actuators embedded in semiconductor chips. MEMS have found widespread applications in the industry, and the market size for MEMS in 2005 is estimated to be $5.7 billion in the February 2004 issue of the Yole development magazine for MEMS and Nanotechnology, Optics, Bio & Micro Fluidic chips and semiconductors.

Natural evolution in MEMS would lead to devices that move by themselves. The concepts of microplanes, microrobots, microcars and microsubmarines have been described in (Fujimasa, 1996).

Currently, MEMS components are manufactured by etching on a silicon substrate using a physical-mask. The chief drawback of this method is that we can't fabricate 3D structures with this technique because in order to fabricate 3D structures, one would need a number of costly masks. Due to its ability to manufacture 3D objects, Stereolithography was perceived to be a potential technique to manufacture 3D micro-parts. This led to the emergence of the field of Micro-Stereolithography (MSL). At present, Mask projection Micro Stereolithography (MPμSLA) is considered to be the most promising Micro-Stereolithography technique to fabricate micro parts.

In this chapter, the motivation behind designing a Mask projection Micro Stereolithography system and modeling its part building process is presented. In Section 1.1, the principle of operation of laser scanning Stereolithography and Mask projection Micro Stereolithography (MPμSLA) is explained. In Section 1.2, the need to model the MPμSLA process is presented. In Section 1.3, the literature on MPμSLA is reviewed to identify the relevant work done in the field. In Section 1.4, the tasks completed in this thesis are delineated and the organization of this thesis is presented.

1.1 STEREOLITHOGRAPHY AND MASK PROJECTION MICRO STEREOLITHOGRAPHY

In this section, the Stereolithography process is explained [Section 1.1.1]. Then, the two ways in which Stereolithography is adapted to fabricate microparts (Scanning Micro Stereolithography and Mask projection Micro Stereolithography) are presented [Section 1.1.2]. In Section 1.1.3, the advantages of the Mask Projection approach over the Scanning approach are enunciated.

1.1.1 Stereolithography

The Stereolithography process begins with the definition of a CAD model of the desired object, followed by slicing of the three dimensional (3-D) model into a series of very closely spaced horizontal planes that represent the X-Y cross sections of the 3-D object, each with a slightly different Z-coordinate value. All the cross-sections are then translated into a numerical control code and merged together into a build file. This build file is used to control the ultraviolet (UV) light scanner and Z-axis translator. The desired

polymer object is then “written” into the UV-curable resist, layer by layer, until the entire structure has been defined.

The schematic of the Stereolithography machine is shown in Figure 1.1.

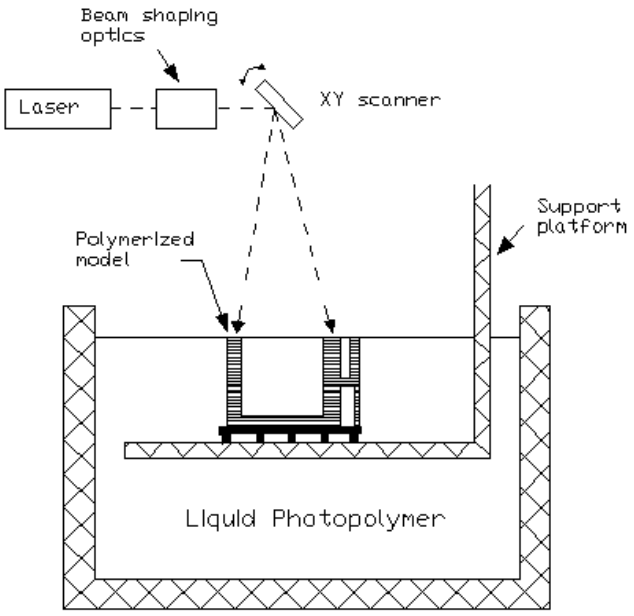

Figure 1. 1 Schematic of a Stereolithography machine

The basic elements of a Stereolithography system are as follows:

- Laser Optics System
- Scanning System
- Elevator and Recoater
- Computer Control and Software

The laser optics system consists of the laser used to cure the resin and the beam shaping optics. The beam shaping optics is responsible for conditioning the laser beam and focusing it on the resin surface with the desired spot size.

The scanning system consists of a set of galvanometric mirrors, which direct the laser beam so that the required cross-section is scanned.

The elevator lowers the cured layer by a distance of one layer thickness. The recoater coats a fresh film of resin on the cured layer. The next layer is scanned on this film by the laser.

Computer and the controlling software are used to control the galvanometric mirrors. The computer also synchronizes the motion of laser, elevator and recoater.

1.1.2 Two approaches to Micro-Stereolithography

When Stereolithography is used to fabricate micro-parts, it is called Micro Stereolithography. The principle of Micro Stereolithography is the same as Stereolithography, i.e. "Writing a cross section on a photopolymer surface by means of UV light". However, the resolution required of a Micro-Stereolithography process is much finer.

Micro-Stereolithography systems developed so far can be divided into two categories:

- Scanning Micro Stereolithography Systems and
- Mask projection Micro Stereolithography Systems, or Integral Micro Stereolithography Systems

<u>Scanning Micro-Stereolithography Systems</u>

It is believed that, in conventional Stereolithography, too many mobile optical elements lead to focusing errors and thereby, poor resolution. Also, the spot size doesn't remain constant throughout the layer cross-section. As a result, lateral resolution is dependent upon the distance of a feature from the center of the vat. In scanning Micro

Stereolithography, this drawback is eliminated by keeping the light beam focused onto a stationary tight spot and scanning the layer by moving the work piece under the spot.

The principle of Scanning Micro-Stereolithography is shown in Figure 1.2.

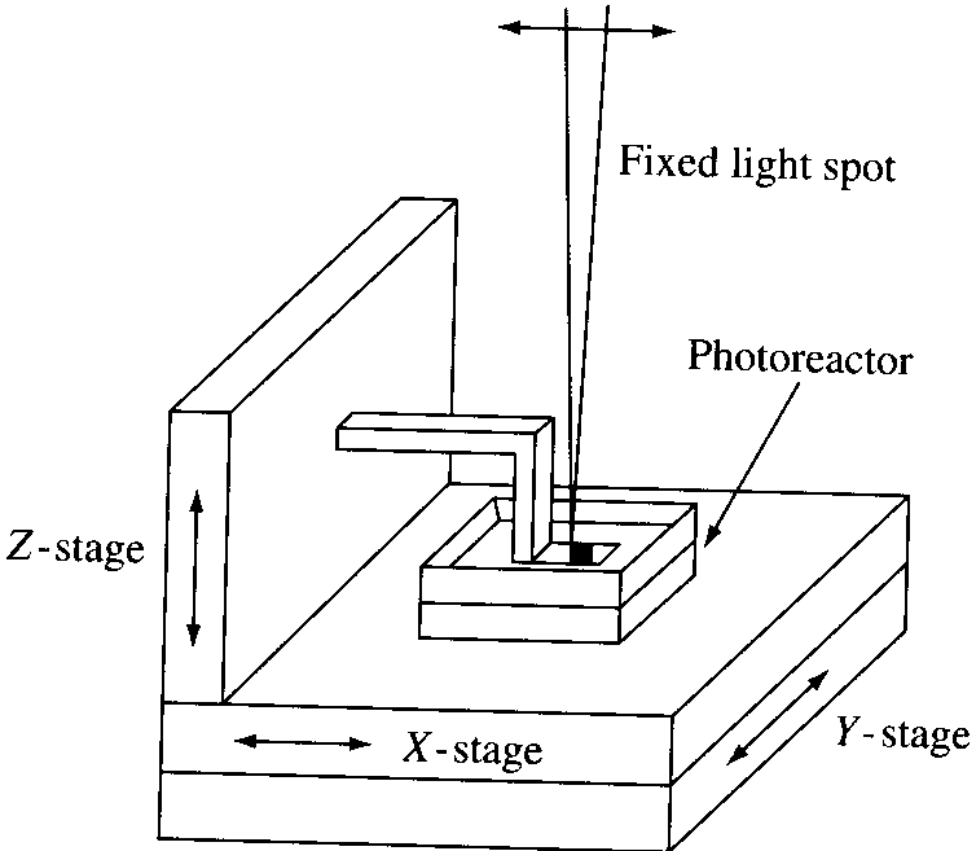

Figure 1. 2 Principle of Scanning Micro-Stereolithography (Beluze et al. 1999)

Scanning Micro-Stereolithography systems have been presented in literature in (Ikuta and Hirowatari, 1993; Nakamoto et al., 1996). The following specifications of a typical scanning Micro-Stereolithography process have been presented in (Gardner et al., 2001):

- 5 μm spot size of the UV beam

- Positional accuracy is 0.25 μm (in the X-Y directions) and 1.0 μm in the Z-direction
- Minimum size of the unit of hardened polymer is 5 μm x 5 μm x 3 μm (in X, Y, Z)
- Maximum size of fabrication structure is 10mm x 10mm x 10mm

Mask Projection Micro-Stereolithography

In Mask projection Micro Stereolithography, also called Integral Micro Stereolithography, a complete layer is polymerized in a single radiation. The principle of Mask projection Micro Stereolithography is shown in Figure 1.3.

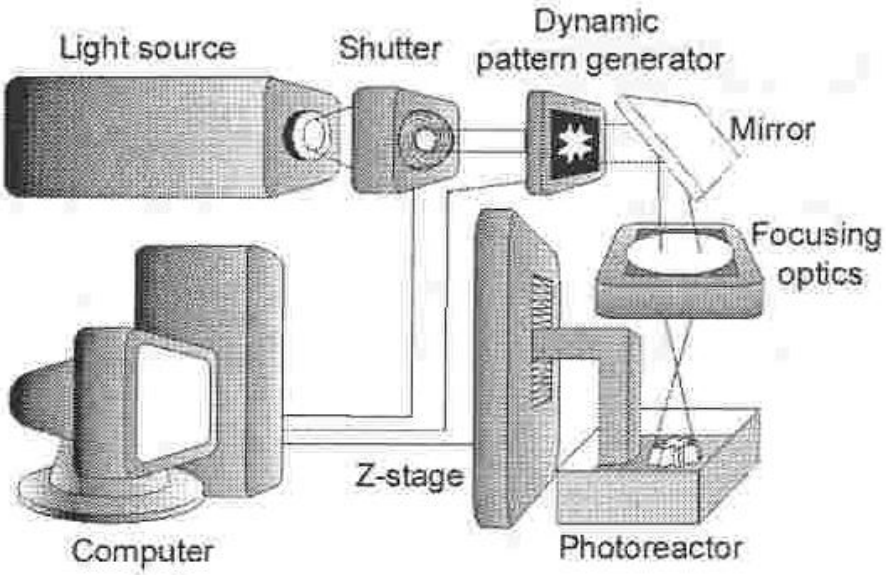

Figure 1. 3 Schematic of a Mask projection Micro Stereolithography apparatus (Bertsch et al., 2000)

The three dimensional CAD model of the object to be cured is scaled, oriented and sliced at uniform increments by horizontal planes. Each slice is converted into a bitmap file. This bitmap file serves as an input to the mask, which displays a pattern corresponding to the layer to be cured.

As shown in Figure 1.3, the beam coming from a light source is shaped by this pattern so that it contains the image of the layer to be cured. Focusing optical components are used to reduce and focus this image onto the surface of a liquid photopolymer, held in a vat. This cures a layer of the cross-section corresponding to the pattern displayed on the mask.

Once the curing of a layer is complete, the already polymerized part of the object is immersed deep in the photopolymer vat so that the polymerized surface is totally covered by fresh photopolymer. It is then lifted up a certain height such that there remains a layer of resin between the last polymerized layer and the free surface of photopolymer.

The process then repeats over the same sequence of operations for the next layers until the object is finished. The polymerized layers are stacked onto one another by the interpenetrating polymer networks. When all the layers have been built, the polymerized part is removed from the vat and washed with the appropriate solvent.

Mask Projection Micro Stereolithography Systems have been presented in literature (Bertsch et al., 1997; Chatwin et al., 1998; Farsari et al., 1999; Chatwin et al., 1999; Monneret et al., 1999; Bertsch et al., 2000; Farsari et al., 2000; Monneret et al., 2001; Hadipoespito et al., 2003). Impressive results have been achieved by these researchers. The results are documents in Table 1.1.

Table 1. 1 Results obtained using Mask projection Micro Stereolithography

Research Team	Light source	Mask	Component Size	Resolution	Reference
Bertsch	Laser 515 nm	LCD[1]	1.3 x 1.3 x 10mm^3	5 x 5 x 5 μm	(Bertsch, Zissi, et al., 1997; Bertsch, Jezequel, et al., 1997)
Chatwin	Laser 351.1nm	SLM[2]	Not reported	5 μm lateral resolution	(Chatwin et al, 1998; Farsari et al., 1999; Chatwin et al., 1999; Farsari et al., 2000)
Monneret	Broad Band Visible	LCD	Not reported	2 μm lateral resolution	(Monneret et al., 1999; Monneret et al., 2001)
Bertsch	Lamp (Visible)	DMD[3]	6 x 8 x 15 mm^3	5 x 5 x 5 μm	(Bertsch et al., 1999)
Bertsch	Lamp (UV)	DMD	10.24 x 7.68 x 20 mm^3	10 x 10 x 10 μm	(Bertsch et al., 2000)
Hadipoespito	Lamp (UV)	DMD	Not reported	Not reported	(Hadipoespito et al., 2003)

1.1.3 Advantages of Mask Projection approach over Scanning approach

The Mask Projection Micro-Stereolithography process has the following advantages over Scanning Micro Stereolithography:

- Mask projection Micro Stereolithography is faster than the Scanning Micro Stereolithography because vector-by-vector scanning is a slower process.

[1] Liquid Crystal Display
[2] Spatial Light Modulator
[3] Digital Micromirror Device

- The accuracy of MPμSLA is better because the errors introduced by the X-Y translation stages are avoided. The only mobile element in the MPμSLA systems is the Z-Stage.

Due to these advantages, current research on Micro Stereolithography is focused on Mask projection Micro Stereolithography.

1.2 NEED TO MODEL MPμSLA PROCESS

Any manufacturing process involves a number of process parameters. Some of these parameters can be explicitly specified by the user (process variables), while the other are fixed by the manufacturing system's design (fixed process parameters). When there are a number of process variables, it is difficult for a user to choose appropriate process values for fabricating a part as per his/her requirements. This problem is accentuated when the part has several and contradictory requirements. Similarly, it is difficult for the designer of a manufacturing system to assign values to the fixed process parameters so that the system is capable of fabricating parts with particular requirements. This necessitates the development of a process planning method for any manufacturing process.

A process planning method computes the values to be assigned to process variables in order to fabricate a part with the required properties. Judicious selection of process parameter values entails modeling their effect on the fabricated part's properties. For example, in case of conventional laser scanning Stereolithography, the effect of the laser power, lasers scan speed, Z wait etc. on the cured parts geometrical and physical properties has been modeled, which allows a manufacturer to cure parts of the requisite

properties. In order to use MPμSLA to fabricate microparts, a process planning method has to be developed. This necessitates the identification of the process parameters and modeling their effect on the cured part's properties. In this thesis, a process planning method for curing microparts of the required geometry is formulated.

In the next section, the literature on MPμSLA is reviewed and it is shown that no work has been done on the process planning.

1.3 MASK PROJECTION MICRO STEREOLITHOGRAPHY LITERATURE

Since 1997, at least five prototype MPμSLA systems have been developed and studied. All research done using these systems is on improving the resolution of the MPμSLA process. Research emphasis has been on characterizing the resins for better vertical (Z) resolution and on experimental determination of the lateral (XY) resolution. In this section, the research done on MPμSLA process is reviewed in detail

1.3.1 Research on resin cure

Bertsch and co-researchers (Bertsch et al., 1997) developed an MPμSLA System that used an LCD screen as the dynamic mask and a laser, emitting visible radiation, as the light source. At high exposures, Stereolithography resins undergo bleaching as the polymerization reactions proceed. Due to bleaching, radiation penetrates the resin easily, which causes polymerization at greater depths. Greater polymerization depths result in lower Z resolution. Bertsch and co-researchers theoretically modeled the effects of photo-bleaching reactions on the evolution of absorbed light energy in the resin. This allowed them to choose the correct exposure times to obtain a resolution of 5μm in the Z direction.

Bertsch and co-researchers (Bertsch et al., 2000) also developed an MPμSLA system that used the Digital Micromirror Device (DMD) as a dynamic mask and a lamp emitting visible light as a light source They plotted a semi-logarithmic plot of cure-depth vs. incident energy (Figure 1.4).

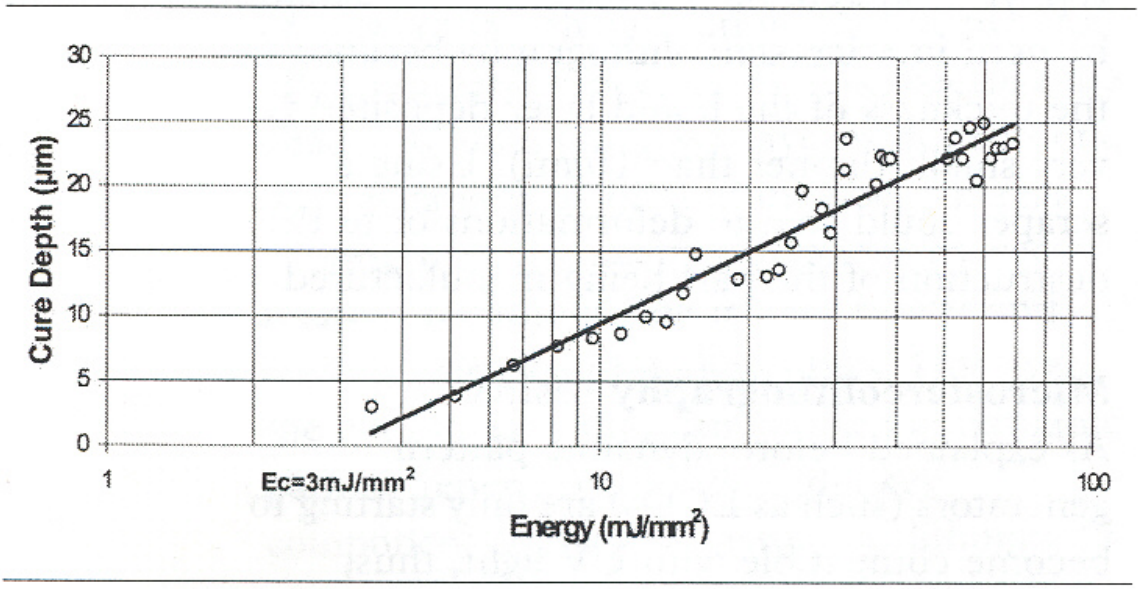

Figure 1. 4 Cure depth vs. incident energy for a resin sensitized by visible wavelengths (Bertsch et al., 2000)

The curve that they obtained was similar to the working curve for commercial Stereolithography resins. The Critical Exposure (E_c) observed from the curve was 300mJ/cm^2, which was much higher than that of the conventional Stereolithography resins, which cure in the UV range (8 to 10 mJ/cm^2). Critical Exposure (E_c) of a resin is the minimum energy per unit area that has to be incident on the resin surface to initiate polymerization reactions. In (Bertsch et al., 2000), the authors have attributed this high value of E_c to the photo initiation mechanism of the polymerization process, which is more complex and less efficient at visible wavelengths than at ultra-violet wavelengths.

This curve allowed the researchers to compute the correct exposure time to obtain very low depth of curing and thereby, high Z resolution. The Z resolution achieved by the research group was 5μm.

1.3.2 Research on XY resolution

All the research done on XY resolution has, so far, been empirical in nature. The best lateral resolution obtained so far is 2 μm (Monneret, 1999). However, the process parameters that gave this resolution have not been specified in the paper. Also, the authors have not stated if this is theoretically the best possible resolution.

Beluze and co-researchers built an MPμSLA system and studied its lateral resolution (Beluze et al., 1999). They plotted the graph of polymerized width vs. number of pixels (Figure 1.5). As seen in the Figure 1.5, the plot is a straight line of slope 2.7μm/pixel. So, Beluze concluded that the best lateral resolution possible with his system was 2.7μm.

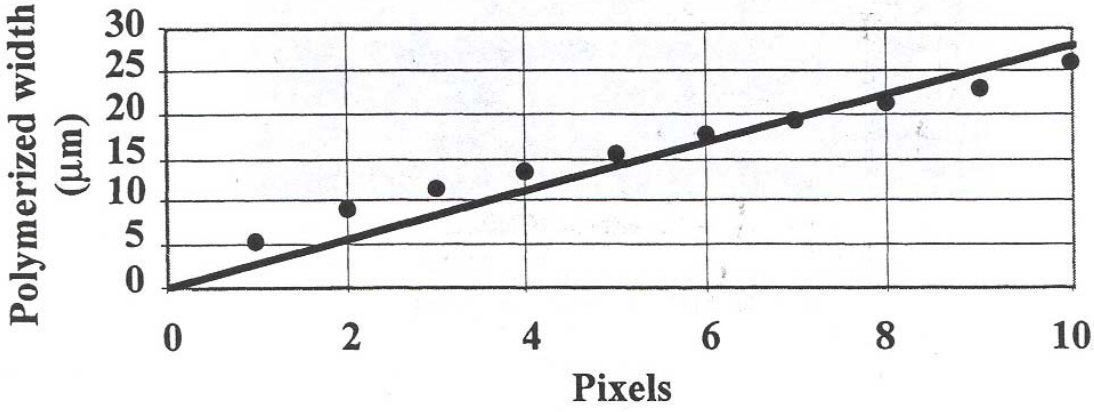

Figure 1. 5 Lateral resolution versus number of pixels (Beluze, 1999)

1.3.3 Scope for research

From the literature review, it is observed that the focus of various research groups has been only on improving the resolution of the MPμSLA process. Apart from resolution, dimensional accuracy is of prime importance for any micro-fabrication process. None of the papers published so far mentions the dimensional accuracy of the MPμSLA system studied.

It can be observed from the literature that the process capabilities have been explored experimentally. No attempt has been made to compute the theoretical limitations on the process resolution. The process has not been analytically modeled and there is no literature on process planning for MPμSLA. The goal in this thesis is to formulate a process planning method for MPμSLA to obtain dimensionally accurate parts.

1.4 TASKS COMPLETED IN THIS THESIS

The goal in this thesis is to develop a process planning method for the MPμSLA process to obtain dimensionally accurate parts. To this effect, a system embodying the principle of MPμSLA (as explained in Section 1.1.2.2) is designed and assembled. Then, the part-building process is analytically modeled. Finally, the model is validated by curing test parts on the system developed. Using this model, a process planning method to obtain dimensionally accurate microparts is formulated.

This work is presented in two distinct parts:

Part 1: Design of a MPμSLA system

Part 2: Modeling the system's part building process

Part 1 is developmental in nature. The Pahl and Beitz Systematic Design Methodology (Pahl and Beitz, 1996) is followed to design the system. Part 1 comprises of Chapter 2 and Chapter 3 of this thesis.

Part 2 is research oriented. In this part, the MPμSLA process is analytically modeled and validated and a process planning method is developed. Specific research questions are developed in this section and hypotheses for these questions are presented and tested. Part 2 comprises of Chapters 4, 5, 6 and 7.

CHAPTER 2

FOUNDATIONS FOR DESIGNING A MASK PROJECTION MICRO-STEREOLITHOGRAPHY SYSTEM

The Mask projection Micro Stereolithography system is designed by following the Pahl and Beitz Systematic Design Methodology in Chapter 3. In this chapter, the Pahl and Beitz Design Methodology (PB Methodology from hereon) is described and adapted to design a MPμSLA.

The methodology has been pictorially represented in Figure 2.1. The PB methodology consists of four phases: Product Planning and Clarification of Task, Conceptual Design, Embodiment Design and Detail Design. These phases are executed depending upon the problem at hand. The PB Methodology starts from searching for a product idea and ends with detail documentation of the design. Since a few Mask Projection Micro Stereolithography Systems are already available in literature for reference, all the phases of PB Methodology need not be executed exactly as suggested. In this chapter, each step of PB methodology is explained and adapted to design the MPμSLA System.

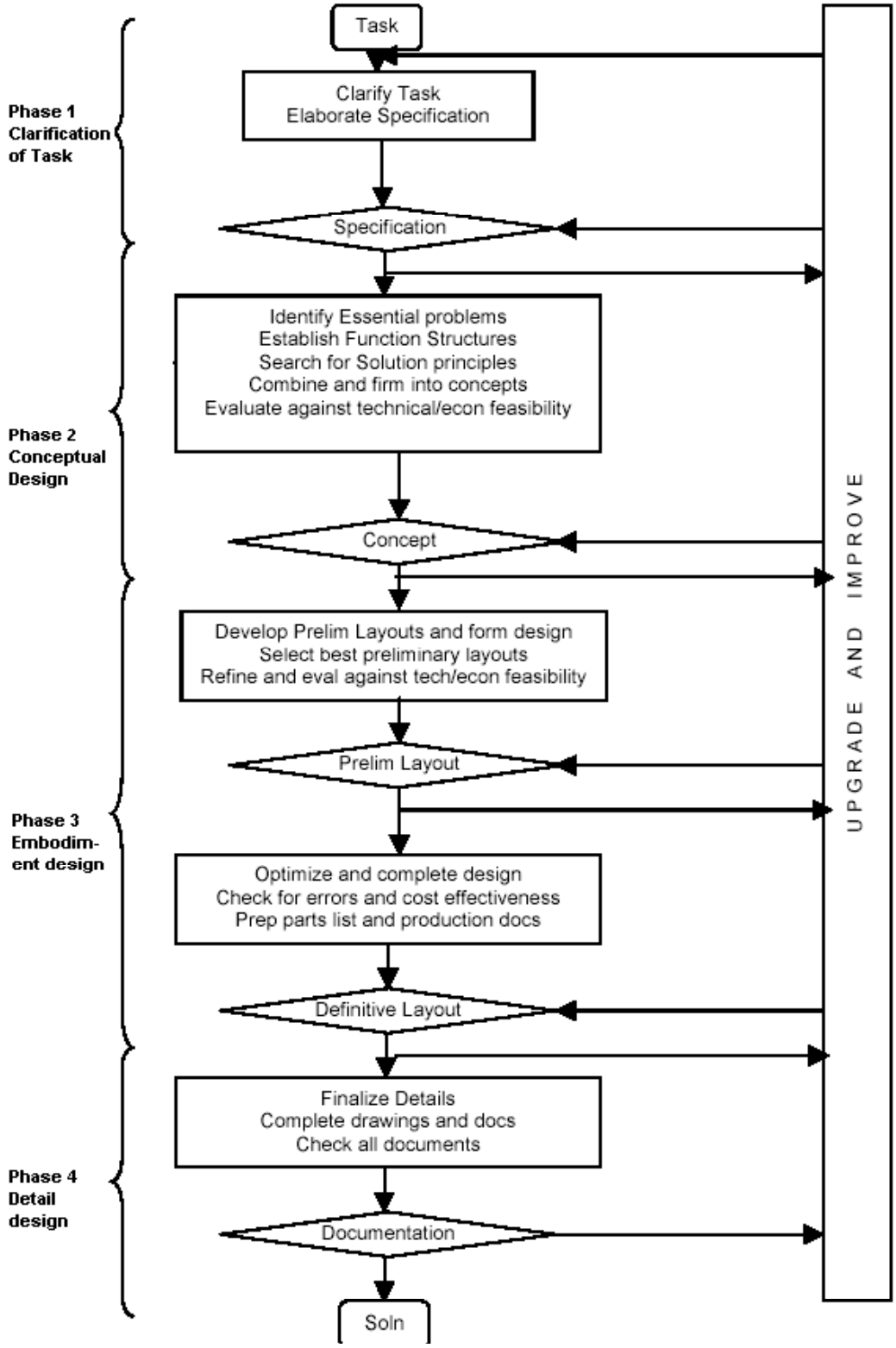

Figure 2. 1 Phases of the Pahl and Beitz Design Methodology (Pahl and Beitz, 1996)

2.1 PLANNING AND CLARIFICATION OF TASK

To start designing a product, a product idea is needed that looks promising. Pahl and Beitz suggest various informal ways of generating product ideas and also evaluating and selecting them. The result of this phase is a detailed product proposal. In our case, this phase was performed in Chapter 1 itself.

The next part of the first phase is "Clarification of Task". The purpose of clarifying a task is to collect information about the requirements that have to be fulfilled by the product and also about the existing constraints and their importance. This phase must answer the following questions:

- What is the problem really about?
- What implicit wishes and expectations are involved?
- Do specified constraints actually exist? And
- What paths are open for development?

This phase ends with the formulation of a "Requirements List" that focuses on, and is tuned to, the interests of the design process and subsequent working steps.

Clarification of Task is performed in Section 3.1. Here, the questions posed above are answered. Then, the Requirements List for the MPμSLA system is formulated.

2.2 CONCEPTUAL DESIGN

After completing the task clarification phase, the conceptual design phase determines the principle solution. This is achieved by abstracting the essential problems, establishing function structures [Section 2.2.1], searching for suitable working principles [Section 2.2.2] and then, combining those principles into a working structures [Section

2.2.3]. The concretization of the Working Principle leads to the formulation of Solution Principles [Section 2.2.4].

2.2.1 Function Structure

When the overall task to be performed by a product has been adequately defined---that is, if the inputs and outputs of all the quantities involved and their actual or required properties are known, then it is possible to specify the overall function. The overall function can thus be considered as a black box that converts the inputs into outputs.

An overall function can often be divided directly into identifiable sub-functions that correspond to various sub-tasks [Figure 2.2]. The relationship between sub-functions and overall function is very often governed by certain constraints inasmuch as some sub-functions have to be satisfied before others. Functions are usually defined by statements consisting of a verb and a noun. For example, "increase pressure, "transfer torque" and "reduce speed".

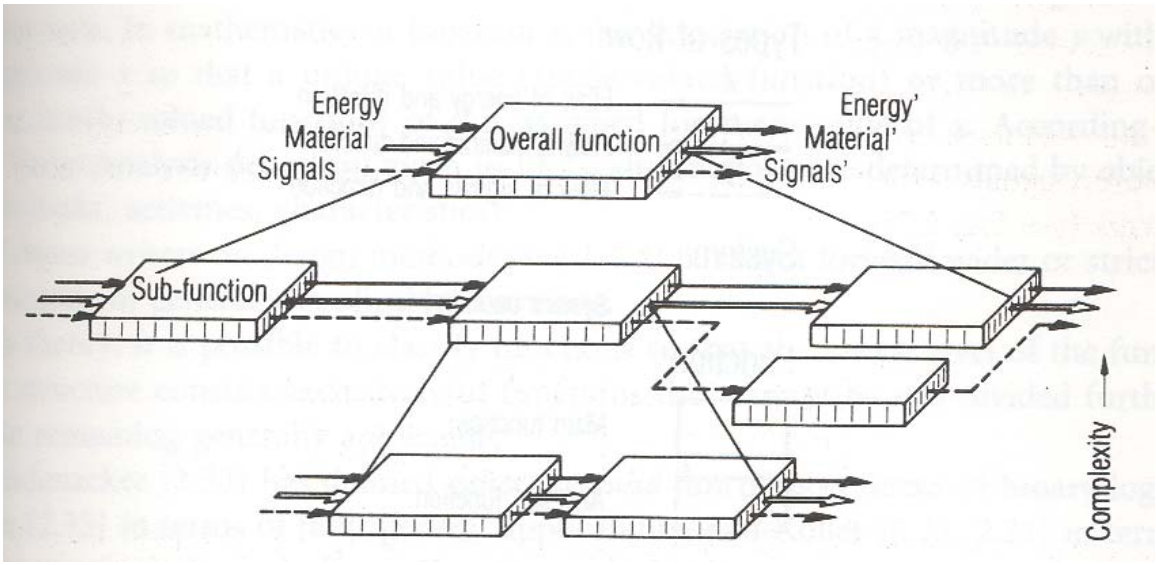

Figure 2. 2 Establishing function structure by breaking down overall function into sub-functions (Pahl and Beitz, 1996)

In the case of Mask-Projection Micro-Stereolithography Systems, the MPμSLA systems developed so far are analyzed. Though the designs of the systems have not been presented in detail, their function structures can be abstracted. It is safe to abstract the function structure from existing systems because the requirements of these systems and my system are going to be more or less similar. So, while designing the MPμSLA system the step of "Developing a Function Structure" is replaced by a step of "Abstracting Function Structure From Existing Systems". This step can be found in Section 3.2.

2.2.2 Working Principles

Once the sub-functions have been identified, we need to think about the physical effects needed to fulfill these functions. A working principle reflects the physical effect needed for the fulfillment of a given function. While searching for Working Principles, Pahl and Beitz recommend conducting a literature search, analyzing technical and natural systems and using intuition-based methods.

While designing the MPμSLA, the working principles for the physical realization of the various sub-functions of the function structure are searched. Various preliminary optical layouts are proposed as working principles for these sub-functions. This step has been presented in Section 3.3.

2.2.3 Working Structures (Combining Working Principles)

To fulfill the overall function, it is now necessary to elaborate the overall solution from the combination of working principles, that is, system synthesis. The main problem with such combinations is ensuring the physical and geometrical compatibility of the

working principles to be combined. Numerous working structures can result by combining different working principles. These working structures are referred to as variants.

While designing the MPμSLA system, the preliminary optical layout generated for the various sub function structures are combined to form working structure variants. These working structure variants are used as the preliminary optical layouts for the entire system.

2.2.4 Generating Solution Principles

The next part is to select the best working structure to embody. The working structures are not concrete enough for informed selection. This is because, as the search for a solution is based on the function structure, it is aimed, first and foremost, at the fulfillment of a technical function. A concept developed from a working structure must however also satisfy the constraints laid down in the Requirements List, at least in essence.

In short, it is necessary to generate some amount of quantitative data about the working structures for selecting the best. This data can be generated by rough calculations based on simplifying assumptions, rough sketches and preliminary experiments.

In the process of designing the MPμSLA system, certain preliminary calculations are performed to firm up the working structures into solution principles. Then, the Solution Principle is selected in light of the Requirements List.

2.3 EMBODIMENT PHASE

During this phase, a designer, starting from a concept (working structure, principle solution) determines the construction structure (overall layout) of a technical system in line with technical and economic criteria. Embodiment design leads to specification of principle. It is often necessary to produce preliminary layouts and sufficiently elaborate these layouts before evaluating them. A definitive layout provides a check of function, strength, spatial compatibility etc. and at this stage at the latest, financial viability of the project must be assessed.

In this phase of designing the MPμSLA system, the detail optical design of the system is completed. The phase includes selection of all the optical components, their spatial layout and mounting equipments.

2.4 DETAIL DESIGN

This is the phase of the design process in which the arrangement, forms, dimensions and surface properties of all individual parts are finally laid down, the material specified, production possibilities assessed, costs estimated and all the drawings and other production documents produced. The result of this phase is the "specification of production."

While designing the Mask Projection Micro-Stereolithography System, this phase includes the cost evaluation of the design and generation of the detailed drawings.

Summary

In this chapter, the various steps of the PB methodology have been adapted to design the MPμSLA system. In Figure 2.3, these adaptations are compiled into steps that are followed when the MPμSLA system is designed.

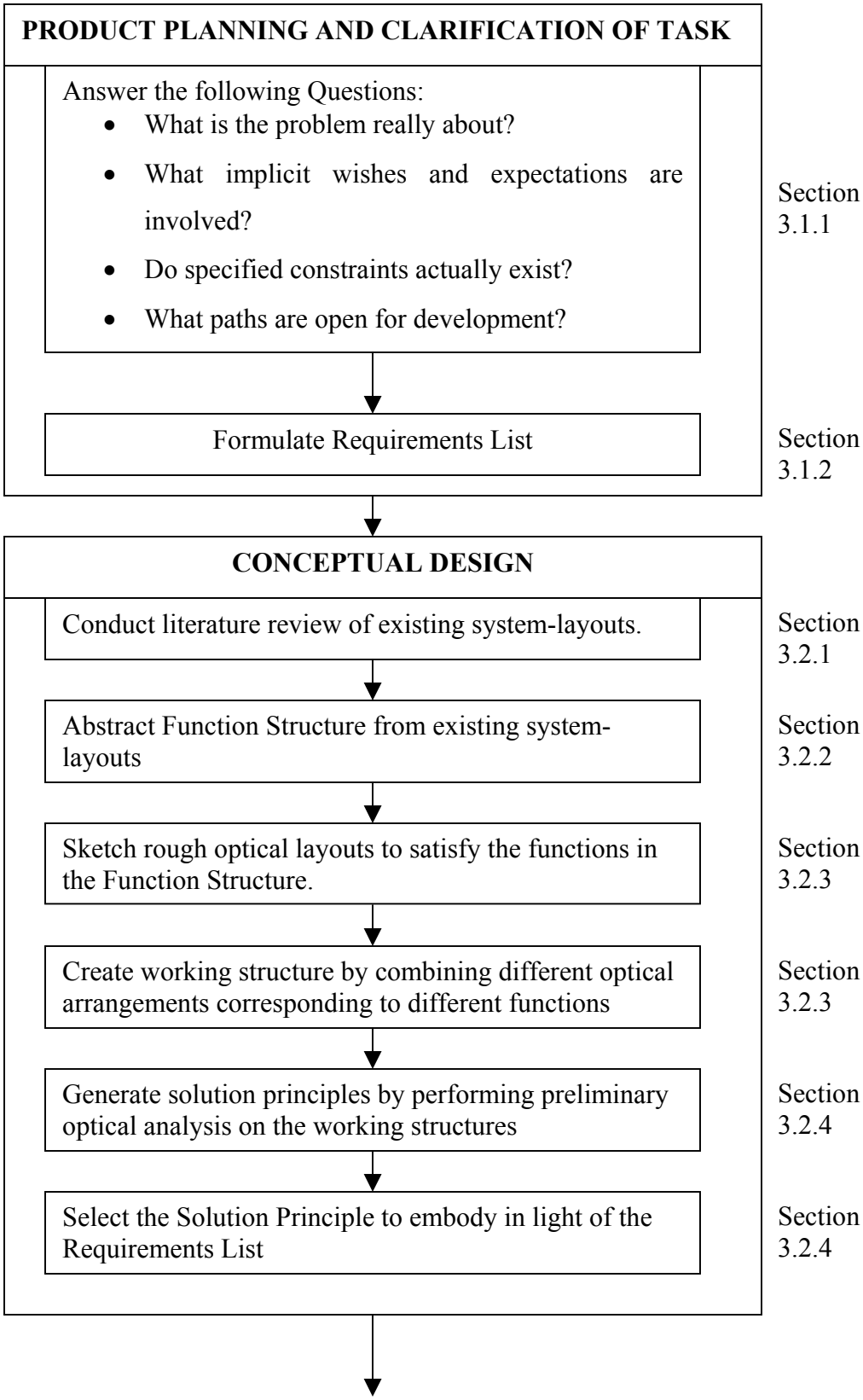
PRODUCT PLANNING AND CLARIFICATION OF TASK
Answer the following Questions:
What is the problem really about?
What implicit wishes and expectations are involved?
Do specified constraints actually exist?
What paths are open for development?
Section 3.1.1
Formulate Requirements List
Section 3.1.2
CONCEPTUAL DESIGN
Conduct literature review of existing system-layouts.
Section 3.2.1
Abstract Function Structure from existing system-layouts
Section 3.2.2
Sketch rough optical layouts to satisfy the functions in the Function Structure.
Section 3.2.3
Create working structure by combining different optical arrangements corresponding to different functions
Section 3.2.3
Generate solution principles by performing preliminary optical analysis on the working structures
Section 3.2.4
Select the Solution Principle to embody in light of the Requirements List
Section 3.2.4

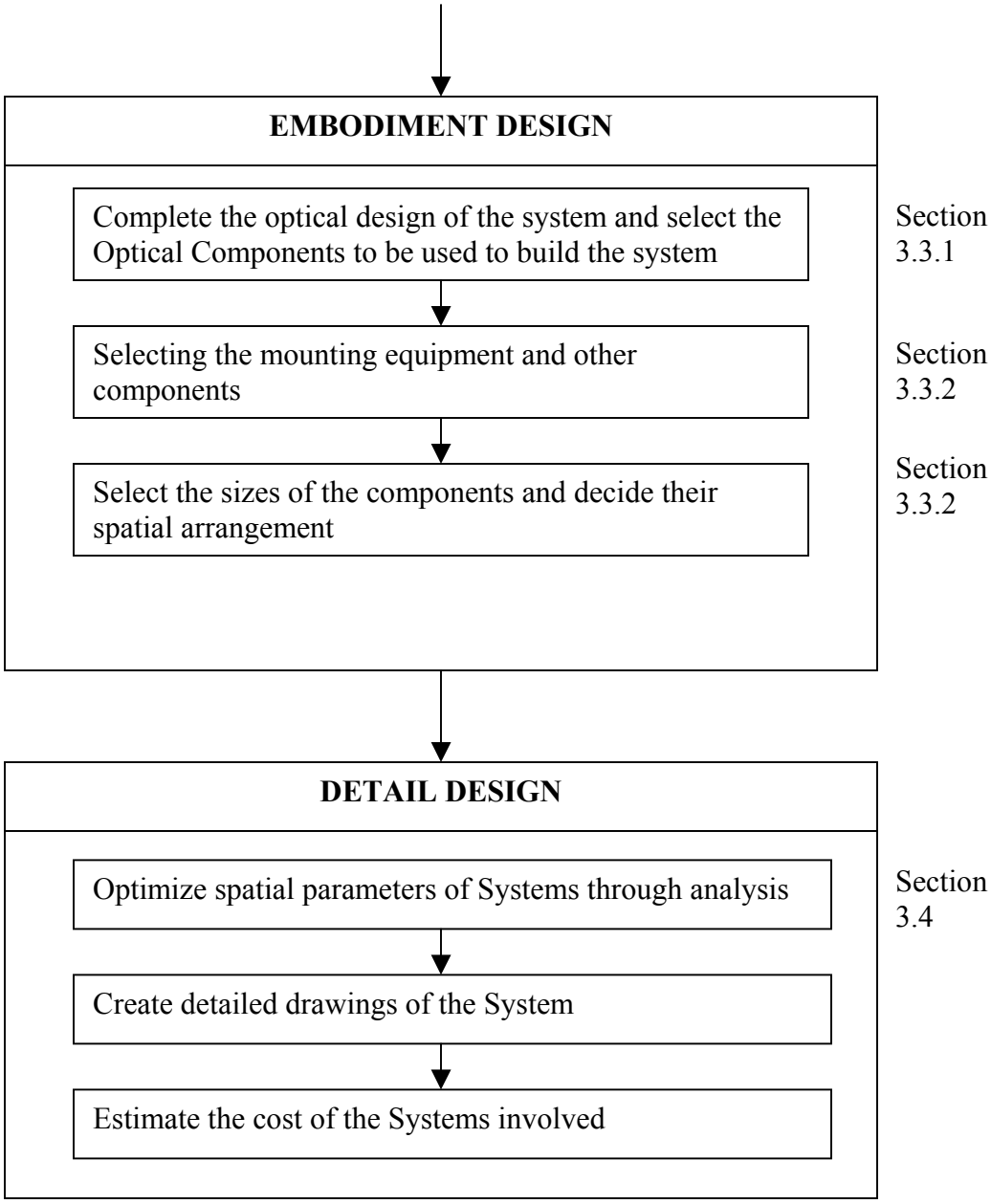

Figure 2. 3 Design Methodology adopted to design the Micro-SLA System

CHAPTER 3

DESIGN OF MASK-PROJECTION MICRO-SLA SYSTEM

In Chapter 2, the PB Methodology has been adapted to design the Mask Projection Micro-Stereolithography System. In this chapter, the adapted methodology is implemented. The design process consists of four phases as shown in Figure 2.3.

3.1 PRODUCT PLANNING AND CLARIFICATION OF TASK

In this phase, the objective behind designing the Mask Projection Micro-SLA system is clarified. Some discussion to this effect has already been presented in Chapter 1 [Section 1.2]. In this section, these objectives are formalized by answering certain fundamental questions [Section 3.1.1]. Then, the Requirements List is created for the system in Section 3.1.2 based upon the objectives stated in Section 3.1.

3.1.1 Clarifying the task

In this section, I shall engage myself in a catechism to have a clear idea of the expectations from the Micro-Stereolithography System, before I even set out to design it.

Question 1: What is the Problem really about?

Answer: The problem is to design and assemble a Mask projection Micro Stereolithography System whose part building process shall be modeled to gain a better understanding of the Process Planning issues in MPμSLA.

Question 2: What are the implicit wishes and expectations involved?

Answer: Since the System is likely to be used to validate theoretical relations about MPμSLA process, it should possible to analytically model the system's working. For this,

we would like the system to be simple and consist of the minimum components, because larger the number of components, larger will be the random errors and the validation will be more difficult. Thus, the implicit wishes are:

Implicit Wish 1: System should be simple and consist of small number of components.

Implicit Wish 2: System should not consist of any black box systems, like say Diffractive Optical Elements, whose effect we can't model.

The System is also to be used to derive experimental relations between certain process-parameters and part properties. For this, the system will have to be run at varying values of process parameters.

Implicit Wish 3: System should be able to function with different process parameter values.

Question 3: Do specified constraints actually exist?

Answer: As an answer to this question, I will identify the constraint, which doesn't exist. The System need not have better resolution than the systems currently developed. The prime aim in this thesis is to increase knowledge about the process rather than develop the best Micro-Stereolithography System. So, this constraint shall be included as a "Wish" and not as a "Demand" in the Requirements List.

Question 4: What paths are open for development?

Answer: The following paths exist for development

1. Replicate a System presented in the literature based upon whatever knowledge is published.
2. Leverage the Function Structure of the System and proceed from there.
3. Design a system from the beginning, leveraging nothing from the current systems.

Of the three paths mentioned above, Path 2 is followed. The designs of the Mask-Projection Micro-Stereolithography Systems developed so far have not been presented in detail and so, replicating one of the existing systems won't be possible. This rules out Path 1. The working of the systems has been described at functional level and so, it is possible to leverage the function structure and thus pursue Path 2. Path 3 shall not be followed to save time and also because Path 3 is likely to yield the same Function Structure as leveraged from existing systems.

3.1.2 Requirements List

The Requirements List will list the demands and wishes from the system that shall be designed. Demands are those expectations from a system, which the system will have to fulfill. Wishes on the other hand are those expectations, whose fulfillment is not a must, but which are preferred as fulfilled.

From the discussion presented in Section 3.1.1, following additions to the Requirements List can be made:

- Demand: No Diffractive Optic Element to be used
- Demand: System should be simple
- Wish: System should consist of minimum number of optical components
- Demand: It should be possible to use a number of resins with the system.

In addition, some other Requirements can be formulated:

Spatial Requirements:

- Wish: The System should not be more than 4x4x4 feet in size, so that it doesn't become unwieldy.

Requirements from cured part:

- Demand: The largest possible size of a cured part must be larger than 2 x 2 x 15mm.
- Wish: It should be possible to cure the same part in different sizes

Cost related:

- Demand: The total cost of the system has to be less than or equal to $16,000.

Requirements from the process:

- Wish: The Process should be as fast as possible. It is expected that greater the part resolution, slower will be the part building speed. For the system that I shall design, I shall relegate the part building speed to the process resolution.
- Demand: The lateral resolution of the process should be better 30μm and vertical resolution better then 10μm
- Demand: The process should dimensionally precise within ± 2μm.

  All these requirements have been presented in Figure 3.1.

REQUIREMENTS LIST FOR THE MASK-PROJECTION MICRO-STEREOLITHOGRAPHY SYSTEM. --Formulated by Ameya Limaye		Date of creation: 10/10/2003
D/W	**Requirement**	**Responsibility**
D	No Diffractive Optic Element to be used	Ameya Limaye
D	System should be simple, i.e. consists of small number of optical components.	
D	It should be possible to use a number of resins with the system	
W	The System should have better resolution that the similar systems that exist currently	
W	The System should not be more than 4x4x4 feet in size	
W	The largest possible size of a cured part must be larger than 3 x 3 x 5mm	
W	It should be possible to cure the same part in different sizes	
D	The total cost of building the system should be less than $16000	
W	Process should be as fast as possible	
D	The lateral process resolution should be better than 30μm and vertical resolution better then 10μm	
D	The process should be dimensionally precise within +-2μm	

Figure 3. 1 Requirements List

3.2 CONCEPTUAL DESIGN

As explained in Section 2.2, Conceptual Design leads to the specification of the principle of operation of a system. In this section, a literature review [Section 3.2.1] of the existing MPμSLA systems is conducted. The function structure of the system to be deigned is abstracted [Section 3.2.2]. Then, the preliminary optical layouts for the sub-functions identified in the Function Structure are sketched in Section 3.2.3. Finally, these optical layouts are combined to create variants of the optical layout of the entire system and select the optical layout to be embodied from among the variants after performing rough calculations [Section 3.2.4].

3.2.1 Literature Review

The Mask Projection Systems developed so far have been presented in Table 1.1. From the table, it can be seen that there are primarily three research groups that have built these research systems. In the publications, the designs of these systems have not been presented in detail. However, their overall operation has been presented. In this section the literature review concerning the design of the systems developed by these groups is presented.

Laser-LCD screen System (Bertsch 1997)

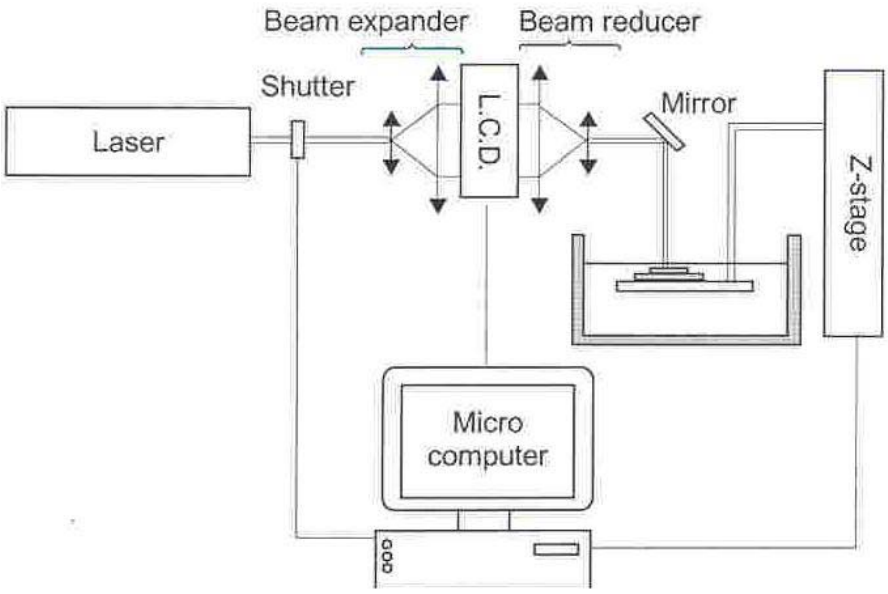

Figure 3. 2 Laser-LCD System layouts from (Bertsch et al. 1997)

This is the first Mask Projection Micro SLA system developed. The layout is shown in Figure 3.2. A laser emitting radiation in the visible range at 515nm is used as a light source. The laser beam is expanded so that it covers the maximum area on the LCD. A pattern corresponding to the layer to be cured is displayed on the LCD. A beam reducer then focuses this pattern onto the resin surface.

The major problems with this design are associated with the use of the LCD as a dynamic mask. The LCD has low contrast because its pixels in their opaque state transmit about 20% of light. Also, the pixel size being large, the resolution obtained is low. Further, the liquid crystal matrix is inserted between four glass windows, which are opaque to UV light. This necessitates the use of a light source emitting in the visible range.

Another disadvantage of this design is the Gaussian energy distribution of the laser beam. Due to this distribution, the polymerization is a function of the distance to the center. There is a risk of unwanted polymerization where the light flux was too high.

UV Laser-Spatial Light Modular System by (Chatwin 1998)

The Mask Projection Micro-Stereolithography System designed by Chatwin et al. in 1998 is an improvement over the design of the System developed by Bertsch in 1997. The layout of the system has been shown in Figure 3.3.

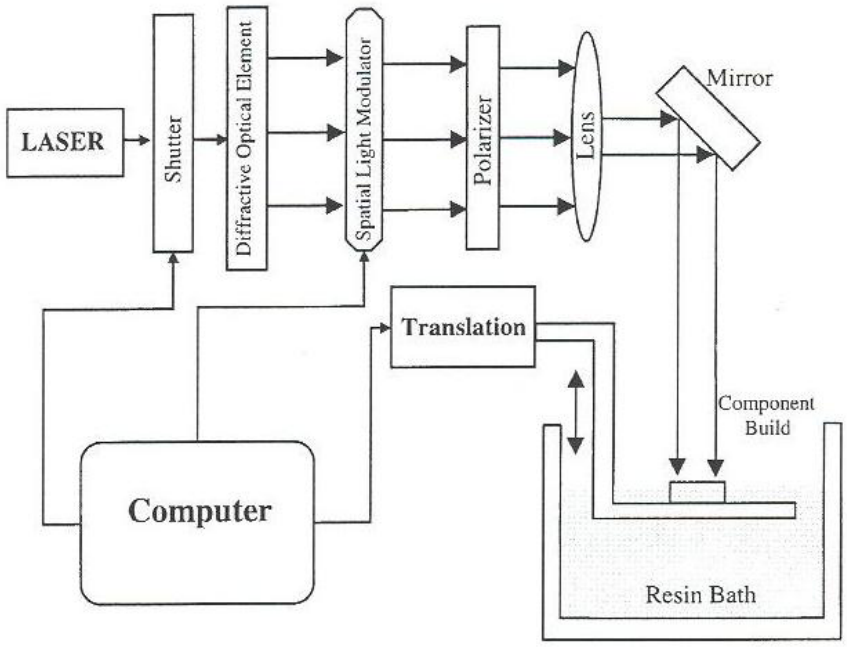

Figure 3. 3 Laser-SLM System from Chatwin 1998

Chatwin used an Argon ion laser, which emitted radiation in the UV range. The Gaussian irradiance distribution is reshaped into a rectangular distribution by using a Diffractive Optical Element (Gaussian to Square Beam Converter by Diagonal Optics Corporation). The speckle of the laser beam emerging from the diffractive optic element

is removed by incorporating a rotating ground screen diffuser. The polarization of the beam is linearized by adding a linear polarized sheet in its path.

A Spatial Light Modulator (SLM) is used as a dynamic mask. The pattern corresponding to the layer to be cured is displayed on the SLM, which acts as a transmissive mask. A focusing lens is used then to focus the pattern onto the resin surface.

Visible Lamp-LCD System (Monneret 1999)

Monneret and co-researchers have developed a Mask Projection Micro-Stereolithography System that employed a visible broadband light source instead of a laser as a light source. Through the use of a lamp instead of a laser, the cost of the apparatus has been greatly reduced. Also, the disadvantages associated with the use of lasers, namely speckle and Gaussian irradiance distribution in the beam have been avoided. The experimental layout presented in (Monneret 1999) is presented in Figure 3.4.

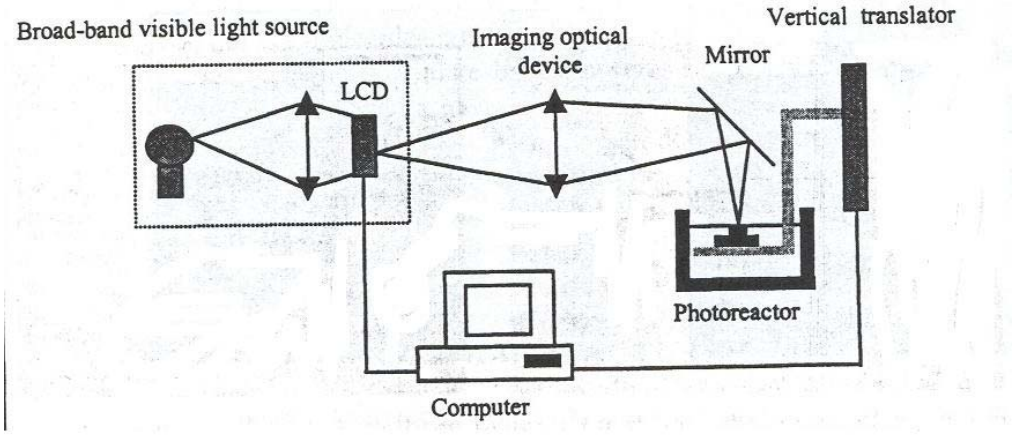

Figure 3. 4 Micro-SLA system layout from Monneret 1999

Lamp-DMD (Bertsch, 1999; Bertsch 2000)

In 1999, Bertsch developed a Mask Projection Micro-Stereolithography System, which employed the Digital Micro-Mirror Display (DMD) as a dynamic mask. Bertsch coupled it with a visible lamp in 1999 and with a UV lamp in 2000 to create his system. No further information about the design and construction of the system has been presented in the literature.

Digital Micromirror Device:

The Digital Micromirror Device (DMD) is an array of individually addressable, bi-stable micro-mirrors (Dudley et al., 2003). A bitmap can be displayed on the DMD by selectively orienting its mirrors in one direction. As opposed to the Liquid Crystal Display (LCD) and Spatial Light Modulator (SLM), the DMD is a reflective mask. As a mask, the DMD has advantages over LCD and SLM. The DMD being reflective doesn't lead to as much diffraction as caused by an LCD. The pixel density of the DMD is higher because the mirrors are smaller in size than the LCD and SLM pixels (12.7μm square as opposed to 24μm square in LCD and SLM) and also because the spacing between mirrors is much less than that between the LCD and SLM pixels.

UV Lamp-DMD System developed at University of Wisconsin (Hadipoespito 2003)

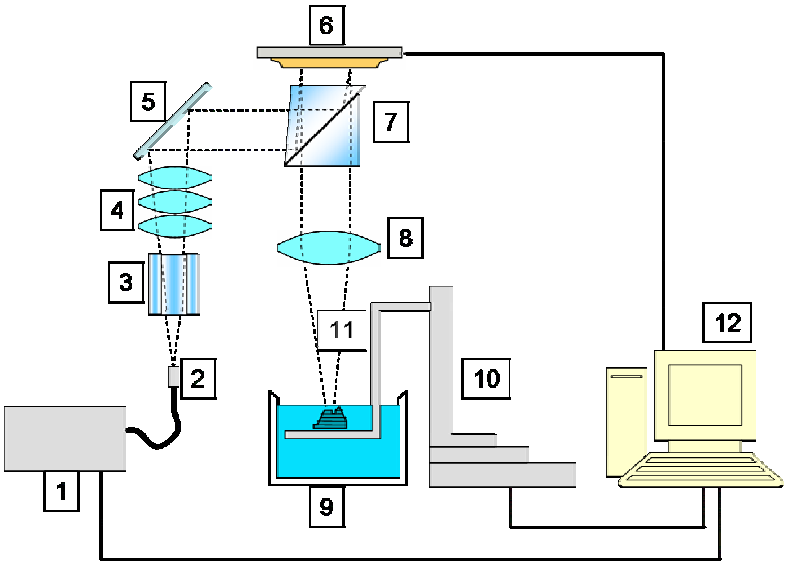

Diagram of the Micro-Stereolithography apparatus: (1) UV light source; (2) light guide; (3) light pipe; (4) condenser lens system; (5) fold mirror; (6) DMD™; (7) TIR prism pair; (8) focusing lens system; (9) photopolymer bath; (10) x-y-z movable stage; (11) building platform; and (12) computer controller.

Figure 3. 5 Micro SLA System layout from (Hadipoespito et al, 2003)

Hadipoespito and co-researchers used a broadband light source, which emitted radiation from 300 to 470nm with a peak at 365nm. The DMD chip was obtained from a DMD-based multimedia projector. The light is collected by condensing lens systems and is made incident on the DMD. A set of focusing lenses was used to image the bitmap displayed on the DMD onto the resin surface.

3.2.2 Leveraging the Function Structure

In this section, the commonality in the working of the systems presented in section 3.1 is identified and the function structure is abstracted [Section 3.2.2.1]. This

function structure is leveraged to generate the function structure for the system that we shall build [Section 3.2.2.2].

Commonality at functional level in the Systems developed so far

From the literature review in Section 3.1, it can be seen that the design of any Mask Projection Micro-Stereolithography system can be divided into five modules:

1. Light Source
2. Beam conditioning module
3. Mask
4. Imaging module
5. Build module.

The following are the functions of these modules:

1. Light Source:

The function of the Light Source is to emit the radiation that will cure the resin

2. Beam Conditioning module:

The design of the Beam Conditioning module is dependent upon the light source used. The following are the functions of this module:

- Collect light from the light source.
- Collimate a beam of light, i.e. send out parallel rays of light.
- Make the irradiance distribution uniform across the light beam.
- Filter the required wavelength.
- Remove speckle.

Thus, a well collimated beam of uniform intensity distribution across its diameter, of the required wavelength and free of speckle emerges out of the Beam Conditioning module and is made incident on the pattern displayed on the mask.

3. Mask

The function of the mask is to display the pattern corresponding to the layer to be cured.

4. Imaging module

The function of the imaging module is to image the pattern displayed on the mask onto the resin surface with the required reduction in image size.

5. Build module

The function of the build module is to lower the cured layer and coat a fresh layer of resin onto the cured layer.

The Function Structure abstracted from the above observation is shown in Figure 3.6.

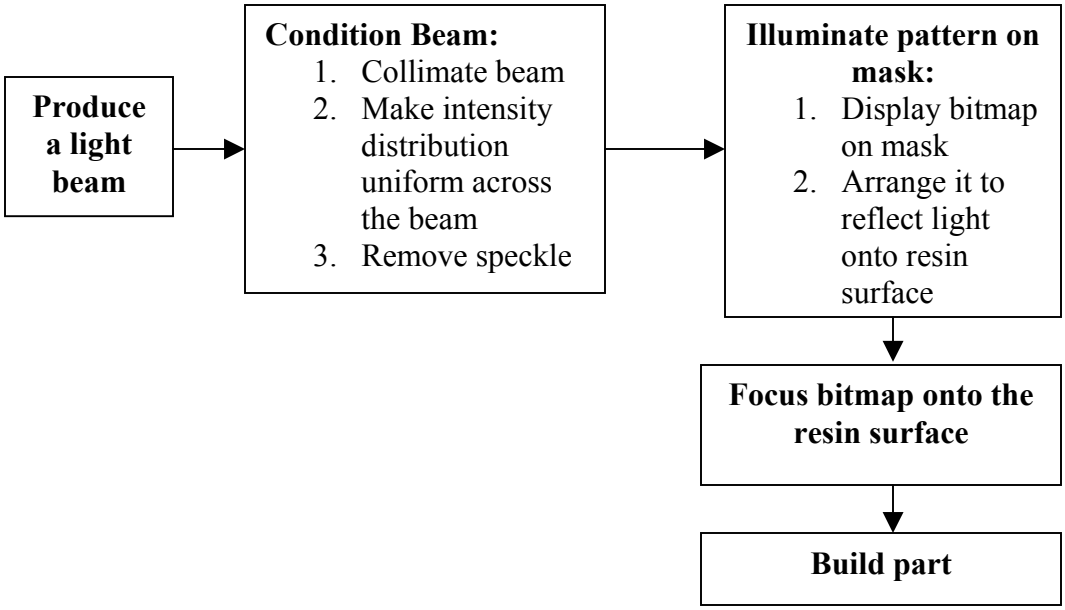

Figure 3. 6 Abstracted Function Structure of any general Mask Projection Micro-Stereolithography System

Leveraging the Function Structure

In this section, the function structure presented in Figure 3.6 is made specific to the system to be designed.

The Beam Conditioning Module, as stated in Section 3.2.2.1, is dependent upon the light source used. Though not in the embodiment –design phase yet, it is possible to decide on the light source to be a UV lamp now itself. This is because a laser costs around $20,000 and one of the Demands in the Requirements List is “Total Cost of the System should not be greater than $16000”.

The dynamic mask to be used with the system can also be decided at this stage. As stated in Section 3.2.1.4, the Digital Micromirror Device has advantages of better resolution and better contrast over LCD and SLM. All the recent systems (over the past three years) employ the DMD as a dynamic mask. So, the DMD is chosen as the dynamic mask for the MPμSLA system to be designed.

Now, given that a UV lamp is going to be used as the light source and a DMD as the dynamic mask, the Function Structure presented in Figure 3.6 is particularized. Since the laser is not to be used, there is no need to remove the speckle and to even out the Gaussian energy distribution in the laser beam. The particularized Function Structure is presented in Figure 3.7.

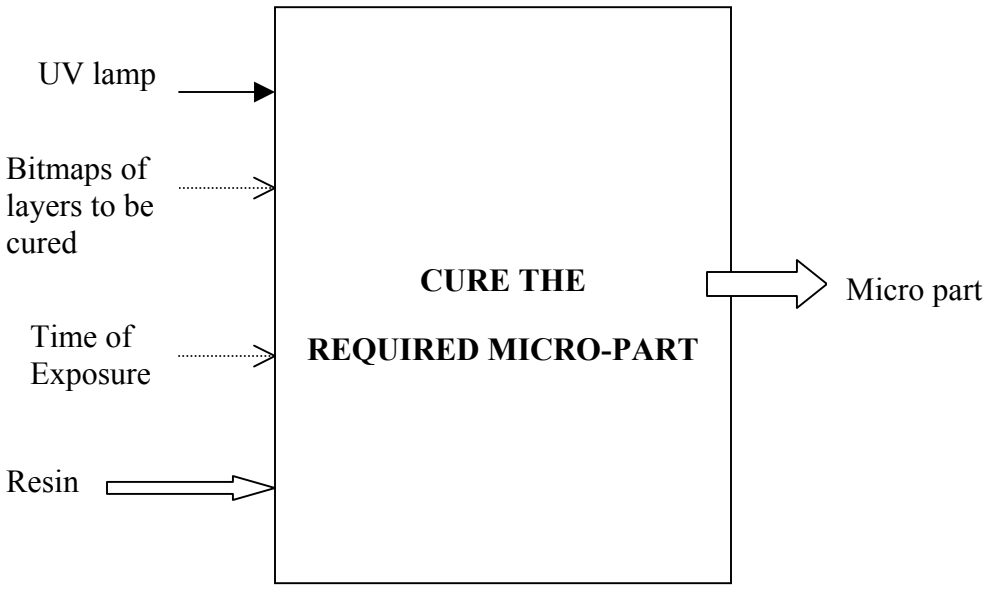

(a)

Figure 3. 7 (a) Overall Function, (b) Sub-functions and (c) Completed Function Structure for the Mask Projection Micro-Stereolithography System

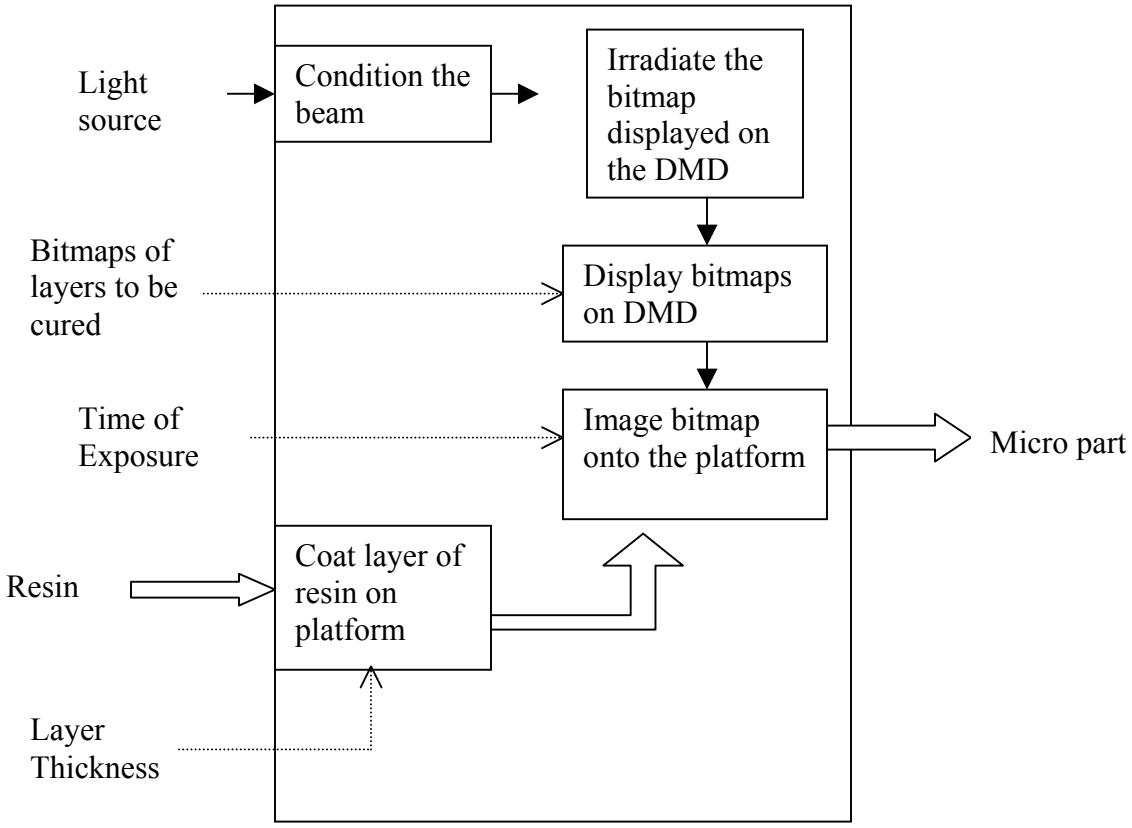

(b)

Figure 3.7 continued

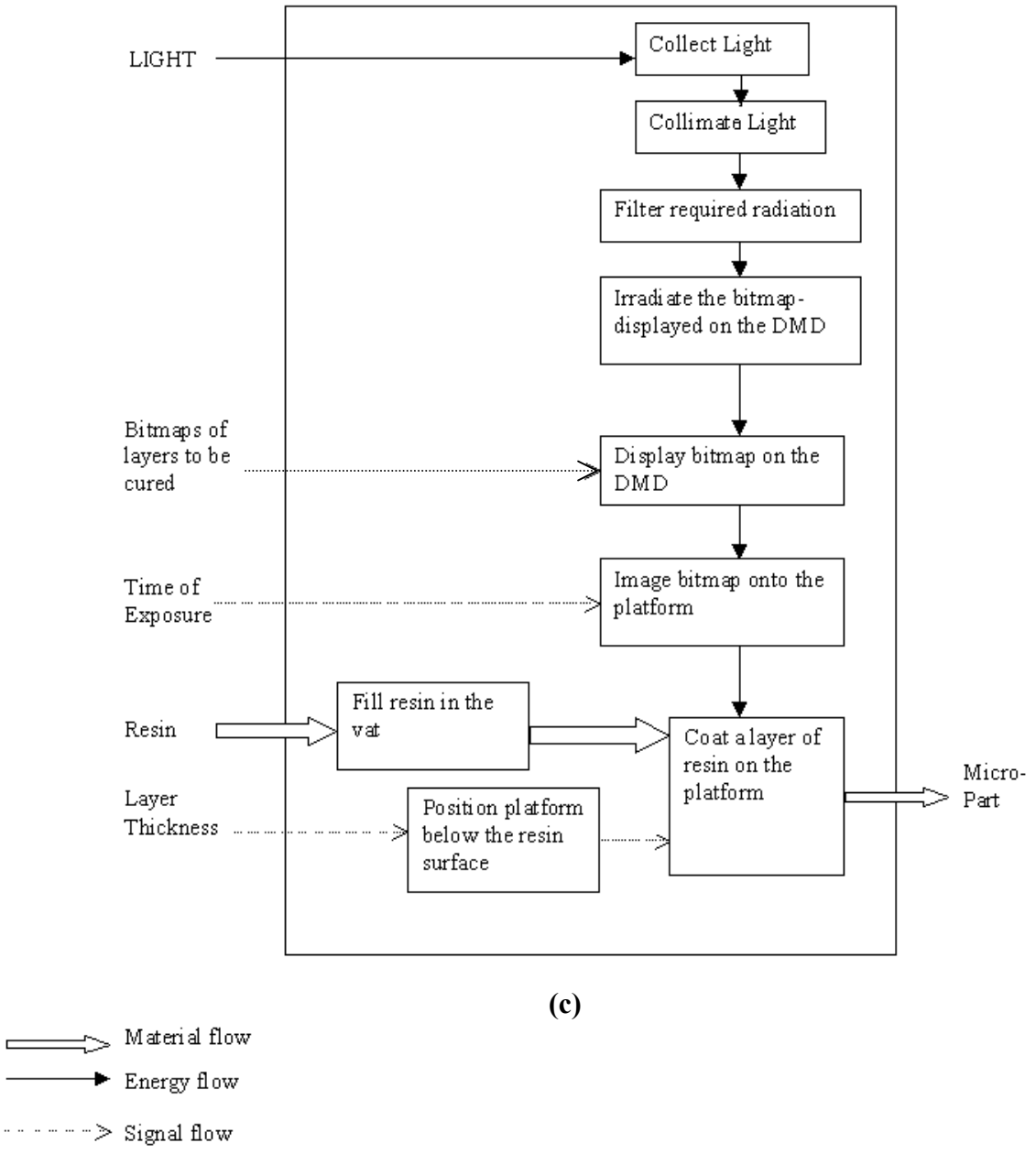

(c)

Figure 3.7 continued

3.2.3 Sketching rough Optical Layouts to satisfy functions in Function Structure

In this section, the preliminary optical layouts are sketched that will satisfy the functions mentioned in the Function Structure as shown in Figure 3.7. In Sections 3.2.3.1 to 3.2.3.3, layouts for three functions: Condition the beam, Image pattern onto resin surface and Build the Part, are sketched. The pros and cons of these layouts are compared and the best layout to be embodied is selected in Section 3.2.4.

Function 1: Condition the beam

The design-module satisfying this function has to satisfy the following sub functions:

Collect light: The light from the UV lamp is diverging. This light needs to be collected and sent out as a beam so that the required amount of irradiance is incident on the DMD.

Collimate the beam: By collimating the beam, we mean sending out a beam with parallel, or more or less parallel rays. This is necessary so that the light reflected from the DMD is not too diverging. This will reduce the demands from the imaging module.

Filter the required wavelength: Since the light source is broadband, all but the required wavelengths will have to be filtered out.

In Figure 3.8, the rough sketches for the realization of the Beam Conditioning System are illustrated. The light of a typical UV lamp is emitted from a liquid guide, which is a tube of about 5 to 10mm diameter. In Rough Sketch 1, a condensing lens is placed at a distance of one focal length from the light guide. The light then passed through a filter. In Rough Sketch 2, a pinhole is placed immediately after the light guide to simulate a point source. Then, a collecting lens kept one focal length away from the

pinhole collects the light, collimates it and sends it through a filter. In Rough Sketch 3, a lens is used to focus the light from the light source onto a point. A second lens collects this light and collimates it.

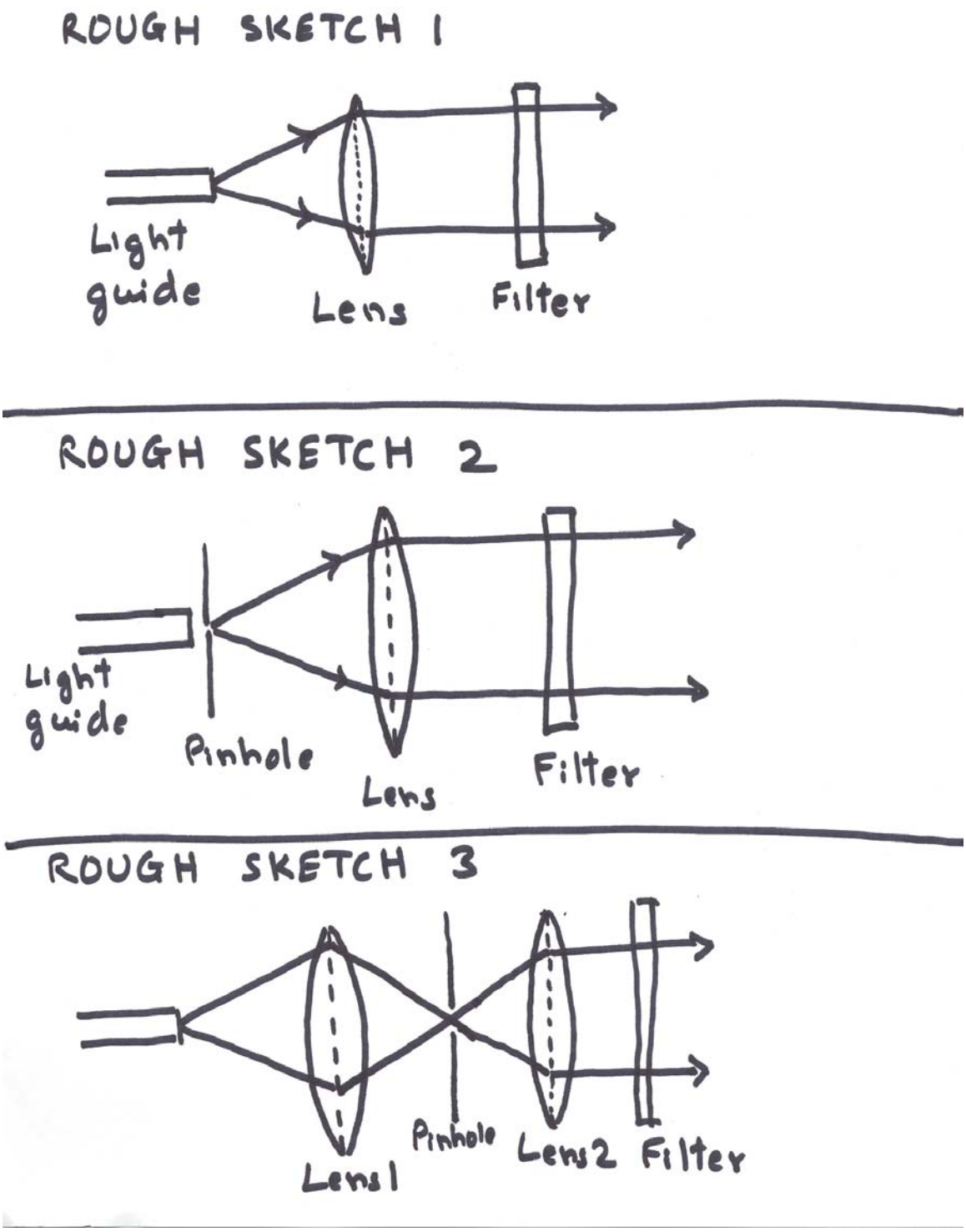

Figure 3. 8 Rough sketches of Beam Conditioning System

Function 2: Image the pattern onto the resin surface

There are two aspects to the Imaging/Focusing System: Location and mounting of DMD, and Method of focusing.

As shown in Figure 3.9, the DMD can be mounted horizontally and irradiated by means of a beam splitter or it can be mounted at 45 degree to the horizontal and the beam splitter can be dispensed with. The imaging can be done using a single convex lens or by using one of the commercial enlarging lens systems used in photography.

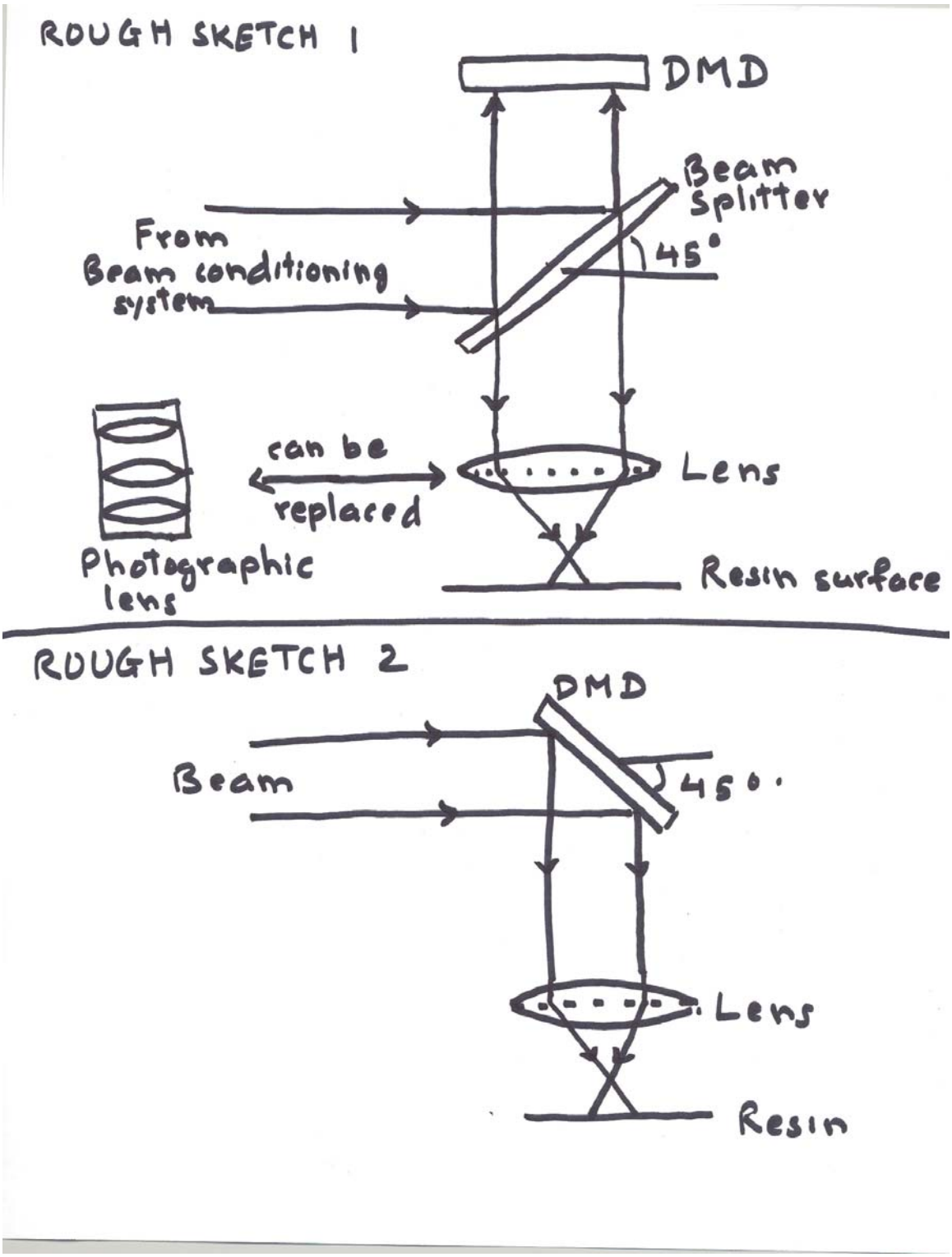

Figure 3. 9 Rough Sketches of Imaging System

Function 3: Build the part

The possible layouts of the Build System have been shown in Figure 3.10. The lowering of the cured layer can be accomplished by attaching the platform to a translation stage. The leveling can be accomplished by relying on the rheological properties of resin, (i.e. purely gravity assisted leveling) or by using an ultrasonic vibrator to assist leveling or by positioning a glass window over the free resin surface to level the resin.

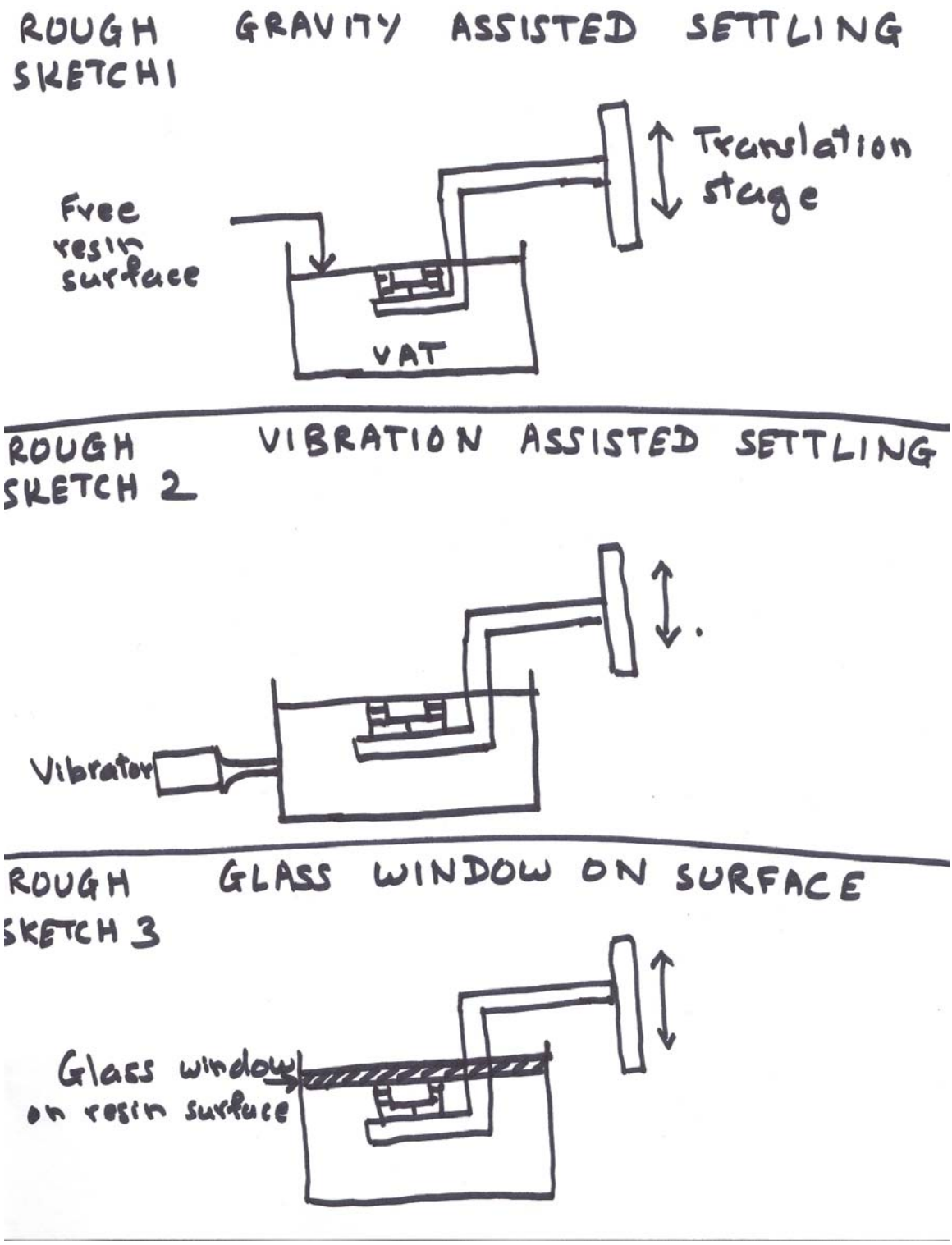

Figure 3. 10 Rough Sketches of Build System

3.2.4 Generating Solution Principle to embody

Working Structures can be created by combining the working principles in the form of rough sketches. Then, the best working structure can be selected from amongst the working structures for embodiment. In this case, a slightly different approach is adopted. The best preliminary rough sketch for each function is selected and then, these are combined to generate the working principle. This can be done because all the optical sketches are compatible with each other. In this section the best layout for every function is selected and the working structure formulated. Optical analysis is performed on the working structure to formulate the solution principle.

Selecting the best rough optical layout for every function

Beam conditioning System:

Please refer to Figure 3.8. Rough Sketch 1 will result in very poor collimation because the end of a typical light guide is about 5mm in diameter and not a point source. Rough Sketch 2 can result in a better collimation. Rough sketch 3 will result in as good collimation as Rough Sketch 2 but it will also result in collecting more light into the system. The recommended incident irradiation on the DMD is given to be 0.68 mW/cm^2. The output of a typical lamp at 365nm is about 3 to $5W/cm^2$. So, we need not collect a large amount of light. Hence, we select Rough layout 2 because it is simpler than Rough Layout 3.

Imaging System:

Please refer to Figure 3.9. The Beam Splitter Design suggested in Rough Sketch 1 will result in loss of 50% of the light every time light passes through it. The irradiance

received from the DMD shall be low because the irradiance incident on it is limited to 0.68mW. Due to the beam splitter, the resin surface will receive very low radiation from the DMD. In case of Rough Sketch 2, which suggests mounting the DMD at 45^{o} with the horizontal, the object distance for the imaging lens will not be constant. Assuming that a bitmap has dimension 6.8mm (i.e. spanning about 500 mirrors on the DMD), the distance of the farthest point from the optical axis will be 3.4mm. So, when the central point on the DMD is focused, the farthest point will be defocused by 3.4 * $\cos 45^{o}$ mm, i.e. 2.4mm. This focusing error appears acceptable.

Using a commercially available imaging system will certainly result in better imaging and thereby higher resolution than using a single focusing lens. However, such systems are costly. Also, such systems being made primarily for visible light will result in lot of losses when UV light is passed through them. Hence, we shall use a single lens to focus the bitmap displayed on the DMD onto the resin surface. This will keep the system simple and low cost.

Build System:

Please refer to Figure 3.10. Rough Sketch 1 is discarded because it will take too long for the resin to level itself purely due to gravity. Placing a glass window over the vat can be a good solution, but using a vibrator to aid leveling will be lot easier. So, Rough Sketch 2 is selected for embodiment.

Finalizing the Optical Layout

By Combining Rough Sketches 2 from Figure 3.8, 3.9 and 3.10, we have the working structure as shown in Figure 3.11. In this section, this rough sketch shall be firmed up into an optical layout through calculation of optical parameters.

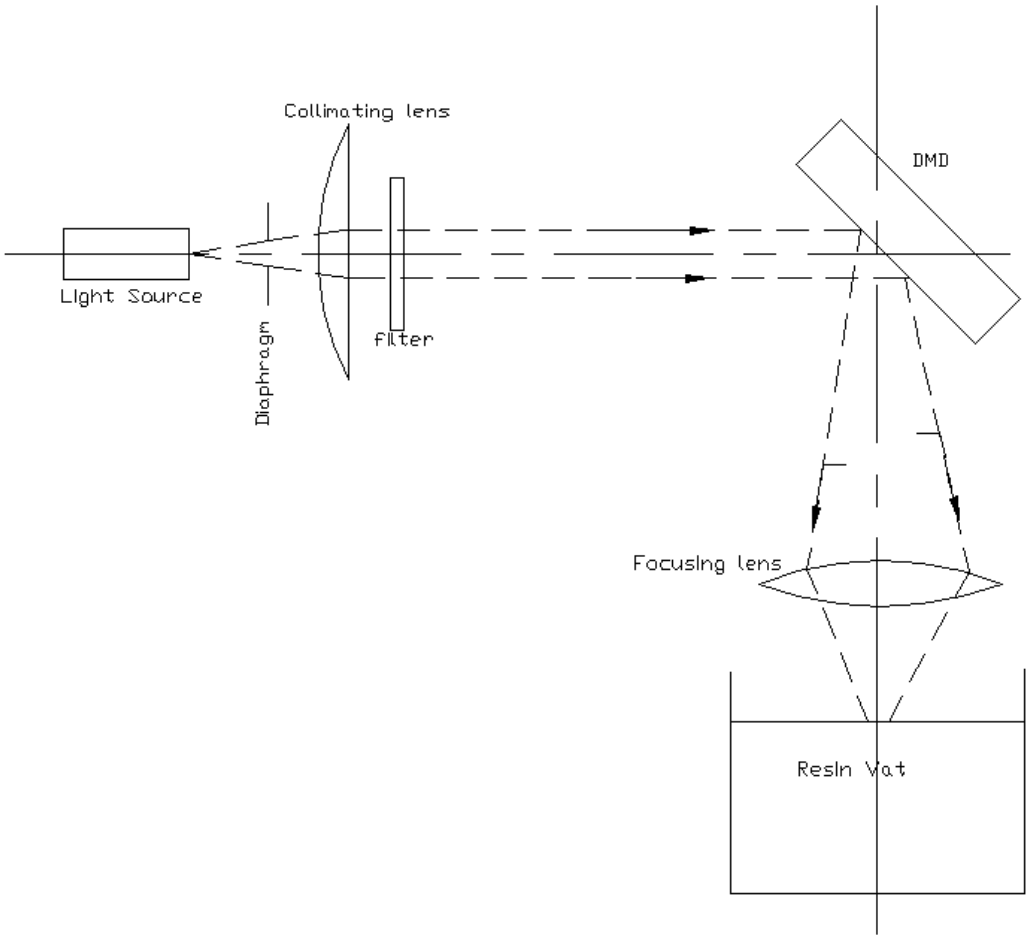

Figure 3. 11 Rough Working Structure to embody

Light Source:

Since the commercially available Stereolithography resins are to be used with the system being designed, a light source whose radiation spectrum peaks around 365nm shall be selected because most resins cure in the vicinity of this wavelength.

Pinhole:

The pinhole shall be placed immediately after the light guide in order to simulate the behavior of a point source. Instead of a pinhole, we shall use a variable aperture diaphragm, which will allow me to increase the light throughput if needed.

Collecting lens:

The Collecting lens, or Collimating lens has to collect as much light coming from the light guide as possible. For this, the lens should have a large diameter and a short focal length, since the diaphragm will be placed at the focus of the lens. The lens should transmit light in the UV range.

Filter:

A filter of diameter at least equal to the diameter of the beam emerging from the collecting lens shall be selected.

DMD:

The DMD shall be mounted at 45 degree to the horizontal.

Focusing Lens:

The focusing lens is responsible for carrying out the required image reduction. A typical bitmap on the DMD will span 500 pixels square, and thus will be 500 x 13.7 = 6850μm = 6.8mm. We need parts about 2mm in lateral dimension. So, we would need a reduction of about 3:1.

Needless to say, this lens should transmit light in the UV range.

It would help to keep the optical path of the focusing system as short as possible to reduce the losses of irradiance. So, a powerful lens will be preferred.

3.3 EMBODIMENT DESIGN

In this section, I shall select the optical components from the catalogs, select the mounting equipment, and decide on their spatial location. The construction and dimensions of the build module comprising of the platform, vat and translation stage shall also be finalized. In Section 3.3.1, the optical components used in the Beam Conditioning System and the Imaging System are selected. In Section 3.3.2, the mounting components are selected and the build module designed. These two tasks are completed together because the mounting components and the vat and platform sizes will have to satisfy the dimensional constraints.

3.3.1 Selecting Optical Components

Light source

The light source should emit radiation in the UV range, mostly at around 365nm. The light source selected is ADAC System's Cure Spot ™ 50. The lamp emits 3000 + mW/cm^2 at 365 nm. The Spectral distribution of the lamp is as shown in Figure 3.12. The typical half cone divergence angle of the light emitted from the light guide is given to be 30^o. This lamp was selected because it was the cheapest lamp available, which emitted in the required spectrum.

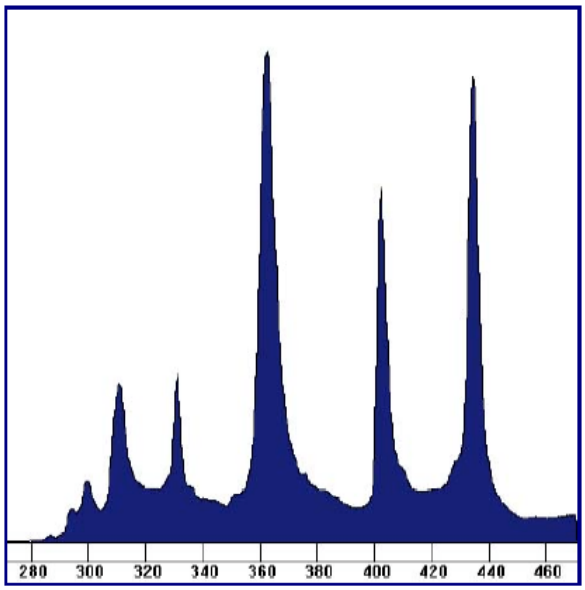

Figure 3. 12 Relative Spectral Distribution of Cure Spot 50

Diaphragm

A mounted iris diaphragm has been selected from Edmund Optics Stock Number H53-914. The diaphragm has clear aperture adjustable within the range 0.8mm to 12mm.

Collecting Lens

The collecting lens should be as fast as possible, i.e. of as small a Focal Number as possible so that it can collect the maximum about of light. The lens selected is an Aspheric Condenser lens from Edmund Optics Stock Number H46-242. The lens has a clear aperture of 26.50mm and an effective focal length (EFL) of 19mm. The lens has a Focal Number of 0.6. The material of the lens is B270, which transmits at 365nm.

Filter

The diameter of the filter can be calculated as follows:

The half cone divergence angle = 30^{o}.The lens is located at a distance = 19mm from the diaphragm (EFL of lens = 19mm). Light rays would come more or less parallel from the lens. The maximum distance of a light ray from the collimating optical axis will be 19 x tan 30^{o} = 10.96mm. So, minimum diameter of the filter = 10.96 x 2 = 21.92mm.

A filter of 24.15mm is selected (Edmund Optics Stock Number H43-103). The filter transmits radiation at 365 nm while blocking all other wavelengths. The wavelength to be allowed is 365 nm because this is the wavelength at which the radiation from the UV lamp peaks.

Focusing Lens

We compute the focal length of the lens:

Let the focal length of the lens be *f* mm. Let object distance be *o* mm and image distance be *i* mm. Then, by simple lens law, $1/o + 1/i = 1/f$

Since reduction $M = 1/3$, $o = 3i$,

$1/3i + 1/i = 1/f$

$4/3i = 1/f$

$i = 4f/3$

$o = 4f.$

$i + o = 16f/3 = 5.33f$ (3.1)

The value of f will thus depend upon the spatial constraints imposed by the system. So, we shall proceed to design the build module and the mounting components for the system because the mounting components and the build module will impose the

spatial constraints. We shall come back and select the focal length of the focusing lens in Section 3.3.3, after we finish designing the build module.

3.3.2 Selecting mounting components and embodying the Build System

Breadboard

To mount any component, we would need an Optical Breadboard. The Breadboard should be sufficiently big and should provide vibration isolation. The Breadboard selected is the Damped Honeycomb Techbase from Oriel Instruments (Model Number 10451). The Breadboard is 30 x 48 inches in size and has ¼-20 tapped holes at 1-inch centers. The Breadboard has a stainless steel top plate with an aluminum honeycomb core, which provides damping.

Optical Rail

The Beam Conditioning System consists of components which are arranged in series one after the other. For relative positioning of these components along a straight line, it will be helpful to mount them on an Optical Rail. The 12inch dovetail Optical Rail sold by Edmund Optics (Stock Number H54-401) has been selected.

Mounts for the light guide, collecting lens and filter

The light guide, collecting lens and filter are mounted using three screw mounts, with maximum inside diameter 39mm (Edmund optics Stock Number H03-668). These three screw mounts are mounted on stainless steel posts 3 inch in length (Edmund Optics Stock Number H36-497), which are in turn held in post holders, 3 inch in length (Edmund Optics Stock Number H03-647). The post-holder is screwed into a carrier

(Edmund Optics Stock Number H54-403), which can slide on the dovetail-rail. The height of the Optical Axis is decided by these components. By sliding the post inside the post holder as shown in Figure 3.13, the height of the collimating system's Optical Axis above the breadboard can be varied.

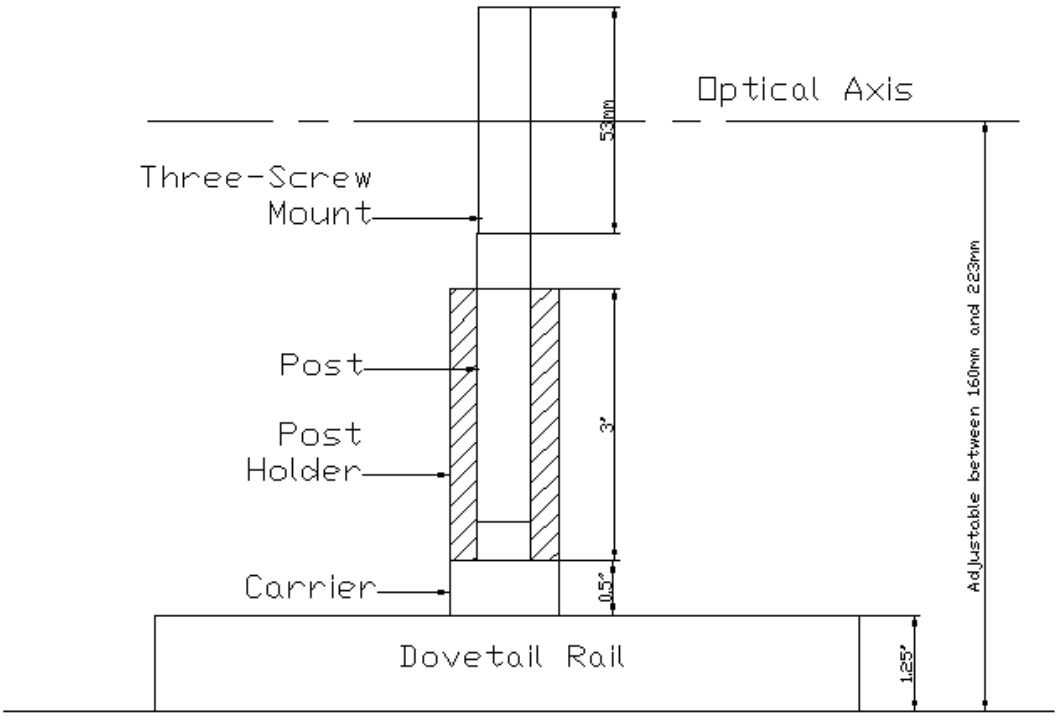

Figure 3. 13 Adjustable height of Collimating Optical Axis

Embodying the Build System

The Build System as shown in Rough Sketch 2 of Figure 3.10 shall now be embodied.

We need a vat that will hold resin. We need a platform that can be raised and lowered inside the vat. The platform thus needs to be attached to a translation stage. The

configuration shown in Figure 3.14 can serve the purpose. A linear translation stage is attached to a right angle bracket. Two cantilever rods are attached to the translation stage. The platform is attached to these two rods. The platform is now raised and lowered in the resin vat by means of this translation stage.

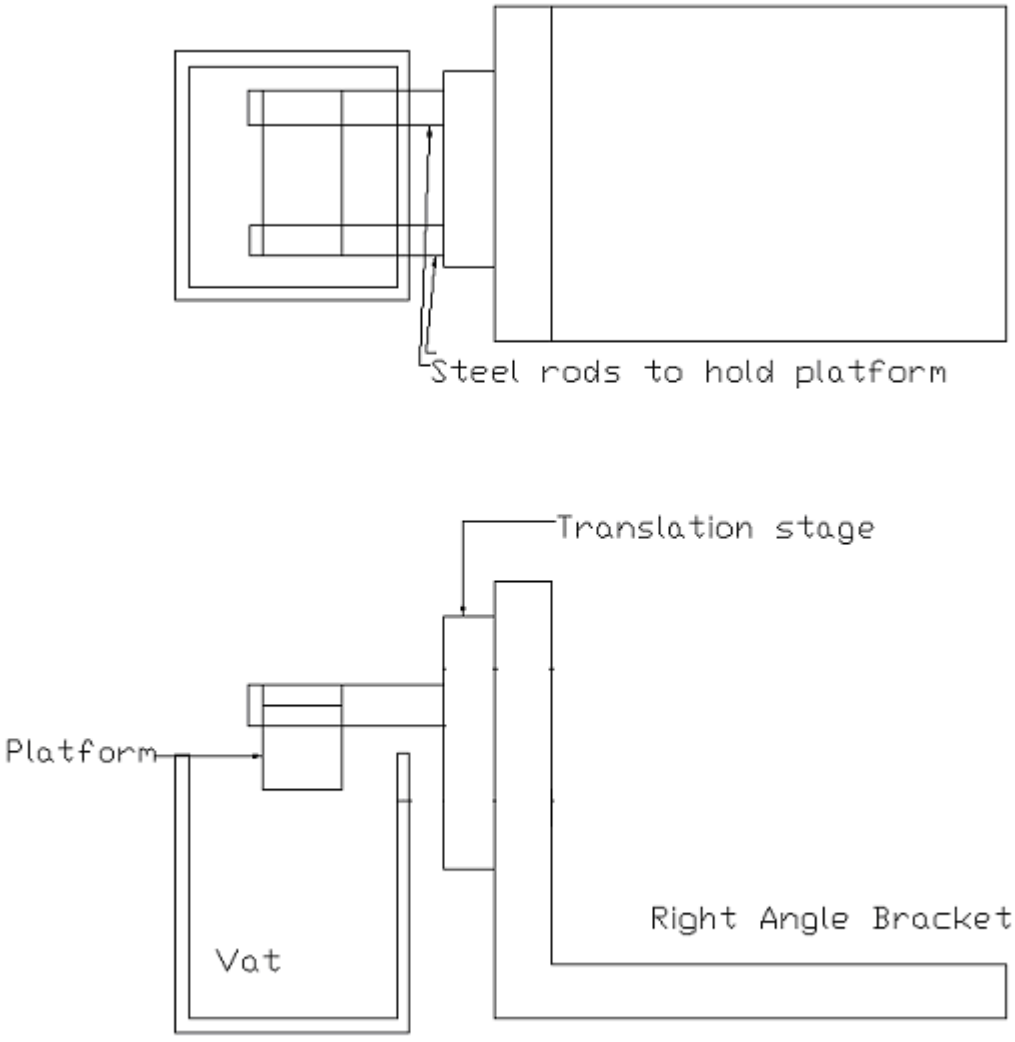

Figure 3. 14 Design of the build system

Now, we shall select the components and their dimensions of the Build Stage as shown in Figure 3.14. The translation stage is purchased from Newport Corporation (Model Number UMR8.25). A micrometer screw of resolution 0.1 μm is used to drive this stage (Newport Corporation Model number DM-17 25). The hole-pattern on the stage is at 1 inch spacing. So, we need a right angle bracket with a similar spacing. The bracket selected is the one supplied by Edmund Optics Stock Number H55-378. Two steel rods, (Edmund Optics Stock Number H36-497) are screwed into the translation stage. When the stage is attached to the right-angled bracket at the lowest possible level, the rods are 95mm from the breadboard. The distance between the lower ends of the rods and the top of the vat must be at least equal to the height of the part to be cured. (Refer to Figure 3.14). The rods being 3mm in radius, the lower ends of the rods are 92mm from the Breadboard. The minimum height of the cured part from the Requirements List (Figure 3.1) is 15mm. So, the height of the vat is to be less than 92-15 = 77mm. We take the height of the vat = 67mm. The vat shall be filled with resin to the brim. Then, the depth of the platform from the rod will be equal to 28.125mm.

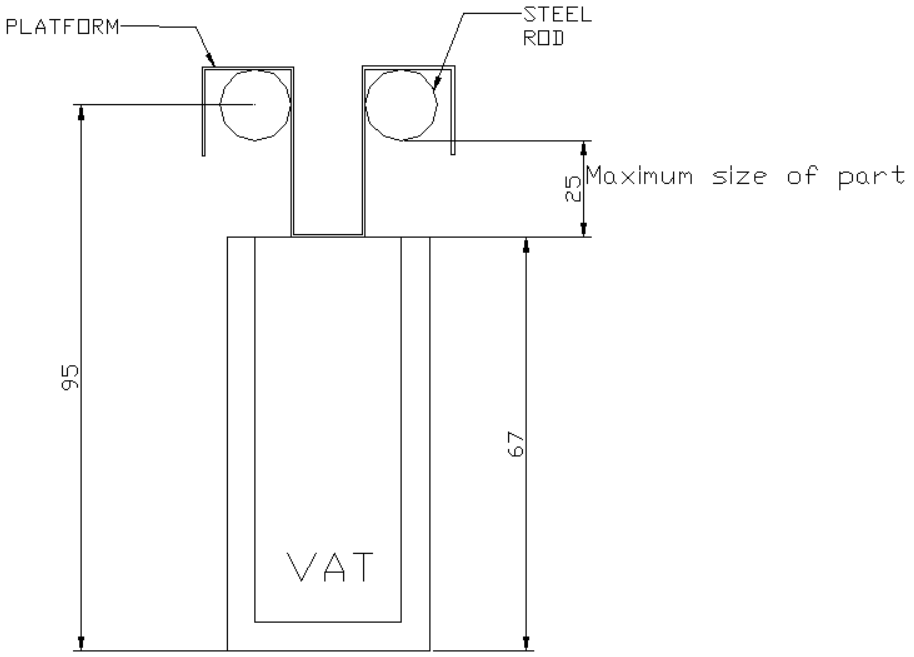

Figure 3. 15 Dimensions of platform and vat

3.3.3 Going back to designing the Focusing System

Now, we shall go back to the design of the Focusing System. The image plane (platform level) is at a distance of 67 mm from breadboard level. The object plane (height of the DMD) is adjustable between 160mm and 223mm (Refer to Figure 3.12). So, the summation of the image and object distances (i + o) is allowable within the range 160-68 = 92mm to 223-68 = 155mm.

From equation (1) presented in Section 3.3.1, we have:

$i + o = 5.33f$

$92 < 5.33f < 155$

$17.2mm < f < 29mm$

Thus, we can choose a lens with focal length between 17.2mm and 29mm.

We choose the lens of focal length 25mm and diameter 25mm, supplied by Edmund Optics (Stock Number H45-098). The lens is MgF_2-coated and has a transmission efficiency of 90% at 365nm.

With this lens, we have:

- Object distance = 100mm
- Image distance = 33.33mm.

Height of DMD from breadboard = 67 (height of image plane) + 33 + 100 = 200mm.

This will also be the height of the optical axis of the beam conditioning system.

3.4 DETAIL DESIGN

In real lens systems, perfect images can't be obtained because of the optical aberrations introduced by the lenses. For detailed explanation on aberrations, please refer Section 6.1. The aberrations can be reduced and the focusing improved by slightly changing the object and image distances. Upon assembling the system, the object and image distances were slightly changed so that the image obtained on the platform was as sharp as possible. Upon these fine adjustments, the object and image distances were manually measured. The image distance was in the range: 32mm to 35 mm, while the object distance was in the range 111m to 114 mm.

The final drawings of the system and the Bill of Materials are presented in Appendix A.

Summary

In Chapter 3, the Pahl and Beitz Methodology is followed to design the MPμSLA system. In Appendix A, the detailed drawings of the system are presented and the components to be purchased are documented. A photograph of the complete assembled system is shown in Figure 3.16. With this chapter, the first part of this thesis is concluded. Chapter 4 onwards, the system's part building process is modeled and its accuracy quantified.

Figure 3. 16 Photograph of the MPμSLA system assembled as a part of this research

CHAPTER 4

FORMULATING RESEARCH QUESTIONS AND RESEARCH TASKS

The focus in the first three chapters of this thesis was on the design of the MP-MSLA system. From here onwards, the focus shall shift to the process of building a micro-part using that system. With the MPμSLA system realized, the next objective is to develop a process planning methodology for the system.

Process planning methodology is the method of choosing the values of process parameters so that a part of required properties can be fabricated. Naturally, the values of process parameters would depend upon the part-properties of interest. In Section 4.1, the properties of interest of microparts to be fabricated are identified and thus, the research objective particularized. In Section 4.2, the research objective is broken down into research questions and research hypotheses. In Section 4.3, the research tasks required to test the hypotheses presented in Section 4.2 are identified. In Section 4.4, the organization of work in this part of the thesis is presented.

4.1 PARTICULARIZING THE RESEARCH OBJECTIVE

The broad research objective is presented as:

"To develop a process planning methodology for the MPμSLA system"

In this section, I identify the properties of critical importance for microparts and thus, particularize the research objective.

The MPμSLA process is a potential supplement to the MEMS fabrication process. Due to its ability to fabricate true 3D structures, this process has an inherent advantage

over the Micro-Systems Technologies, which fabricate 2 ½ D structures. As of now, the MPμSLA process is not capable of achieving the degree of miniaturization that the Micro-Systems Technologies have achieved. However, with further research, this process is sure to supplement, if not replace, the conventional MEMS fabrication processes. Futuristically speaking, the MPμSLA process will have widespread applications in a variety of fields ranging from bioengineering to automotive to the jewelry industry. We might also have micro-robots, micro-cars and other self-translating micro machines in the future (Fujimasa 1996). MPμSLA holds promise for the fabrication of such machines.

There is a plethora of potential application areas for micro-parts and thus a very strong future for the MP-MSLA process. However, to exploit these application areas, the process must fulfill certain requirements. The most critical parameters of a micro-part are its dimensions. There is very little allowance for dimensional errors in a micro-part. So, the chief requirement of any micro-fabrication process is that it should fabricate parts with a high degree of dimensional accuracy. There is thus a need for a process planning methodology for MPμSLA that would enable a manufacturer to fabricate dimensionally accurate parts.

Another process parameter of importance is resolution. Resolution of the process will determine how small a feature can be built using that process and how close two features can be placed. The chief advantage of the micro-manufacturing processes over the conventional macro-manufacturing processes is that the former have a much finer resolution. This single advantage has opened up a variety of application areas for the micro-manufacturing processes. The number of application areas will increase with the

betterment of resolution. Thus, it is necessary to run any MPμSLA system at the process parameter values that will give the best possible resolution.

In the literature review presented in Section 1.3, it has been shown that most of the work on MPμSLA systems has been directed at achieving the best possible resolution using the existing system. However, all this work has been experimental in nature. The researchers have experimentally measured the limiting resolution of their respective systems. There is no attempt to determine the theoretical limit on resolution of any system.

The theoretical limiting resolution of a system can be determined by modeling the part dimensions in terms of process parameters. This work will also enable us to identify the modifications in a MPμSLA system required to attain better resolution.

Thus, the research objective is particularized as:

"To develop a process planning methodology for the MPμSLA process to obtain dimensionally accurate parts"

Due to limitations of time, the scope of this work is restricted only towards developing a process planning method for obtain a single layer of accurate dimensions. Thus, the research question is further particularized as:

"To develop a process planning methodology for the MPμSLA to cure dimensionally accurate layers"

4.2 RESEARCH QUESTIONS AND HYPOTHESES

The research objective shall be broken down into research questions and hypotheses.

Research Question 1: How can the lateral dimensions of a cured layer be modeled in terms of the process parameters?

Hypothesis 1: The lateral dimensions of a layer can be modeled by modeling the layer curing process in two steps:

Step 1: Modeling the process of irradiation of the resin surface

Step 2: Empirically modeling the curing process that occurs in a resin upon receiving irradiation

Explanation: The layer curing process occurs in two steps: Irradiation of the resin surface and Curing of the irradiated surface. In Step 1 mentioned in the hypothesis, irradiance received by the resin surface can be modeled as a function of the process parameters (Irradiance model). A ray tracing procedure shall be used to formulate the Irradiance model. In Step 2 mentioned above, the relation between the Time of Exposure (time for which the bitmap is imaged onto the resin surface) and the depth to which the resin gets cured is established experimentally (Cure model). If the depth of cure at any point on the resin surface is greater than on equal to the layer thickness, the point would become a part of the cured layer. Thus, the Irradiance model and the Cure model can be used in conjunction to formulate the Layer Cure model which models the dimensions of an entire layer in terms of the process parameters. The proposed structure of the Layer cure model is presented in Figure 4.1.

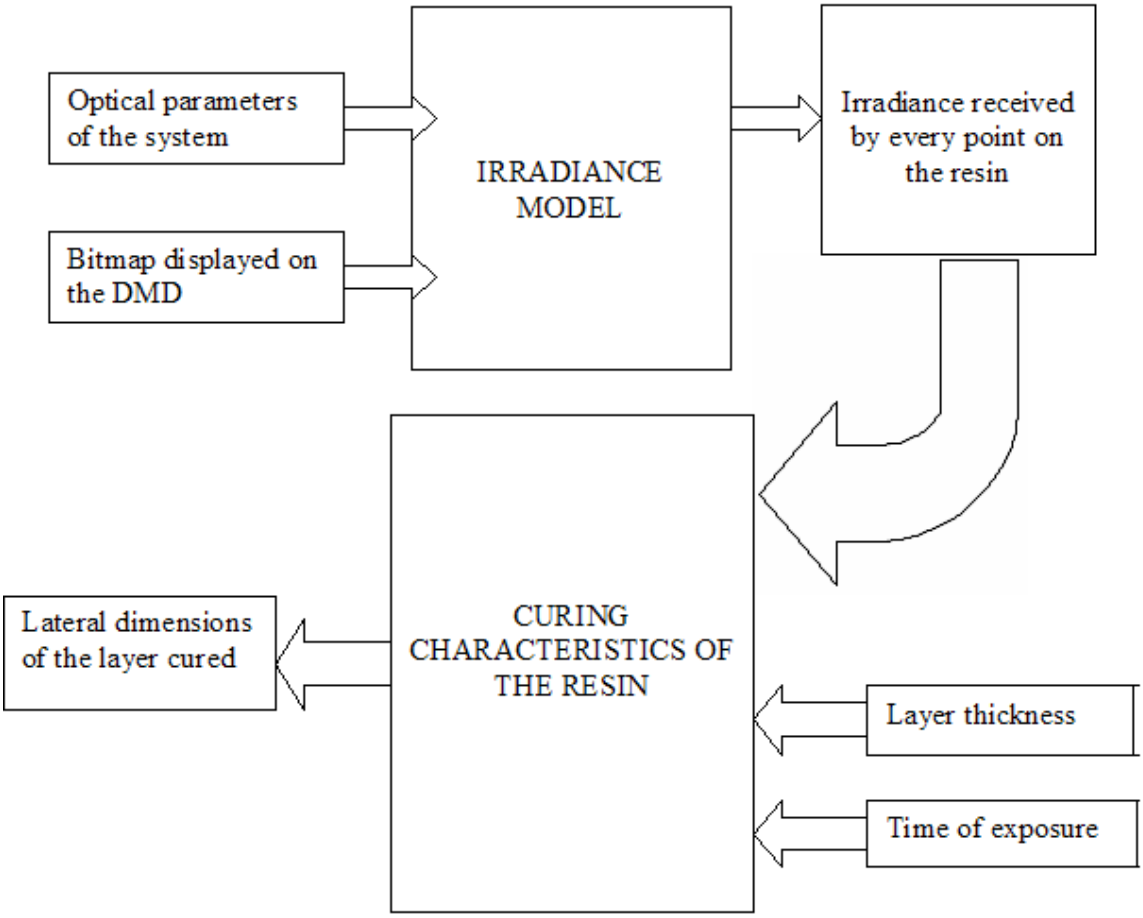

Figure 4. 1 Proposed Structure of Layer cure model

Research Question 2: How can a process planning methodology be formulated for the MPμSLA process in order to cure dimensionally accurate layers?

Hypothesis 2: The dimensions of a cured layer are modeled in terms of the process parameters as mentioned in Hypothesis 1. This model can then be inverted to determine the values of process parameters that will cure a layer of the required dimensions.

Explanation: Using the Layer cure model a correspondence between the "ON" micromirrors on the DMD and the cured pixel on the layer can be established. This would

enable us to determine the micromirrors that need to be turned ON in order to irradiate a required aerial image. This would enable us to generate the bitmap to be supplied to the DMD. Using the Cure model, the time for which the bitmap should be exposed onto the resin surface so that the entire exposed area (aerial image) cures down to a depth of one layer thickness or more can be computed.

Research Question 3: How can the theoretical limit on lateral resolution on the MPμSLA system be determined?

Hypothesis 3: The theoretical limiting resolution of the MPμSLA system can be determined by using the Layer cure model developed as a response to Research Question 1.

4.3 FORMULATING RESEARCH TASKS

In this section, the research tasks required to test the hypotheses presented in Section 4. 2 are identified.

Research Task 1: Classification of process parameters

It is necessary to identify the process parameters and classify the process parameters based on their role in the MPμSLA process before formulating any analytical model. The MPμMSLA process is analyzed in detail to identify the parameters that are fixed by the system's design and those that are variables. This task is performed in Chapter 5.

Research Task 2: Model the layer curing process

The layer curing process is modeled as the Layer cure model. The model consists of two parts:

- Irradiance model: This models the irradiance on the resin surface in terms of process parameters.
- Cure model: This models the curing of resin in response to the irradiance received by the surface.

The Layer cure model is validated by building single layer parts using the MPμSLA system assembled. Hypothesis 2 is tested by completing this task. This work is presented in Chapter 6.

Research Task 3: Formulating the process planning methodology

The inverse of the Layer cure model is formulated as the "Inverse Layer cure model." This model allows us to compute the values of process variables needed to cure a layer of the required dimensions. This model is also validated by curing test layers on the system. Using this model, the theoretical limit on the lateral resolution of the MPμSLA system is computed.

Hypotheses 1 and Hypothesis 3 are tested by completing this task. This work is presented in Chapter 7.

4.4 ORGANIZATION OF THIS THESIS

In **Chapter 5**, the process parameters are identified and classified according to the classification schemes presented in Research Task 1. This Chapter also presents the foundations required to formulate the analytical models in Chapter 6.

In **Chapter 6**, the "Irradiance model" is formulated, which computes the irradiance received by the resin surface given the Irradiance Parameters. Then the "Cure model" is empirically formulated which returns the depth to which a resin will get cured

upon exposure to a given dose of radiation. The Irradiance Model and the Cure model are combined to formulate the "Layer Cure Model" which computes the dimensions of a layer in terms of the values of the process parameters used to cure it. The Layer Cure Model is validated by building test layers on the MPμSLA System.

In **Chapter 7**, the Inverse Layer cure model is formulated and validated.

Chapter 8 is on conclusion of this work and identification of future work.

The organization of the thesis has been presented pictorially in Figure 4.2.

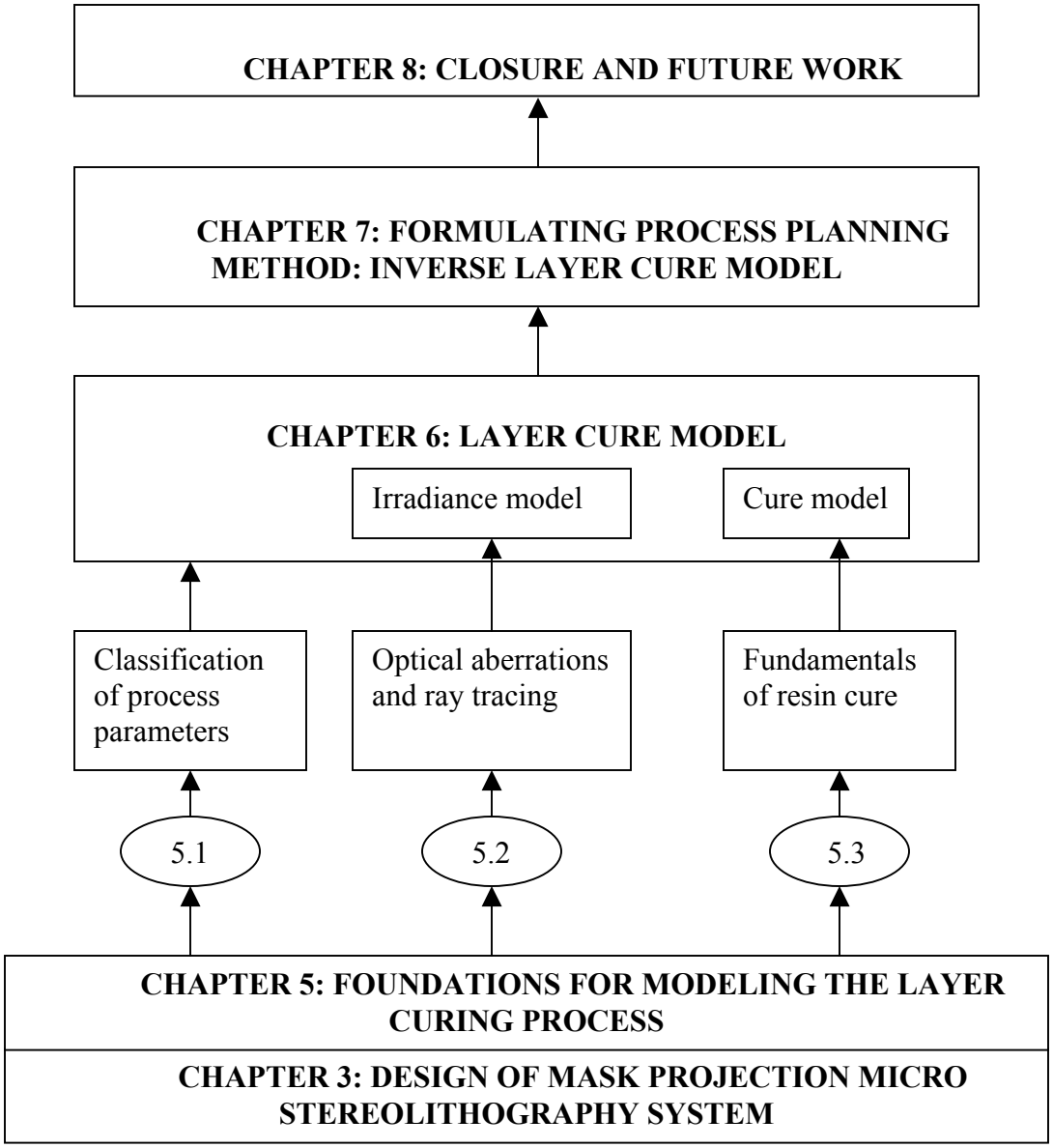

Figure 4. 2 Organization of work in Part 2 of the thesis

CHAPTER 5

FOUNDATIONS FOR MODELING THE LAYER CURING PROCESS

In this chapter, the foundations for formulating the Layer cure model are presented. In Section 5.1, the various process variables and fixed process parameters of the MPμSLA process are identified and classified as fixed process parameters and process variables. The role of every parameter in the process is identified. Finally, the values for the fixed process parameters are stated. In Section 5.2, the fundamentals of image formation are presented. Here, the concept of optical aberrations is introduced and the procedure of ray tracing is explained. In Section 5.3, the fundamentals of resin cure are presented. Here, the chemistry behind the curing reactions in a typical photopolymer resin is presented.

5.1 IDENTIFYING AND CLASSIFYING PROCESS PARAMETERS

In Section 5.1.1, the MPμSLA process shall be analyzed in detail and the process variables shall be identified. Process variables are those process parameters which a user can control while building a part. In Section 5.1.2, the design of the MPμSLA system shall be analyzed to identify the fixed process parameters. Fixed process parameters are system parameters, which a user cannot control. In Section 5.1.3, the values for fixed process parameters and the uncertainties involved in these values are stated. Finally, in Section 5.1.4, the process parameters are classified depending upon the role that they play in the part building process.

5.1.1 Identifying process variables

In this section, the process variables shall be identified by going through the part building process step by step. The following are the steps of the process:

1. Fill the vat with resin to the brim.
2. Slide the platform onto the rods attached to the translation stage. The translation stage has been so adjusted that when it is at its top most position, the platform is just covered by a thin film of resin.
3. Display a bitmap on the DMD. **Process variable: Bitmap displayed on DMD**
4. Image this bitmap on the resin surface for the required time. This time is called the "Time of Exposure". **Process variable: Time of Exposure**
5. Lower the platform by a considerable amount. This step is called as "Deep Dip". The Deep Dip should be enough to ensure that the cured layer is completely covered by resin. It has been found through experimentation on this MPμSLA system that a Deep Dip of 2mm is sufficient to ensure that any cured layer gets completely covered by resin.
6. Raise the platform so that the distance between the cured layer and the free surface of the resin is equal to one layer thickness. **Process variable: Layer Thickness**
7. When a part is raised after the deep dip, excessive resin is observed on top of the cured layer. So, the resin needs to be allowed to stand for some time and level out its free surface. The time allowed for the resin surface to level itself is called the "Leveling Wait" (LW). **Process variable: Leveling Wait**
8. Display the next bitmap on the DMD and irradiate the next layer on the resin. Continue the process till the entire part is built.

5.1.2 Identifying the fixed process parameters

In this section, the MPμSLA system shall be analyzed module by module to identify the fixed process parameters.

Following are the four modules of the MPμSLA system:

Beam conditioning system

This includes a broadband light source, a diaphragm with 0.8 mm diameter clear aperture placed immediately after the light guide outlet, a plano-convex lens placed one focal length away from the diaphragm and a filter placed about 1 inch away from the lens.

Fixed process parameters:

- Power of the light source
- Distance between the diaphragm and the collecting lens
- Distance between the collecting lens and the filter
- Focal length of the collecting lens

DMD

Parameters related to the DMD as well as its mounting are fixed

Fixed process parameters:

- Size of micro mirrors on the DMD and the gap between adjacent micro mirrors
- Angle that the DMD makes with the horizontal

Imaging system

The imaging system includes the imaging lens, which images the bitmap onto the resin surface.

Fixed process parameters:

- Distance between DMD and the imaging lens
- Distance between the imaging lens and the resin surface
- Imaging lens parameters, namely radii of curvature, lens thickness and refractive index

Resin parameters

DSM SOMOS 10120 Water Clear resin shall be used with this system. All the parameters related to this resin can be treated as fixed process parameters:

Fixed process parameters:

- Critical Exposure (E_c): This is the minimum amount of irradiation that a resin must receive in order to polymerize.
- Depth of Penetration (D_p): This is the depth in a resin at which the incident radiation falls to 1/e times its value on the surface of the resin.
- Viscosity (V): This is viscosity of the resin.

5.1.3 Values of fixed process parameters

Fixed Process Parameters have unchanging values. The exact values of some of these parameters are specified by the manufacturers. The values of the remaining parameters have been measured manually to a limited degree of precision. So, there is an

uncertainty surrounding these values. In this section, the values of all the fixed process parameters are presented and the uncertainties in these values are estimated.

The distances in the optical setup can be measured up to a precision of +/- 2 mm. The exact values of lens parameters are known from manufacturer's catalog. The values of resin parameters are also specified by the resin manufacturer. The fixed process parameter values are summarized in Table 5.1.

Table 5. 1 Values of fixed process parameters

Fixed process parameter	**Value**
Beam conditioning optical system parameters	
Power of light source	3 W/cm^2 at 365nm
Distance between diaphragm and collecting lens	19 mm (+/- 2 mm)
Distance between collecting lens and filter	25 mm (+/- 2 mm)
Focal length of collecting lens	19 mm
Imaging optical system parameters	
Distance between DMD and first surface of imaging lens	100 mm (+/- 2 mm)
Thickness of imaging lens	10.9 mm
Distance between second surface of imaging lens and resin surface	29 mm (+/- 2 mm)
Radii of curvatures of imaging lens	+21.49 mm and -21.49 mm
Refractive index of lens material	1.45848
Mask parameters	
Angle made by DMD with the horizontal	Computed in Chapter 6
Size of every micro mirror on DMD	12.7 µm
Gap between adjacent micro mirrors	1 µm
Resin Parameters	
Critical Exposure of resin (E_c)	9.7 mJ/cm^2
Depth of penetration of resin (D_p)	0.16 mm
Viscosity	130 cps

The DMD consists of micromirrors mounted on a chip. In their neutral state, the mirrors are parallel to the plane of the chip. When a bitmap is supplied to the DMD, every micromirror rotates about its diagonal by an angle of +10^o or -10^o depending upon

whether the micromirror corresponds to a white pixel on the bitmap or a black pixel. This flaw in the design of the DMD forces us to align the DMD chip at an angle that compensates for the angle made by the micromirrors with the chip in their "ON" position.

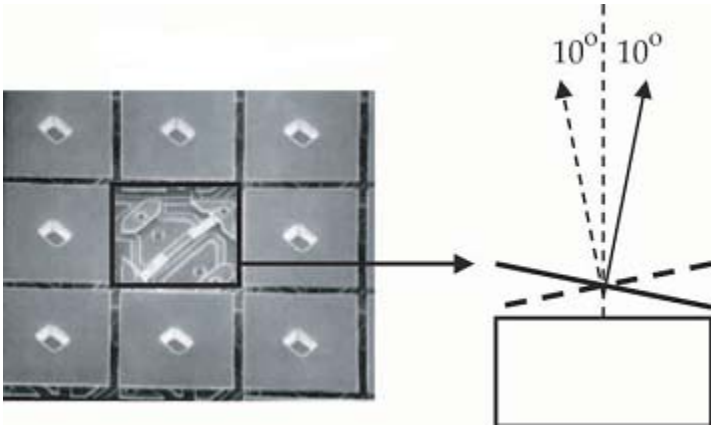

Figure 5. 1 Angle made by a micromirror with the DMD chip (Nayar et al., 2004)

While aligning the experimental setup, the DMD chip was so arranged that it directed the horizontal light beam vertically downwards. At this position, the micromirrors are definitely at 45° to the horizontal. The angles made by the DMD chip with the horizontal are required in order to execute the Layer cure model. This angle is analytically computed in Chapter 6.

5.1.4 Classification of process parameters

In Table 5.2, the process parameters are classified according to the role that they play in the part building process.

Table 5. 2 Classification of process parameters

Sub-process	Process parameters		Model to be formulated to characterize the sub-process
	Process variables	**Fixed process parameters**	
Formation of aerial image on the resin surface	Bitmap displayed on the DMD	Power of the light source	**Irradiance Model**
		Distance between diaphragm and collecting lens	
		Distance between collecting lens and filter	
		Collecting lens parameters	
		Distance between DMD and imaging lens	
		Distance between imaging lens and resin surface	
		Angle made by the DMD with the horizontal	
		Size of mirrors on the DMD	
		Gap between mirrors on the DMD	
Curing of the irradiated area of resin	Irradiation received by resin surface	Critical Exposure of resin (E_c)	**Cure Model**
	Time of exposure	Depth of penetration of resin (D_p)	
	Layer thickness		

5.2 FUNDAMENTALS OF IMAGE FORMATION

During the irradiation step, a bitmap displayed on the DMD is imaged onto the resin surface. Modeling the irradiance on the resin surface is, essentially, modeling the process of image formation by the imaging lens. In this section, the fundamentals of image formation, from the standpoint of geometrical optics, as opposed to wave optics, shall be presented.

In Section 5.2.1, the concept of optical aberrations is introduced and thereby the need for formulating a rigorous Irradiance model is accentuated. In Section 5.2.2, the procedure of tracing rays through a spherical lens is described.

5.2.1 Need for formulating a rigorous Irradiance model: Introduction to optical aberrations

When a perfect lens focuses any object onto an image plane, all rays emanating from any one point on the object meet at one and the same point on the image. Under this condition, the image formed is termed as the perfect image. For a thin lens, this condition occurs when the image distance (i) and the object distance (o) are related to the focal length (f) of the lens by the thin lens equation:

$$1/i - 1/o = 1/f$$[4]

The magnification of the image is given by $M = -(i/o)$.

For a spherical lens with finite thickness, even if the image and object distances are set as calculated using the thin-lens equation, all rays from any one point on the object do not converge to the same point on the image. Also, the focal length of a spherical lens is not the same for all object points. This results in optical aberrations. Optical aberrations can be thought of as imperfections caused in an image. They lead to the formation of a distorted image, with lower contrast. Aberrations are classified as follows:

- Spherical aberration
- Astigmatism
- Coma

[4] In this equation, only the magnitudes of i and o are considered

- Distortion
- Chromatic aberration

Spherical aberration

Spherical aberration can be defined as variation of focus with aperture. Figure 5.2 is an exaggerated sketch of a spherical lens forming an image of an axial object point situated a great distance away. It can be seen that the rays away from the optical axis come to focus (intersect the axis) earlier than the rays closer to it. In Figure 5.2, point A is the paraxial focus. The distance from the paraxial focus to the axial intersection of the marginal rays (i.e. rays from the edges of the lens) is called longitudinal spherical aberration. In Figure 5.2, LA_R is the longitudinal spherical aberration. Transverse, or lateral spherical aberration is the name give to the aberration when it is measured in a direction perpendicular to the optical axis. In Figure 5.2, TA_R is the transverse spherical aberration.

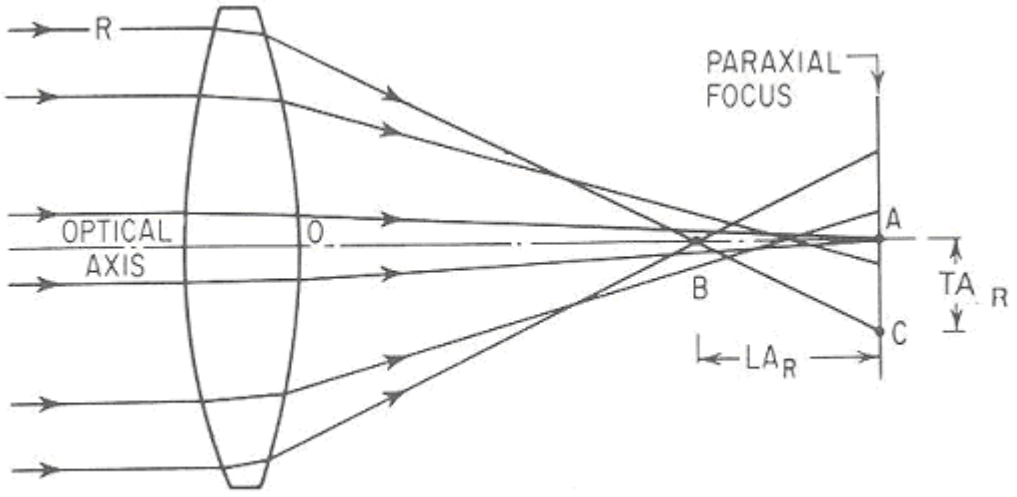

Figure 5. 2 Spherical aberration (Smith, 1996)

Coma

Coma can be defined as variation in magnification with aperture. When a bundle of oblique rays is incident on a lens with coma, the rays passing through the edge portions of the lens are imaged at a different height than those passing through the center portion. In Figure 5.3, the upper and lower rim rays A and B intersect the image plane above the ray P which passes through the center of the lens. The distance from P to the intersection of A and B is called tangential coma of the lens.

$Coma_T = H_{AB} - H_p$

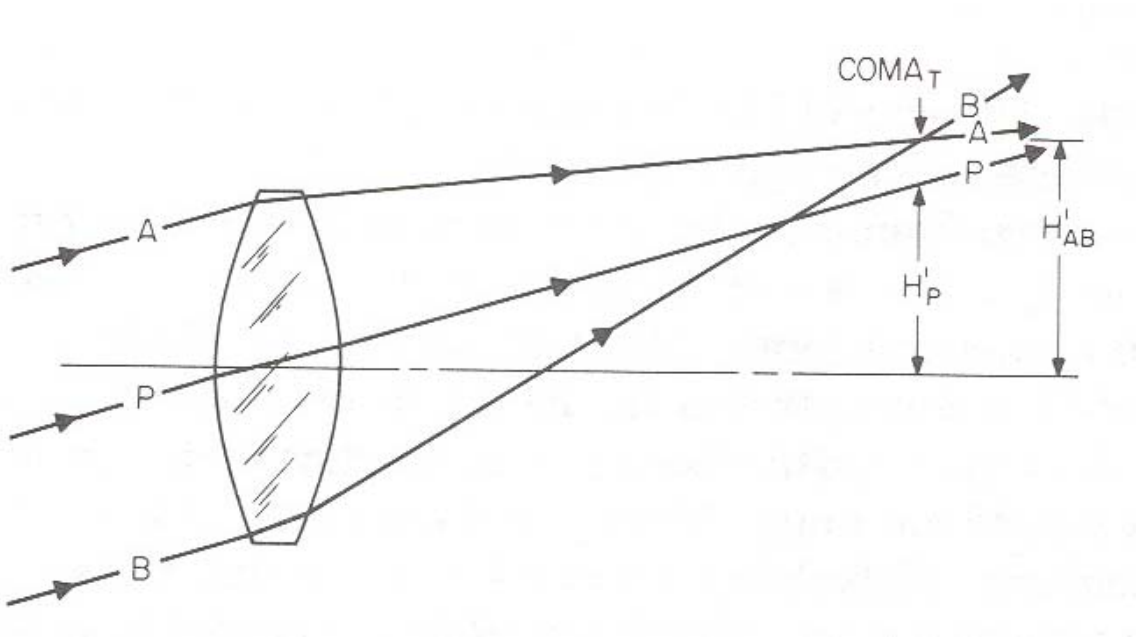

Figure 5. 3 Coma (Smith, 1996)

The appearance of a point image formed by a comatic lens is indicated in Figure 5.4.

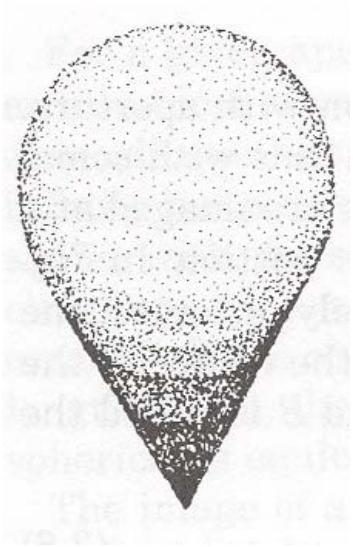

Figure 5. 4 The coma patch. The image of a point source is spread out into a comet-shaped flare

Astigmatism

Any plane through the optical axis is called as the meridional, or the tangential plane. The imaginary plane passing through the chief ray (an oblique ray passing through a point on the object and the center of the lens) and perpendicular to the meridional plane is called the sagittal plane. All the rays from the object, which lie in this plane, are called sagittal rays. See Figure 5.5.

Astigmatism occurs when the tangential and the sagittal images don't coincide. In the presence of astigmatism, the image of a point source is not a point, but takes the form of two separate lines as shown in Figure 5.5.

Unless there is some manufacturing defect in a lens, there is no astigmatism when an axial point is imaged. However, as the imaged point moves further from the axis, the amount of astigmatism gradually increases.

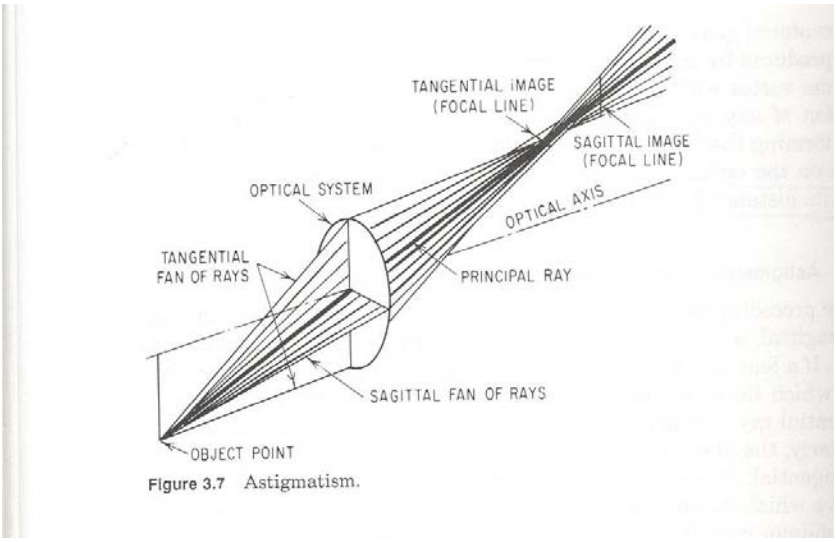

Figure 5. 5 Astigmatism (Smith, 1996)

Distortion

When the image of an off axis point is formed farther from the axis or closer to the axis than the image height given by the paraxial expressions (i.e. expressions derived by assuming that rays pass through an infinitesimal threadlike region on the lens around the optical axis), the image of the extended object is said to be distorted. The amount of distortion increases as the cube of the image height. Thus, if a centered rectilinear object is imaged by a system afflicted with distortion, it can be seen that the images of corners will be displaced more than the images of the points making up the sides. In Figure 5.6, the appearance of a square figure imaged by a lens system with distortion is shown. In Figure 5.6a, the distortion is such that the images are displaced outwards from the correct position. This is called positive or pincushion distortion. In Figure 5.6b, the distortion is

of opposite type and the corners of the square are pulled inward more than the sides. This is called the negative of the barrel distortion.

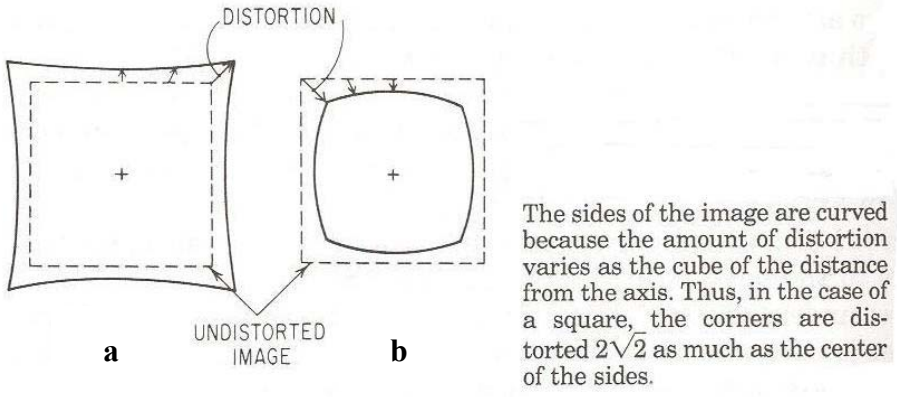

Figure 5. 6 a) Pincushion or positive distortion b) Barrel or negative distortion (Smith, 1996)

Chromatic Aberration

Chromatic aberrations are caused because the refractive index of any material is different for different wavelengths of lights. Since the MPμSLA system filters a single wavelength in the Beam conditioning system, this aberration is not a concern.

It is clear from the preceding discussion that the size and shape of an image formed by a lens is not intuitive. Due to optical aberrations, the thin lens equation will calculate erroneous dimensions of the aerial image formed on the resin surface. The exact image size can be calculated by adopting the procedure of tracing rays through a lens as explained in the next sub-section.

5.2.2 Exact ray tracing

From Section 5.2.1, it is clear that the size of the expected image cannot be determined from the simple lens equation. The exact size of the image can be obtained through "exact ray tracing procedures." In an exact ray trace, the object is considered as a collection of point sources. Rays in all possible directions are traced from each of these point sources. The rays undergo refraction at every surface separating two media. The refraction is governed by Snell's law:

sine i / n_1 = sine i'/n_2,

where i and i' are the angles of incidence and refraction, and n_1 and n_2 are the refractive indices of the media on either side of the surface on which the rays are incident. By tracing rays, their points of intersection with the image plane are calculated. The farthest points of intersections give the size and shape of the image.

Exact ray tracing is an involved procedure, especially because the angle of incidence (i) for every ray is in a different plane. In this section, the ray tracing procedure presented in (Smith, 1996) is described. This ray tracing procedure was first published by D. Feder in the Journal of the Optical Society of America vol. 41, pp. 630-636, 1951.

Exact Ray Tracing Procedure for spherical surfaces

A skew ray is a perfectly general ray. The ray is defined by the coordinates x, y and z of its intersection with a surface and by its direction cosines X, Y and Z. The origin of the coordinate system is at the vertex of each surface. Figure 5.7 shows the meanings of these terms.

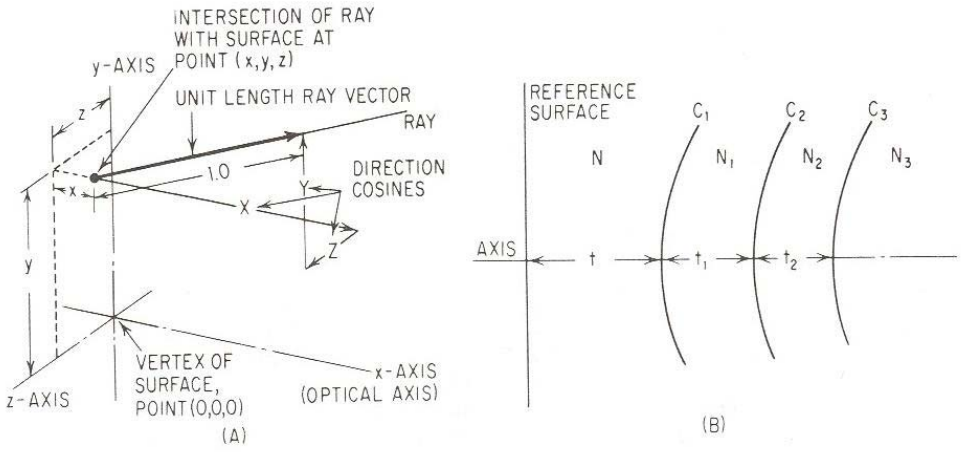

Figure 5. 7 Symbol used in Transfer and Refraction equations. a) The physical meanings of the spatial coordinates (x,y,z) of the ray intersection with the surface and of the ray direction cosines, X, Y, and Z. b) Illustrating the system of sub-script notation

The computation is opened by determining the values for x, y, z, X, Y and Z with respect to an arbitrarily chosen reference surface which is usually chosen to be the object plane. Then, the following "Transfer equations" give the coordinates (x_1, y_1, z_1) of the point of intersection of the ray with the next surface:

$$e = tX\ (xX + yY + zZ)$$

$$M_{1x} = x + ex - t$$

$$M_1^2 = x^2 + y^2 + z^2 - e^2 + t^2 - 2tx$$

$$E_1 = \sqrt{X^2 - c_1(c_1 M_1^2 - 2M_{1x})}$$

$$L = e + (c_1 M_1^2 - 2M_{1x}) / (X + E_1)$$

$$x_1 = x + LX - t$$

$$y_1 = y + LY$$

$$z_1 = z + LZ$$

The direction cosines of a ray after it undergoes refraction at a surface are given by the following "Refraction equations":

$$E_1' = \sqrt{1-(N_1/N_2)^2(1-E_1^2)}$$

$$g_1 = E_1' - (N/N_1)E_1$$

$$X_1 = (N/N_1)X - g_1c_1x_1 + g_1$$

$$Y_1 = (N/N_1)Y - g_1c_1y_1$$

$$Z_1 = (N/N_1)Z - g_1c_1z_1$$

In the above Transfer and Refraction equations, the symbols have the following meanings:

t	Distance between to surfaces
x, y, z	The spatial coordinates of the ray intersection with the reference surface
x_1, y_1, z_1	The spatial coordinates of the ray intersection with surface #1
M_1	The distance (vector) from the vertex of surface # 1 to the ray, perpendicular to the ray
M_{1x}	The x component of M_1
E_1	The cosine of the angle of incidence at surface #1
L	The distance along the ray from the reference surface (x, y, z) to surface #1 (x_1, y_1, z_1)
E_1'	The cosine of the angle of refraction (I') at surface #1

X, Y, Z	The direction cosines of the ray in space between the reference surface and surface #1 (before refraction)
X_1, Y_1, Z_1	The direction cosines after refraction by surface #1
c	The curvature (reciprocal radius = 1/R) of the reference surface
c_1	The curvature of surface #1
N	The refractive index between the reference surface and surface #1
N'	The refractive index following surface #1
T	The axial spacing between the reference surface and surface #1

5.3 FUNDAMENTALS OF RESIN CURING

In this section, the chemistry behind the photo polymerization reactions that occur when a Stereolithography resin cures is presented. Then the expected curing characteristics of a resin are presented along with a chemical explanation to it.

5.3.1 Chemistry behind resin cure

Polymerization is the process of linking small molecules (monomers) into larger molecules (polymers) comprised of many monomer units. Most Stereolithography resins contain the vinyl monomers and acrylate monomers. Vinyl monomers are broadly defined as monomers containing a carbon-carbon double bond. Acrylate monomers are a subset of the vinyl family with the carboxylic acid group (-COOH) attached to the carbon-carbon double bond. For an acrylate resin system, the usual catalyst is a free radical. In Stereolithography, the radical is generated photo chemically. The source of the

photo chemically generated radical is a photo initiator, which reacts with an actinic photon as shown in the photo-polymerization scheme presented in Figure 5.8. This produces radicals (indicated by a large dot) that catalyze the polymerization process.

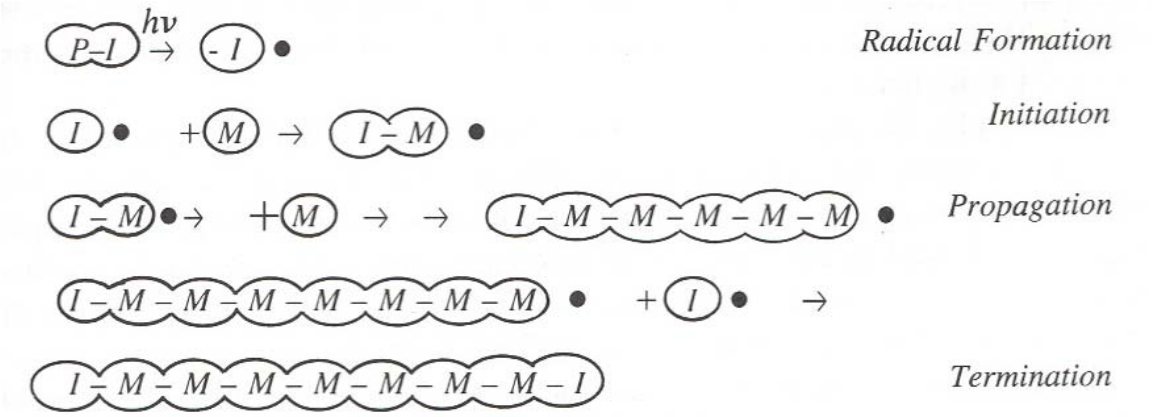

Figure 5. 8 Scheme of the photo-polymerization process (Jacobs, 1996)

5.3.2 Beer Lambert's law of light absorption

As the photons penetrate the resin, they are progressively absorbed by initiators. According to Beer Lambert's law of absorption, the exposure (mJ/cm^2) decreases exponentially with depth.

$$E(z) = E_{max} \exp(-z/D_p) \quad (1)$$

where D_p is the resin "penetration depth" (a resin parameter) at the given wavelength and E_{max} is the exposure at the surface of the resin ($z = 0$).

In practice, polymerization doesn't proceed beyond a limited depth where the exposure falls below a threshold value. This is primarily due to oxygen inhibition (Drobny 2002), which imposes a minimal threshold to start polymerization. The exposure

level where the gel point is reached is still higher. The exposure threshold for the formation of gel is known as the "Critical Exposure" (E_c).

Suppose that a point on the resin surface receives an exposure E_{max}. If the point gets cured to a depth C_d then the exposure received at the depth C_d will be equal to E_c.

Putting $z = C_d$ and $E(z) = E_c$ in Beer Lambert's law:

$E_c = E_{max} \exp(-C_d/D_p)$

Rearranging the terms,

$C_d = D_p \ln(E_{max}/E_c)$

Thus, the plot of C_d versus $\ln(E_{max})$ is straight line with slope equal to D_p and the X intercept = $\ln(E_c)$. This plot is called as the Working curve of the Stereolithography resin. See Figure 5.9.

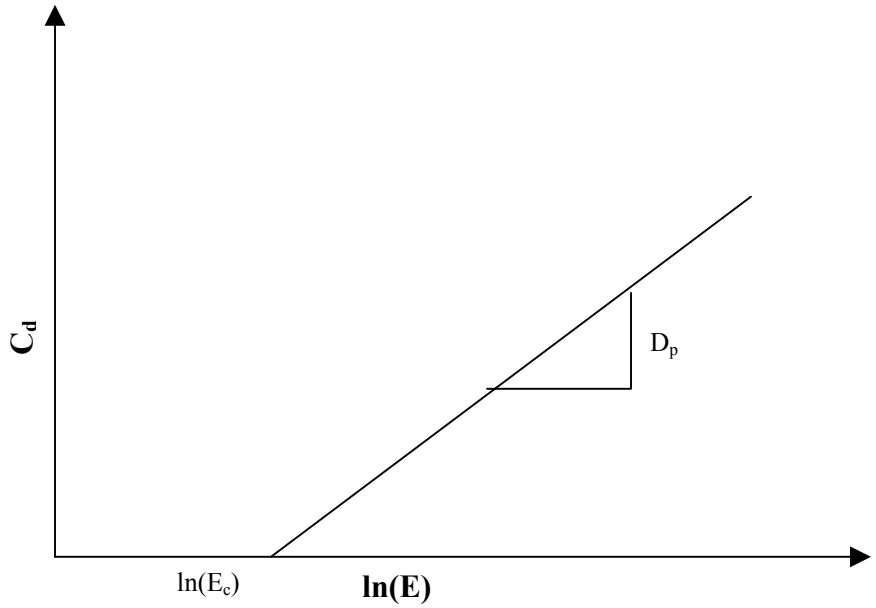

Figure 5. 9 Theoretical Working curve of a Stereolithography resin

The values of E_c and D_p are fixed for any resin and so, the working curve of any resin is, theoretically, invariant.

Summary

In this chapter, the process of curing of a micropart using the MPμSLA system is analyzed. The different process variables and fixed process parameters are identified. The foundational knowledge required to formulate the Layer cure model is presented. In the next chapter, the Layer cure model is formulated and validated.

CHAPTER 6

FORMULATING AND VALIDATING THE LAYER CURE MODEL

In this chapter, the process of curing a single layer in resin is modeled as the "Layer cure model". This model analytically relates the dimensions of a layer with the process parameters used to cure it.

The process of curing a layer in resin occurs in two steps:

1. Irradiation of the resin surface
2. Curing of the resin in response to the irradiation received

In order to reduce the process planning errors occurring during the curing of a layer, both the steps mentioned above must be modeled. The process of irradiation of the resin is modeled in the form of Irradiance model, which computes the irradiance received by every point on the resin surface in terms of the optical parameters of the system. The second step is empirically modeled as the Cure model. The resin is characterized to determine the relationship between the time of exposure and the depth of cure. The Irradiation model and the Cure model can be used in conjunction to obtain the lateral dimensions of the layer that will be cured when a particular bitmap (pattern) is imaged onto the resin surface for a particular duration of time. The structure of the Layer cure model is presented in Figure 6.1.

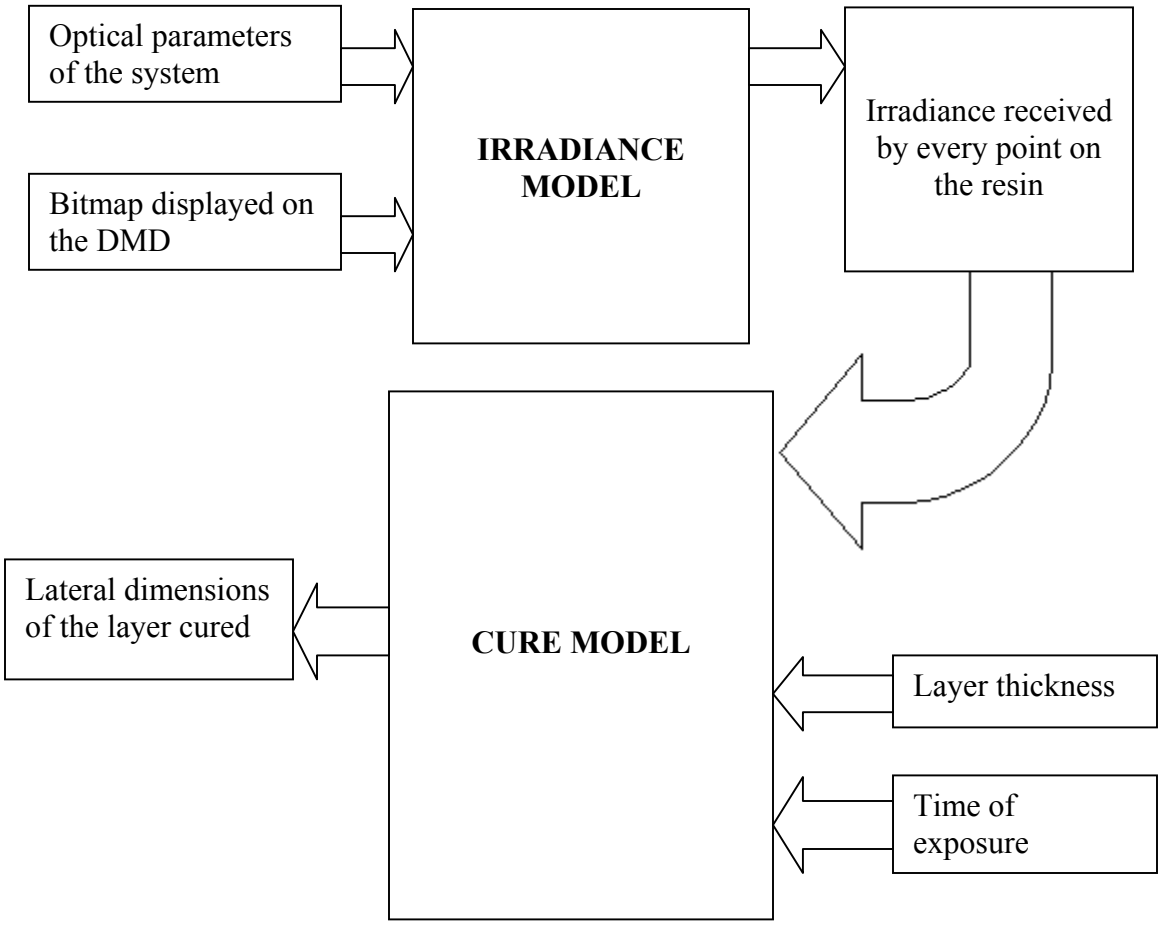

Figure 6. 1 Structure of the Layer cure model

In Section 6.1, the Irradiance model is formulated. In Section 6.2, the Cure model is formulated. In Section 6.3, the Layer cure model, which is a combination of the Irradiance model and the Cure model, is validated and the accuracy and precision of the process are discussed. In Section 6.4, pictures of some microparts cured using the MPμSLA system are shown.

6.1 IRRADIANCE MODEL

In this section, the Irradiance model is formulated. This model computes the irradiance received at every point on the resin surface in terms of the optical parameters of the system and the bitmap displayed on the DMD. See Figure 6.2.

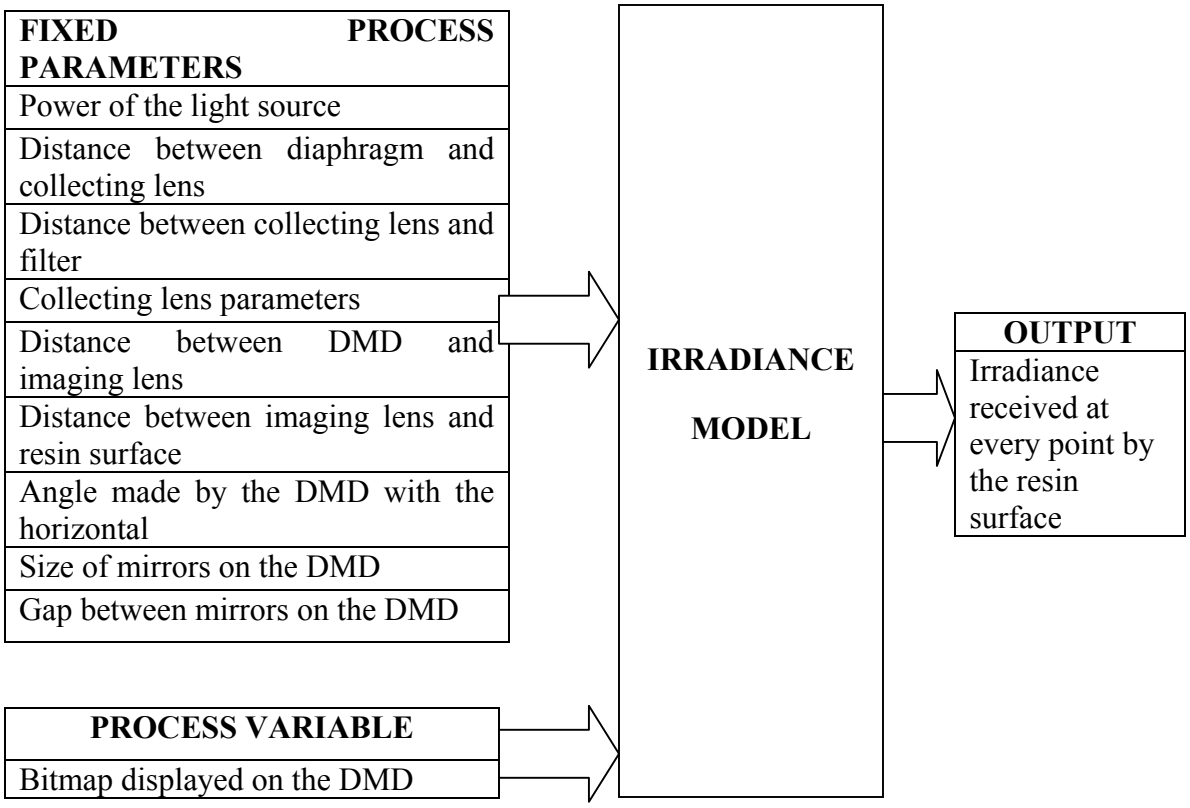

Figure 6. 2 Irradiance model

The irradiance received at every point of the resin surface is a function of the Beam conditioning system parameters and the Imaging system parameters. The Beam conditioning system parameters influence the characteristics of the beam that is incident on the DMD. The Imaging system parameters influence the image formation process. In Section 6.1.1, the characteristics of the beam emerging out of the Beam conditioning

module of the MPμSLA system and incident on the DMD are measured. In section 6.1.2, the image formation process is modeled. The characteristics of the beam measured in Section 6.1.1 are one of the inputs to this Image formation model. In Section 6.1.3, the method of solving the Irradiance model numerically is presented. The structure of the Irradiance model after separating the effects of the Beam conditioning system parameters and the Imaging system parameters is shown in Figure 6.3.

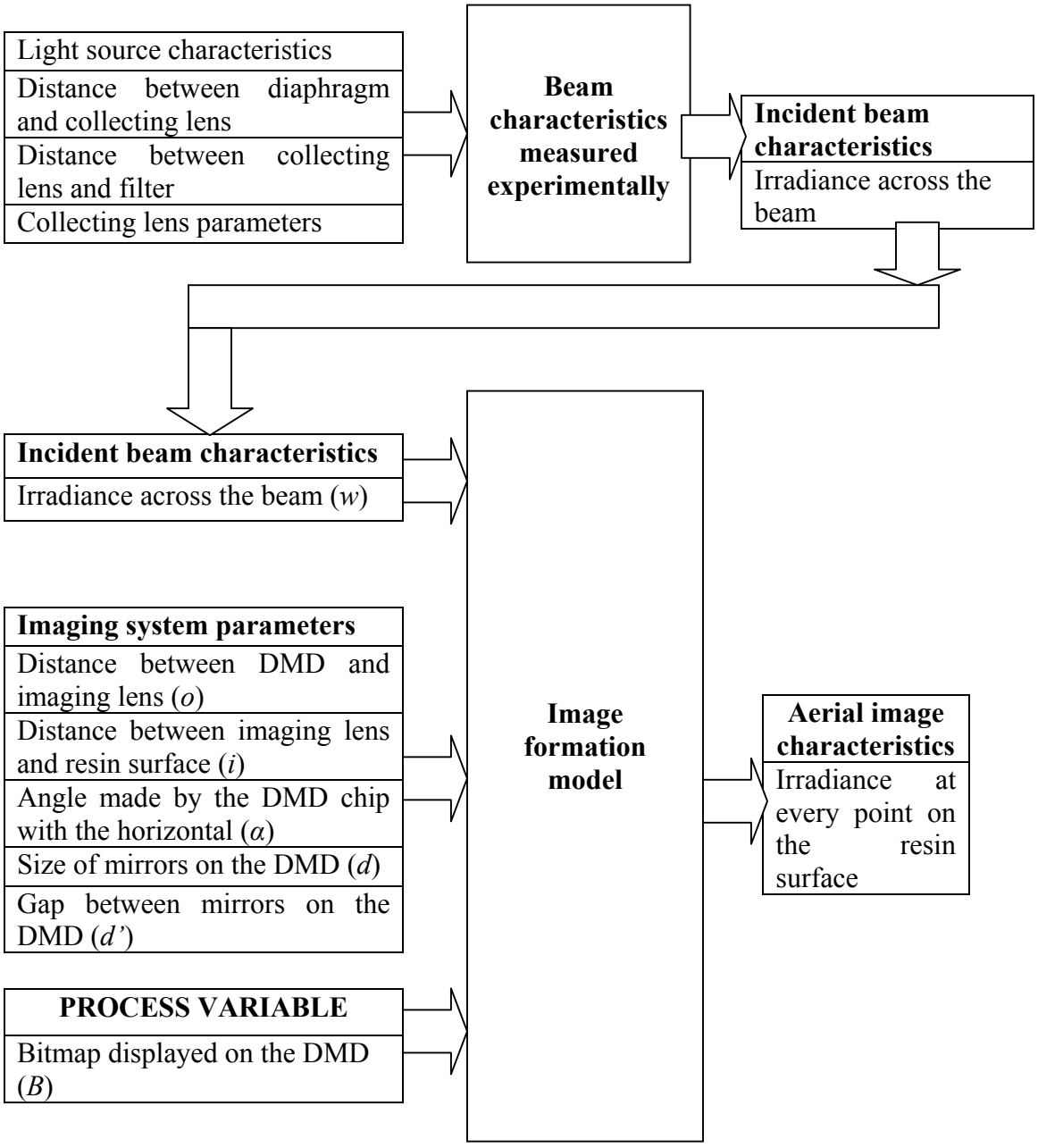

Figure 6. 3 Factored Irradiance model

6.1.1 Characteristic of beam incident on the DMD

The beam characteristic of interest from the point of view of modeling the aerial image on the resin surface is the irradiance distribution across the beam. This is experimentally measured in this section. During research, this experiment was performed before mounting the DMD and adjusting the imaging optical setup.

A radiometer was attached to the translation stage. The translation stage was mounted in a tall bracket in the path of the beam coming out of the beam conditioning system. Using the translation stage, the radiometer sensor was moved across the diameter of the beam. Thus, the irradiance distribution across the beam was determined. The readings of the radiometer are recorded in Table 6.1.

Table 6. 1 Irradiance distribution across the irradiating beam

Distance from beam center (mm)	Reading of the radiometer (μm)	Normalized irradiance distribution
0.0	771	1
0.5	771	1
1.0	769	0.997
1.5	761	0.987
2.0	750	0.973
2.5	735	0.953
3.0	716	0.929
3.5	688	0.892
4.0	658	0.853
4.5	626	0.812
5.0	595	0.772
5.5	564	0.732
6.0	532	0.690

Fitting a curve through the data presented in Table 6.1, the irradiance distribution across the beam incident on the DMD is given by the equation

$$I_{irr} = 1 - 0.00086\,p - 0.00883p^2 \qquad (6.1)$$

where I_{irr} is the normalized irradiance and p is the radial distance from the center of the beam incident on the DMD.

6.1.2 Modeling the image formation process

The process of image formation is analytically modeled in this section. When a bitmap displayed on the DMD is imaged onto the resin surface, all rays emanating from all points on the bitmap are directed onto the resin surface by the imaging lens. Every ray irradiates the infinitesimal area centered at the point where it intersects the resin surface. The pattern can be assumed to be composed of n number of points: $p_1, p_{2,\ldots}p_n$, where n→ ∞. Since a UV lamp is used as the light source, the beam incident on the DMD is not perfectly collimated. So, every bitmap point receives rays coming from different directions. These rays reflect from every point on the pattern in the form of a cone. There is an uncertainty as regards the angle of this cone and the distribution of energy within it. Nevertheless, since the beam incident on the DMD is fairly collimated, most of the rays are expected to be directed vertically downwards, parallel to the imaging system's optical axis. In general, the directions in which rays are emitted from every point on the pattern can be represented by direction vectors $v_1, v_2, \ldots v_m$, where m→ ∞. The resin surface can be assumed to be composed of x number of points $pr_1, pr_{2,\ldots,} pr_x$, where x→ ∞. Refer to Figure 6.4.

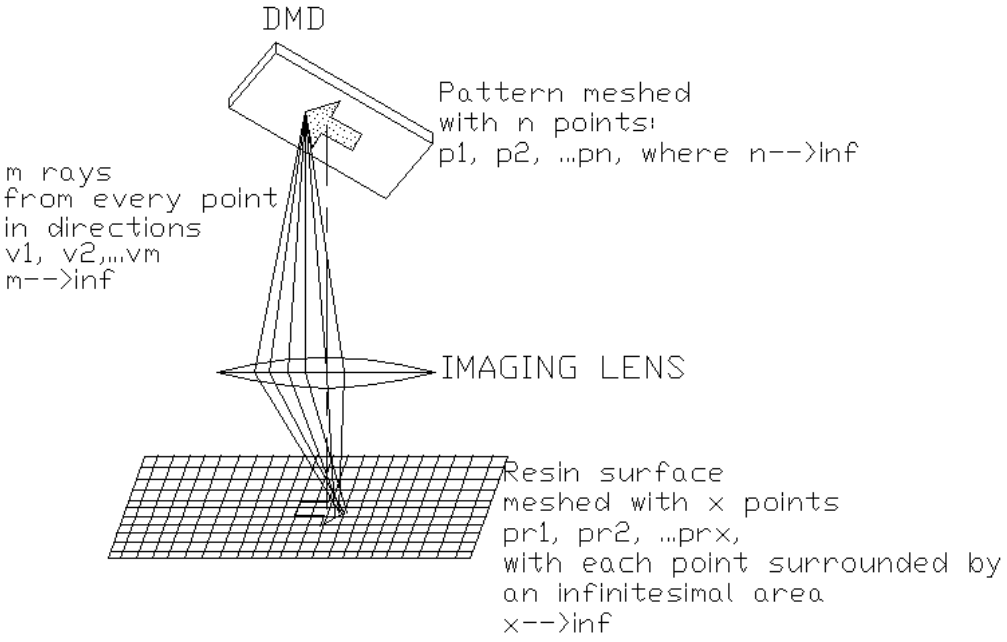

Figure 6. 4 Nomenclature used in theoretical derivations

We introduce a function δ, which evaluates whether a particular ray will strike an infinitesimal area centered on a given point on the resin surface or not. For example, $\delta(p_j, v_k, pr_i, o, i, \alpha, d, d', \phi)$ will determine whether the ray originating from the point p_j on the bitmap in the direction of vector v_k will strike an infinitesimal area centered on point pr_i on the resin. The rays are expected to be emitted from every point on the bitmap in the form of a cone. ϕ is the half plane angle of this cone of rays. Note that o, i, α, d, d' are the fixed optical system parameters as shown in Figure 6.3.

If the ray does strike the infinitesimal area surrounding point pr_i,

then, $\delta(p_j, v_k, pr_i, o, i, \alpha, d, d', \phi) = 1$;

else, $\delta(pri, p_j, v_k, o, I, \alpha, d, d', \phi) = 0$

The function δ is evaluated by adopting the exact ray tracing procedure as explained in (Smith, 1996). In an exact ray trace the path of every ray is traced through the lens, and the coordinates of the point where it intersects the image plane are analytically computed. The imaging system parameters are used in the evaluation of the function δ. The procedure of ray tracing has been explained in Section 5.2.2.

The irradiance received by any point on the resin surface will be proportional to the number of rays striking an infinitesimal area centered on that point. The number of rays striking a point pr_i on the resin surface will be given by the function:

$$N(pr_i) = \sum_{j=1}^{n}\sum_{k=1}^{m}\delta(p_j, v_{k,} pr_{i,} o, i, \alpha, d, d', \phi) \tag{6.2}$$

Since the irradiance at a point on the resin surface is proportional to the number of rays striking that point, the irradiance can be given by:

$$H(pr_i) = c\sum_{j=1}^{n}\sum_{k=1}^{m}\delta(p_j, v_{k,} pr_{i,} o, i, \alpha, d, d', \phi) \tag{6.3}$$

where c is a constant.

The constant c is calculated as follows:

Using a radiometer, the average irradiance across an aerial image can be measured. Let the average irradiance be H_{av}. The average number of rays striking a point on the resin surface will be given by (total number of rays/total number of points on the resin surface) = nm/x. So, nm/x rays correspond to an irradiance of H_{av}. The constant c is thus determined to be $H_{av}/(nm/x)$. Substituting for c in the equation (6.3),

$$H(pr_i) = (H_{av}x / nm)\sum_{j=1}^{n}\sum_{k=1}^{m}\delta(p_j, v_{k,} pr_{i,} o, i, \alpha, d, d', \phi) \tag{6.4}$$

Equation (6.4) will give accurate results when $n \rightarrow \infty$ *and* $m \rightarrow \infty$.

An assumption made while formulating equation (6.4) is that all rays carry the same amount of energy. This is not true because the irradiance across the beam incident on the pattern is not constant as explained in Section 6.1.1.The irradiance distribution is measured to be as given by equation (6.1). So, the energy emitted by different points on the pattern is different. This effect can be accounted for by assigning weights to the rays emitted from different points on the bitmap. If the weight assigned to the rays emitted from the j^{th} point on the pattern (point p_j) is w_j, equation (6.4) can be modified as:

$$H(pr_i) = (H_{av}x / \sum_{j=1}^{n} w_j m) \sum_{j=1}^{n} \sum_{k=1}^{m} \delta(p_j, v_k, pr_i, o, i, \alpha, d, d', \phi) \tag{6.5}$$

The weights assigned to different pattern points are a function of the distance of that point from the center of the beam measured in the plane perpendicular to the direction of beam propagation. If w_j is the weight assigned to a pattern point, which is at a distance p from the center of the incident beam, then, w_j is given by:

$w_j = f(p)$

where $f(p)$ is the irradiance distribution across the beam. The irradiance distribution across the beam and hence, the weight function are as given by equation (6.1).

To summarize, the Irradiance model can compute the irradiance received at every point on the resin surface by the following set of equations:

$$H(pr_i) = (H_{av}x / \sum_{j=1}^{n} w_j m) \sum_{j=1}^{n} \sum_{k=1}^{m} \delta(p_j, v_k, pr_i, o, i, \alpha, d, d', \phi)$$

where $w_j = 1 - 0.00086p - 0.00883p^2$

and where the function δ is evaluated by ray tracing

6.1.3 Numerical solution to the Irradiance model

To solve the Layer cure model, it is not possible to assign *n, m* and *x* values equal to ∞. In other words, we can mesh the bitmap with only a finite number of points, trace rays only in a finite number of directions from every mesh point on the pattern and can evaluate the irradiance at only a finite number of points on the resin surface. So, while solving the model, we take larger and larger values of n, m for a chosen value of x till the irradiance distribution on the resin surface converges to its final value. This is exemplified in Section 6.3, when the Layer cure model is validated.

Also, there is an uncertainty regarding the angle of the cone formed by the rays leaving every point on the bitmap. This angle depends upon the collimation of the beam and is hence a fixed parameter of the MPμSLA system. Since the beam incident on the DMD is fairly collimated, this angle is expected to tend to 0°. When the Layer cure model is validated in Section 6.3, the model is run for various values of half plane angles of the cone, from 0° to 4°. It is shown in Section 6.3 that the best agreement with the experimental results is obtained when this angle is chosen to be 0°.

In order to trace rays from any bitmap point, it is essential to know the location of the point relative to the optical axis and also the distance of that particular point from the imaging lens. In order to obtain these quantities, it is first necessary to compute the orientation of the DMD (the angles made by the DMD with all the three axes). This is computed in Section 6.3, while validating the Layer cure model.

6.2 CURE MODEL

From the foundations presented in Section 5.3, the expected relation between the depth of cure (C_d) and the exposure on the resin surface (E) is given by:

$$C_d = D_p \ln(E/E_c)$$

where D_p and E_c are constant resin parameters. D_p is the depth in the resin to which the irradiance falls to (1/e) times the irradiance on the resin surface. E_c is the minimum exposure required to initiate the photopolymerization reactions.

The working curve presented in Figure 5.8 has been validated on the conventional laser-scanning Stereolithography systems. However, the practically observed working curves for Mask-projection Stereolithography systems differ from the theoretical working curves. It has been reported in papers published on MPμSLA that the experimentally observed value of E_c is much greater than its value specified by the resin manufacturer (Beluze et al., 1999; Bertsch et al., 2000; Farsari et al., 2000). However, no explanation has been provided by the authors in order to explain this discrepancy. The DSM SOMOS 10120 resin was characterized by (Hadipoespito et al., 2003). They found that the cure depth varied linearly with exposure, as opposed to varying logarithmically. From the past experiments, it can be seen that the manufacturer's values of E_c and D_p can't be used directly to predict the cure depth. It is necessary plot the working curve for the resin for the specific system being characterized.

In section 6.2.1, the E_c and D_p values of the resin are calculated experimentally. In Section 6.2.2, using the Beer Lambert's law, the relation between the Layer Thickness, Time of Exposure and the lateral dimensions of a layer is formulated.

6.2.1 Experiments performed to characterize the resin

The following experiments are performed to plot the working curve of the DSM SOMOS 10120 resin. A polymer thread is photo polymerized, supported on a U-shaped micro-part as shown in Figure 6.5. The supporting micro-part is U shaped because it offers rigidity and is easy to handle and place under a microscope.

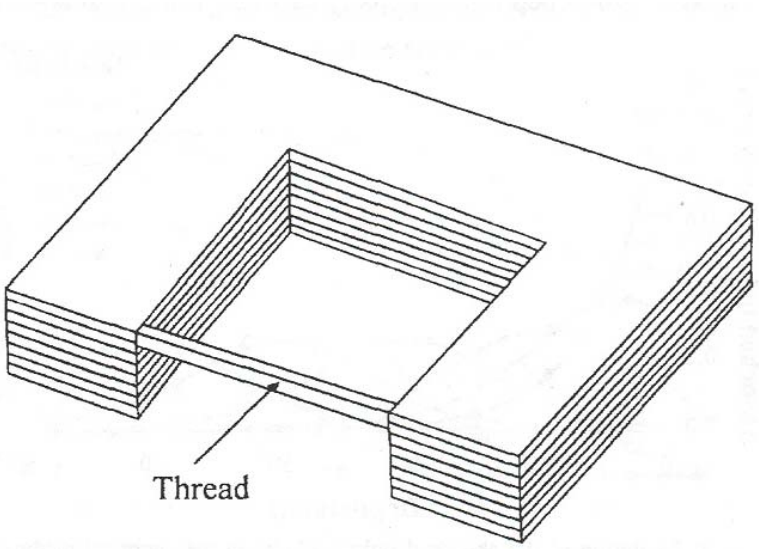

Figure 6. 5 Polymer thread for cure-depth measurements

The thread is located approximately at the center of the imaged area of the mask. The thread is cured by exposing it to radiation for different durations of time. The thickness of the thread in the vertical direction is measured and plotted against the time of exposure. Using a radiometer, the average irradiance on the image is measured to be 5mW/cm^2. The exposure received by thread is calculated by multiplying the average irradiance with the time of exposure. The microscope pictures of the threads are attached in Appendix B.

The thickness of the threads has been tabulated against the exposure in Table 6.2.

Table 6. 2 Thickness of cured thread vs. exposure

Thickness of polymerized thread (μm)	Time of Exposure (s)	Exposure (mJ/cm^2)
32.6	3	15
53.3	5	25
68.1	7	35
130.4	20	100
160	30	150

The plot of cure depth versus the natural logarithm of Exposure (C_d vs. E) has been shown in Figure 6.6.

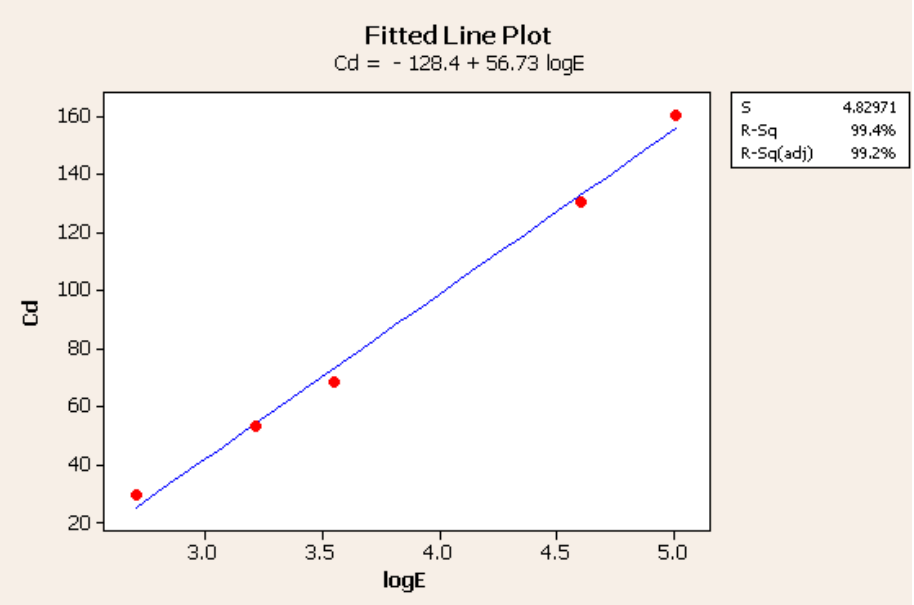

Figure 6. 6 Working curve for DSM SOMOS 10120 with the MP-MSLA system

From Figure 6.6, it can be seen that the X intercept of the plot is 2.26. So, ln (Ec) = 2.26. So, E_c = 9.58 mJ/cm^2. The slope of the plot is 56.73 micron. So, D_p = 0.05673mm.

6.2.2 Formulating the cure model

When a resin is exposed to radiation at any point, it cures up to a certain depth, which depends upon the exposure it receives. For the cured layer to bind to the layer cured beneath it, it should cure to a depth at least equal to the layer. So, all those points on the aerial image at which the resin cures to a depth greater than or equal to the layer thickness will sustain and will be a part of the layer cured. The rest of the cured area will get washed away and will not be a part of the cured layer.

Suppose *TOE* (Time of Exposure) is the time for which the resin is exposed to radiation and *LT* is the layer thickness used to build the part. The Irradiance received by the resin surface is given by $H(pr_i)$. A point pr_i will be a part of the cure layer if the resin at that point cures to a depth greater than *LT*. The layer will be a collection of all these points at which the resin cures to a depth greater than or equal to *LT*.

The cure depth at any point pr_i is given as

$$C_d(pr_i) = D_p \ln (H(pr_i)\ TOE/E_c) \tag{6.6}$$

We introduce a function $L(pr_i)$, which checks if the cured depth at a particular point is greater than or equal to LT.

$$\text{If } C_d(pr_i) \geq LT, \text{ then } L(pr_i), = 1; \text{ Else, } L(pr_i) = 0 \tag{6.7}$$

The cured layer will be a collection of all the points pr_i for which $L(pr_i) = 1$.

The Layer cure model, which is composed of the Irradiance model and the Cure model can thus be presented in the form of the following set of equations:

$$H(pr_i) = (H_{av}x / \sum_{j=1}^{n} w_j m) \sum_{j=1}^{n} \sum_{k=1}^{m} \delta(p_j, v_k, pr_i, o, i, \alpha, d, d', \phi)$$

where

$H(pr_i)$ is irradiation received at point pr_i on the resin surface,

H_{av} is the average irradiance received by the resin surface,

w_j is the weight given to the ray, calculated as $w_j = 1 - 0.00086p - 0.00883p^2$ where p is the distance of the point on the pattern from which the ray is emanating from the center of the beam incident on the DMD,

$\delta(pri, p_j, v_k, o, i, \alpha, d, d', \phi)$ is a ray tracing function that operates on the imaging system parameters to determine whether the ray starting from pattern point p_j in the direction of vector v_k will intersect the point pr_i on the resin surface or not,

$n \rightarrow \infty$, $m \rightarrow \infty$

Cured layer is a collection of points satisfying condition:

$L(pr_i) = 1$

$L(pr_i) = 1$ *if and only if* $C_d(pr_i) \geq LT$

$C_d(pr_i) = D_p \ln (H(pr_i) TOE/E_c)$

where

$C_d(pr_i)$ is the cure depth at the point pr_i on the resin surface,

$H(pr_i)$ is the irradiance received by the point pr_i on the resin surface

LT is the layer thickness used to build the micro-part

TOE is the time for which the pattern is imaged onto the resin surface

D_p is the depth of penetration of the resin

E_c is the critical exposure of the resin

6.3 VALIDATING THE LAYER CURE MODEL

The Layer cure model is validated by comparing the analytical and experimental dimensions of some test layers. The bitmap used to cure these test layers has been presented in Figure 6.7.

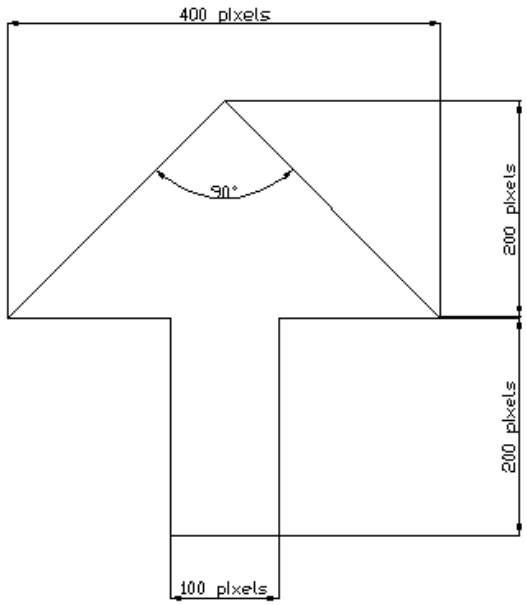

Figure 6. 7 Bitmap used to cure validation-layers

An arrow shaped bitmap is chosen for validation because it has sides in different directions. So, such a bitmap can be used to validate the model in all directions. Consider that this bitmap is imaged for 50s on a 30-micron thick film of resin to cure a layer. In Section 6.3.1, the dimensions of the layer cured are analytically calculated using the Layer cure model. In section 6.3.2, fifteen such single layer parts are experimentally cured and their dimensions measured. The accuracy of the layer cure model and the precision of the process are discussed in Section 6.3.3.

6.3.1 Analytical dimensions of the arrow-shaped layer

The analytical dimensions of the layer are calculated in the following steps:

1. **Value of α, the angle subtended by the DMD chip with the axes computed**

In order to have the micromirrors at an angle 45° to the horizontal, the chip has to be first mounted at 45° to the horizontal and then rotated about its diagonal by 10°. For conducting the analysis in Chapter 6, the angle made by the chip with the X and Y axes is needed. In order to compute these angles, the angle of 10° about the diagonal has to be factored into its component angles about the X and Y axes.

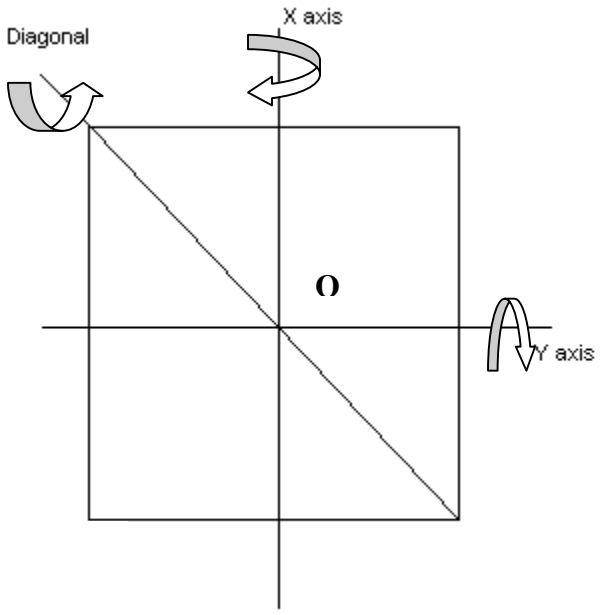

Figure 6. 8 Determining the angle made by the DMD with the horizontal

Consider the corner point 'P' of the chip as shown in Figure 6.8. 'O' is the center of the chip. Suppose the side of the active area of the chip (which is square: 450 x 450 pixels) be *d* units. Then, the diagonal will be of length $d\sqrt{2}$ units. The distance from

O to P will be $d\sqrt{2}/2 = d/\sqrt{2}$ units. So, a rotation about the diagonal by 10° will result in the point P being raised by $d/\sqrt{2}\ \sin 10°$ units. If we factor this rotation into two rotations: one by an angle α about the X axis and another, again by an angle α about the Y axis, then the point P must be raised by the same amount. Since the chip is square, the same amount of "raise" shall be supplied to P during each of the two rotations. So, angle α will be such that:

$(d/2) \sin \alpha = (d/\sqrt{2}) \sin 10°$.

$\sin \alpha = \sin 10°/\sqrt{2}$

$\alpha = \sin^{-1} (\sin 10°/\sqrt{2})$

$\alpha = 7.05°$

Thus, the angle made by the DMD chip with the horizontal, about the Z-axis is 45 + 7.05 = 52.05° and that with the horizontal with a rotation about the Y-axis is 7.05°.

2. Meshing the bitmap with points

The bitmap is meshed with equally spaced points. The separation of points in the Z direction of the bitmap is *1/cos 45°* times the spacing in the Y direction. As a first iteration, the mesh spacing is taken to be 2.5 pixels in the Y direction. Later, in Step 4, this meshing is made denser and denser iteratively till the irradiance on the resin surface converges to its final value.

3. Resin surface of 2x2 mm meshed with a 25 x 25 point grid. Average irradiance across this area experimentally measured

The resin surface of 2x2 mm is meshed with 25x25 grid points. The average irradiance across this 2x2 mm area is determined as follows:

A radiometer sensor is placed under the image. The average irradiance is measured by the radiometer as 1.02 mW/cm^2. With the sensor diameter as 5mm, its area is 0.1963 cm^2. So, the total power in the image is 0.2002 mW. The formed image is smaller that the 2x2 mm area and will definitely lie within it. The average irradiance across the 2x2 mm area is given as $H_{av} = 0.2002/0.04 = 5mW/cm^2$.

4. **Rays traced from all the bitmap points. Determining the value of Φ, the half angle of the cone in which rays emit from every bitmap point**

Rays are traced from every point on the bitmap. The location of every point on the bitmap relative to the optical axis and its distance from the imaging lens is calculated, given the orientation of the DMD chip as derived in Step 1 in this section. As said in Section 6.1.3, there is an uncertainty as regards the angle of the cone (Φ) formed by the rays emitted from every bitmap point. Various cone angles are assumed, from 0° to 4° and rays are traced. The angle which gives results that agree the best with the experimental results (as obtained in Section 6.3.2) is considered as the half cone angle. It has been found that smaller the assumed value of Φ, better is the agreement with experimental results.

5. **Mesh on the bitmap made denser and denser till solution converges**

The mesh density on the bitmap is progressively made denser and denser till the irradiance computed at the grid on the resin surface converges. It has been observed that when the grid spacing is reduced to 1.6 micromirrors, the solution converges. The matrix showing the irradiance at the grid on the resin surface is shown in Figure 6.9. The actual Irradiance matrix is 25 x 25. In the Figure 6.9, only its relevant portion is shown.

0	0	0	0	0	0	0	0	0	0	0	0	0	0
0	0	0	0	0	0	0	0	0	0	0	0	0	0
0	0	0	0	0	0	3.3308	3.3324	3.3308	0	0	0	0	0
0	0	0	0	0	0	20.0034	20.0128	20.0031	0	0	0	0	0
0	0	0	0	0	0	20.0326	20.0421	20.0323	0	0	0	0	0
0	0	0	0	0	0	20.0588	20.0683	20.0586	0	0	0	0	0
0	0	0	0	0	0	21.7565	21.7669	21.7562	0	0	0	0	0
0	0	0	0	0	0	21.7800	21.7905	21.7797	0	0	0	0	0
0	0	0	0	0	0	21.5758	22.0340	21.7993	0	0	0	0	0
0	0	0	0	0	0	21.9270	25.0726	23.4936	0	0	0	0	0
0	0	0	0	0	0	21.9394	25.0873	23.5069	0	0	0	0	0
0	0	0	0	0	0	20.7150	23.3040	22.1711	0	0	0	0	0
0	1.5437	22.6710	23.7719	24.3042	24.7052	39.9785	43.0291	40.6507	24.8171	24.3041	23.6609	22.7818	1.8745	0
0	0	25.5676	47.5399	48.6042	49.4058	47.2501	46.6079	47.3621	49.4056	48.7152	47.3175	26.4522	0	0
0	0	1.7725	41.2075	48.4786	49.1668	49.8090	50.0626	49.6972	49.5020	48.3668	41.5401	2.1049	0	0
0	0	0	13.0034	47.7877	48.9180	49.5575	49.6976	49.5575	48.9179	47.6764	13.7811	0	0	0
0	0	0	0	30.2929	45.3124	45.4969	45.8573	45.7205	45.2008	31.1830	0	0	0	0
0	0	0	0	5.6802	43.3800	45.3448	45.4805	45.1213	43.6029	6.1257	0	0	0	0
0	0	0	0	0	22.9602	44.8502	44.8733	44.6271	23.8515	0	0	0	0	0
0	0	0	0	0	1.8939	37.3337	40.9171	37.4449	2.2281	0	0	0	0	0
0	0	0	0	0	0	16.7003	40.4182	17.2568	0	0	0	0	0	0
0	0	0	0	0	0	0.6674	27.4671	0.7787	0	0	0	0	0	0
0	0	0	0	0	0	0	0.4444	0	0	0	0	0	0	0
0	0	0	0	0	0	0	0	0	0	0	0	0	0	0
0	0	0	0	0	0	0	0	0	0	0	0	0	0	0
0	0	0	0	0	0	0	0	0	0	0	0	0	0	0

Figure 6. 9 Irradiance matrix

It can be seen that the minimum irradiance received by any grid spacing is equal to 0.4444 mW/cm^2. This is the value of the variable *minH(pr)* in the Layer cure model as presented in Section 6.2.

The Matlab code written to execute Steps 1 to 5 above is documented in Appendix C.

6. Computing lateral dimensions of the layer

The bitmap is exposed for 50s, the depth to which the area receiving irradiance *minH(pr) = 0.4444mW/cm^2* will get cured will be given as:

$C_d = D_p \ln (\min(H(pr)*50/E_c)$

$= 0.056 * \ln(0.4444*50/9.6)$

$= 0.0469mm$

$= 46.9\ \mu m.$

Thus, the entire exposed area shall be cured to a depth greater than the layer thickness (30µm) and hence, the lateral dimensions of the cured layer will be equal to those of the aerial image.

The simulated image of the layer is shown in Figure 6.10.

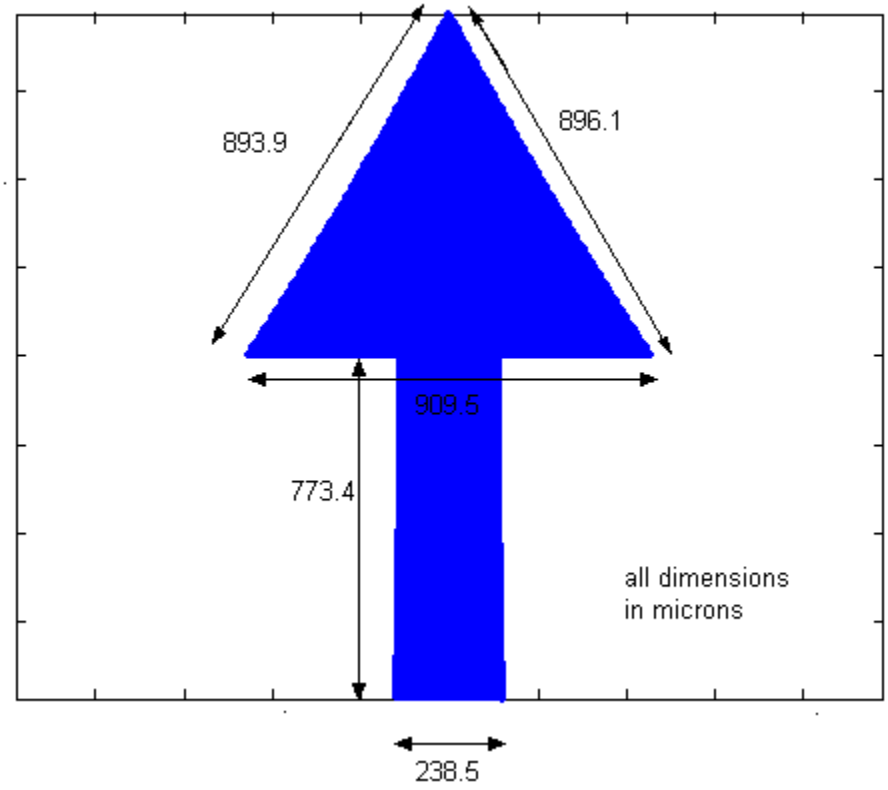

Figure 6. 10 Aerial image formed on the resin surface

6.3.2 Curing of test layers

The bitmap shown in Figure 6.7 is imaged onto a 30µm thick film of resin for 50s to cure arrow shaped layers. In all, 15 such single layer microparts are cured. The dimensions of these layers are measured under an optical microscope. The picture of one of the layers is shown in Figure 6.11. The pictures of all 15 layers are attached in Appendix D.

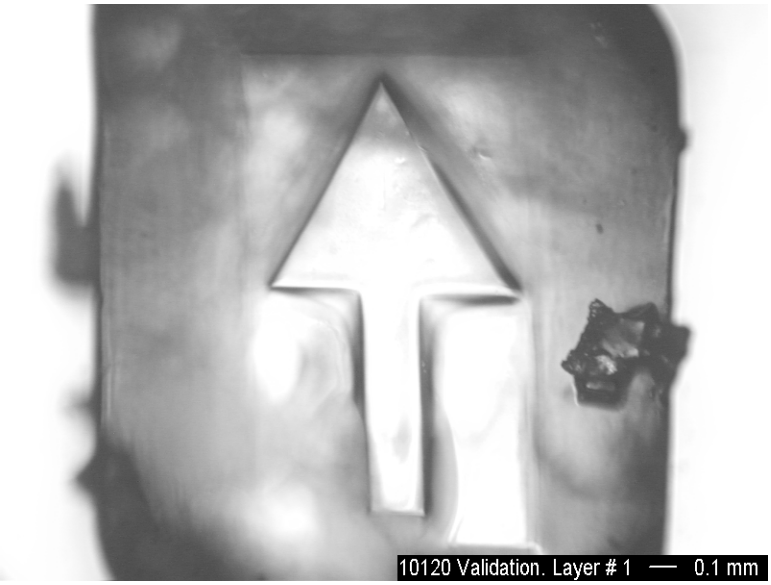

Figure 6. 11 Arrow shaped layer

The dimensions of the various sides of these layers and the corresponding dimensions computed by the Layer cure model have been documented in Table 6.3. The sides whose dimensions are compared are shown in Figure 6.12.

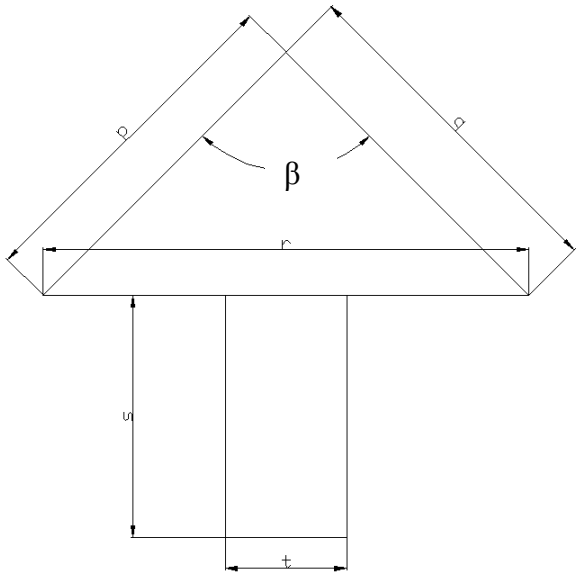

Figure 6. 12 Dimensions compared to validate the Layer cure model

Table 6. 3 Experimental and analytical dimensions of the arrow shaped layers

	Dimensions in microns					β
Layer #	p	q	r	s	t	Angle in degrees
1	900	875	887.5	775	212.5	53
2	887.5	850	887.5	762.5	200	60
3	912.5	900	887.5	775	212.5	55
4	912.5	887.5	875	775	212.5	53
5	912.5	900	887.5	787.5	225	57
6	900	875	875	787.5	212.5	53
7	937.5	912.5	887.5	787.5	212.5	56
8	900	900	875	787.5	212.5	57
9	912.5	900	887.5	775	212.5	57
10	925	900	887.5	787.5	212.5	55
11	900	875	875	775	212.5	51
12	912.5	900	887.5	787.5	212.5	52
13	912.5	887.5	887.5	787.5	212.5	54
14	887.5	875	875	775	212.5	56
15	912.5	900	887.5	787.5	212.5	54
Average dimension	**908.3333**	**889.1667**	**883.3333**	**780.8333**	**212.5**	**54.86667**
Standard Deviation (σ)	**13.0817**	**16.27516**	**6.099375**	**7.999256**	**4.724556**	**2.356349**
3 σ	**39.24511**	**48.82549**	**18.29813**	**23.99777**	**14.17367**	**7.069047**
Percent Precision	**4.320562**	**5.491152**	**2.071486**	**3.073353**	**6.669961**	**12.88405**
Analytical dimension	**896.1**	**893.1**	**909.5**	**773.4**	**238.5**	**52**
Error	**12.23333**	**-3.93333**	**-26.1667**	**7.433333**	**-26**	**2.866667**
Percent Error	**1.365175**	**0.44041**	**2.87704**	**0.961124**	**10.9015**	**5.512821**

From Table 6.3, it can be seen that the layer dimensions computed using the Layer cure model agree well with the dimensions of the test layers cured on the system. The resolution of measurement of these layers is 12.5µm. The absolute error varies from 3.93µm to 26µm and the standard deviation varies from 4.72µm to 16.26µm. Given the resolution of the measuring device, this accuracy and precision is very good. This validates the analytical model. Nevertheless, there is some discrepancy in the analytical

and experimental results. This discrepancy is due to the accuracy and precision errors in the process as discussed in the next section.

6.4 ACCURACY AND PRECISION OF THE MPμSLA PROCESS

In section 6.4.1, the accuracy and precision of the MPμSLA process is determined. In Section 6.4.2, the methods of improving the accuracy and precision of the process are discussed.

6.4.1 Accuracy and Precision of the process

Accuracy is defined as the degree of agreement [of an experimental value] with its true [target] magnitude (Kalpakjian, 1992). Suppose that we wanted to cure an arrow shaped layer with dimensions as returned by the Layer cure model, i.e. with target dimensions as:

$p = 896.1\mu m$

$q = 893.1\mu m$

$r = 909.5\mu m$

$s = 773.4\mu m$

$t = 238.5\mu m$

$\beta = 52°$

We would then image the bitmap in Figure 6.7 on the resin for 50s. The dimensions of the experimental layers would be as documented in Table 6.3. From the definition of "accuracy" stated above, the agreement of the dimensions of the 15 test layers with the target dimensions would give us the accuracy of the process. Accuracy error is always present when the numerical average of successive readings (measurements) deviates from

the known correct [target] reading. (Schenck, 1979). In case of the MPμSLA process, the average measurements of the dimensions of the arrow shaped layer are as follows:

p = 908.3μm

q = 889.2μm

r = 883.3μm

s = 780.8μm

t = 212.5μm

β = 54.9°

The difference in the target dimensions and the mean of the experimental dimensions would be a measure of the accuracy of the process. The accuracy and the percent accuracy of the process are presented in Table 6.3.

Precision is the degree to which an instrument gives repeated measurements of the same standard (Kalpakjian, 1992). Precision error is always present when successive measurements of a quantity yield different numerical values (Schenck, 1979). The dimensions of the 15 validation layers are presented in Table 6.3. Same process parameters were used to cure each of these 15 layers. The standard deviation of the dimensions from their mean is a measure of the precision of the process. The standard deviation and precision of the process are computed in Table 6.3

6.4.2 Improving accuracy and precision of the MPμSLA process

The accuracy and precision of the process are caused by different types of errors. Accuracy can be improved by reducing the accuracy errors (as defined in Section 6.4.1),

also called as systematic errors. Precision can be improved by reducing the precision errors (as defined in Section 6.4.1) also called as random errors.

In case of the MPμSLA process accuracy errors exist due to the following reasons:

- Incorrect alignment of the optical components: The collimating lens, the imaging lens and the DMD are aligned only manually. The errors due to misalignment will be introduced in all the layers cured by the system
- Errors in the optical components: Some manufacturing defects are likely to exist in the optical components. These defects will introduce errors in all the layers cured using the MPμSLA system

Accuracy errors can be eliminated by calibrating the Layer cure model. It should be noted that the calibration can correct only for the accuracy errors and not the precision errors.

Precision (random) errors are introduced in the layer dimensions due to the following reasons:

- Errors introduced by variation of the height of resin in the vat
- Errors introduced by the variation in the curing characteristics of the resin used
- Errors introduced by the post-cure operations

Errors introduced by variation in the height of resin in the vat

The image distance (i) of the imaging system of the MPμSLA system is equal to the distance between the imaging lens and the free surface of the resin. Since the level of resin in the vat is adjusted only manually, the image distance doesn't remain constant from experiment to experiment and thus introduces errors. Small defocusing errors tend

to simply enlarge or reduce an image proportionately. This is verified by running the Layer cure model for different values of image distances and calculating the ratios of the sides of the arrow that would be obtained. It is seen from Table 6.4 that the ratio of sides remains nearly unchanged by variation in image distance. Thus, variation in resin level from experiment to experiment would create lateral scaling of the layer and will not be the cause of distortion of a layer. A layer appears distorted if there is an error in the dimension of a side relative to the others. Thus, the effect of random errors introduced by change in resin level can be factored out if we consider the variation in the ratios of the various sides of the arrow from experiment to experiment.

Table 6. 4 Quantifying the effect of variation in resin level on layer dimensions

Dimension (all in μm)	**Image distance: 33.45 + 0.5mm**	**Image distance: 33.45**	**Image distance 33.45 – 0.5mm**
p	960.3	896.1	832.4
q	959.5	893.9	831.7
r	976.2	909.5	842.8
s	827.9	773.4	718.9
t	255.3	238.5	221.7
p/q	1	1.002	1
p/r	0.9837	0.9852	0.9876
p/s	1.1599	1.1586	1.1578
p/t	3.7614	3.7572	3.7546

The errors in the ratios of the sides of the arrows cured using the MPμSLA system are tabulated in Table 6.5. From Table 6.3 and Table 6.5, it can be seen that the precision of the process has improved after factoring out the effect of the variation in resin level.

.

Table 6. 5 Precision of process after factoring out errors due to variations in resin level

Layer #	p/q	p/r	p/s	p/t
1	1.028571	1.014085	1.16129	4.235294
2	1.044118	1	1.163934	4.4375
3	1.013889	1.028169	1.177419	4.294118
4	1.028169	1.042857	1.177419	4.294118
5	1.013889	1.028169	1.15873	4.055556
6	1.028571	1.028571	1.142857	4.235294
7	1.027397	1.056338	1.190476	4.411765
8	1	1.028571	1.142857	4.235294
9	1.013889	1.028169	1.177419	4.294118
10	1.027778	1.042254	1.174603	4.352941
11	1.028571	1.028571	1.16129	4.235294
12	1.013889	1.028169	1.15873	4.294118
13	1.028169	1.028169	1.15873	4.294118
14	1.014286	1.014286	1.145161	4.176471
15	1.013889	1.028169	1.15873	4.294118
Average dimension	**1.021672**	**1.028303**	**1.16331**	**4.276008**
Standard Deviation (σ)	**0.010784**	**0.013072**	**0.013942**	**0.091626**
3σ	**0.032353**	**0.039217**	**0.041825**	**0.274877**
Percent Precision	**3.166659**	**3.813786**	**3.595371**	**6.428351**

Errors introduced by the variation in the curing characteristics of the resin used

So far we have assumed that the resin behavior doesn't change with time. However, with every part cured, the resin in the vat gets exposed to radiation. This exposure is likely to change the curing characteristics of the resin from experiment to experiment. Also, it is assumed that the resin doesn't cure in the lateral direction. Since there is no rigorous analytical model for resin cure and also since the chemical composition of the DSMS SOMOS 10120 resin is unknown, it is not possible to incorporate these variations in resin properties in the analytical model.

Errors introduced by the post-cure cleaning operations

Every cured layer is submerged in resin. This resin is removed by dipping the platform and cured layer briefly (2 or 3 seconds) in a beaker containing isopropyl alcohol and vibrating it gently. This is the only cleaning that has been done to remove the excess resin surrounding the cured layer. A variation in the time for which the part was dipped in the alcohol bath and in the frequency and amplitude of vibrations imparted to platform is likely to cause some random errors in the layer dimensions.

6.5 LIMITING LATERAL POSITIVE RESOLUTION

Using the Layer cure model, the limit on the lateral positive resolution of the system can be quantified. A line of micromirrors one micromirror thick shall cure the thinnest feature. By running a bitmap of size 5 pixel x 1 pixel through the Layer cure model, the thickness the aerial image is found to be 2.1 μm. In order to validate this limit, the curing of a line one pixel thick was attempted. However, the line couldn't withstand the rinsing under alcohol. Nevertheless, since the Layer cure model has been validated, it can be concluded that the limiting resolution computed using it would be correct. In order to check the validity of the Layer cure model for very small features, a line 3-pixel wide was cured. This line could withstand the cleaning procedures. The Layer cure model computed the width of the cured line to be 6.2 μm. The width of the actual line cured was found to be 6μm. The picture of the line is shown in Figure 6.13. This shows that the Layer cure model is valid even for small feature sizes.

Figure 6. 13 Three-pixel wide line cured on the MPμSLA system

Before the theoretical limiting resolution of the system can be specified be 2.1 μm, it needs to be ascertained that the diffraction limit on the minimum feature size that can be irradiated by the imaging lens is smaller than 2.1μm. Resolution of the imaging system is determined by the wavelength and the numerical aperture using the Rayleigh's formula (Sheats, 1998),

$$D = \frac{k_1 \lambda}{NA} \tag{6.8}$$

where D is the minimum dimension that can be printed, λ is the exposure wavelength and NA is the numerical aperture of the imaging lens, and the proportionality constant k_1 is a dimensionless number in an approximate range from 0.6 to 0.8.

The numerical aperture of the imaging lens is 0.492. So, the diffraction-imposed limit on the resolution of the imaging system is:

$$D = \frac{0.8 * 0.365}{0.492}$$

= 0.593μm.

This is far less than the resolution computed as 2.1μm. Thus, the theoretical limiting lateral resolution of the MPμSLA system is 2.1μm.

The theoretical limit on resolution has been computed using the Layer cure model. The Layer cure model however is based on the assumptions that the optical system is aligned perfectly and that the resin cures only in the downward and not in the lateral directions. These assumptions introduce some errors in the Layer cure model. Thus, the theoretical limit of resolution calculated to be 2.1μm is also likely to contain certain errors. Since the layer cure model has been found to be inaccurate within about 10% for small features, the error in the theoretical limiting resolution is also likely to be in the range of ± 10%.

6.6 PICTURES OF SOME MICROPARTS CURED USING THE MPμSLA SYSTEM

In this section, the pictures of some of the microparts cured using the MPμSLA system are presented. In Figure 6.14, the four wheels and axle of a micro-SUV cured using the MPμSLA system developed is shown. The width of the axle is measured to be 57.14μm while the width computed by the Layer cure model is 57.6μm. It is to be noted that the axle is an overhang, supported on the four wheels. The part shown is 9 layers thick, each layer being 20μm thick.

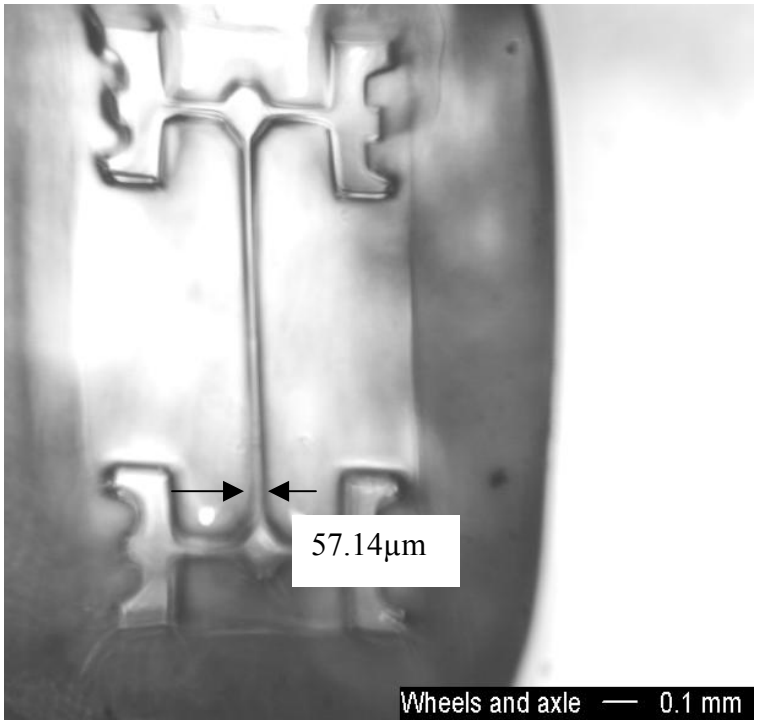

Figure 6. 14 Four wheels and axle of an SUV

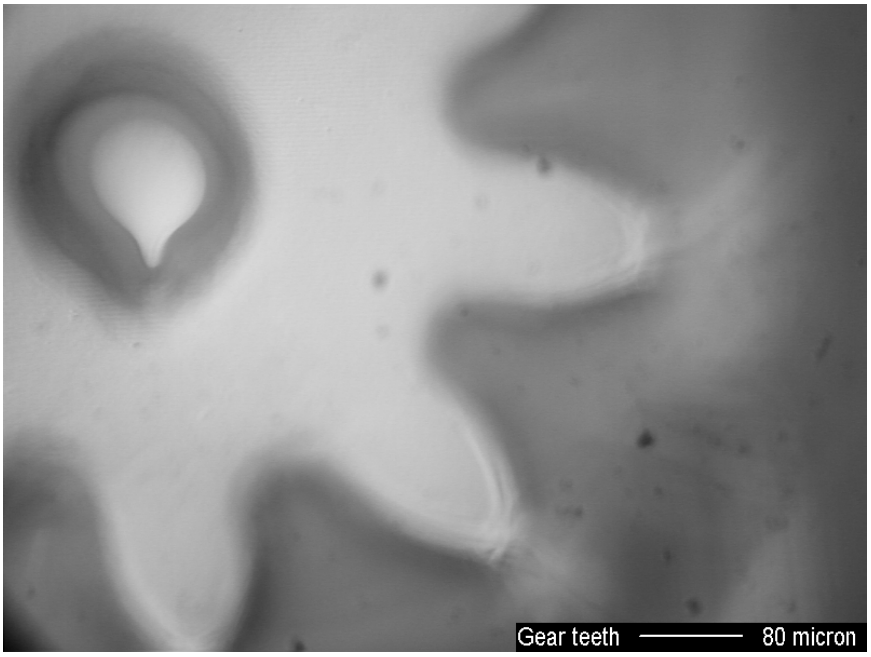

Figure 6. 15 Teeth of a spur gear

In Figure 6.15, the teeth of a spur gear cured on our system are shown. The thickness of the gear teeth at the pitch-circle diameter of the gear is measured as 40μm. This part is made up of 2 layers, each layer being 30 μm thick.

Figure 6. 16 RPMI logo

In Figure 6.16, the logo of the Rapid Prototyping and Manufacturing Institute at Georgia Institute of Technology is shown. This logo is a single layer part 50 μm thick.

Layer cure model can compute the distortions in a layer cured when a bitmap is imaged onto the resin surface. The Layer cure model can be flipped over to compute the compensatory distortions necessary in a bitmap in order to cure a layer of the required

dimensions. This is achieved by the Inverse Layer cure model, which is formulated in Chapter 7.

Summary

Using the Layer cure model, the effect of the process variables, namely layer thickness (*LT*), time of exposure (*TOE*) and bitmap (*B*), on a cured layer's lateral dimensions is quantified. It is shown that when a bitmap is imaged onto the resin surface, the aerial image formed is distorted. This is due to optical aberrations. The irradiance distribution across this aerial image is not constant, with the center portions of the image receiving more energy than the edges. The time of exposure should be such that that the resin at the edges of the aerial image cures down to the previously cured layer, i.e. to a depth of one layer thickness

The use of a UV lamp as opposed to a laser offers an advantage. With a laser the irradiance distribution across the beam incident on the pattern is Gaussian. This creates a large variation in irradiance across the aerial image formed. The irradiance distribution across the beam obtained from the UV lamp is much more uniform. Refer to Table 6.1. The advantage of using a laser is that the beam is collimated. So, rays are reflected vertically downwards from every pattern point, parallel to the optical axis. Such rays reduce the optical aberrations, which results in less distortion of the aerial image and uniform irradiance distribution across it. On the other hand, with a UV lamp, a cone of rays emits from every pattern points. This results in increased optical aberrations.

The layer cure model is accurate within an error of 26μm. The precision of the process is 7%. The methods of improving the accuracy and precision of the process are discussed in Section 6.4.2.

In the formulation of the layer cure model, the effect of the following process parameters was not considered:

Resin Viscosity (*V*)

Deep Dip (*DD*)

Time of leveling (*TOL*)

All these parameters are related to the recoating of a layer. DD is the depth to which a cured layer is lowered into the resin vat. TOL is the time allowed for the recoated film of resin to level itself. The effect of these variables will be studied if the build time of the micro part is to be modeled.

CHAPTER 7

CURING DIMENSIONALLY ACCURATE LAYERS: INVERSE LAYER CURE MODEL

The Layer cure model computes the lateral dimensions of a layer in terms of the process parameters. A manufacturer would be more interested in knowing the values of process parameters that would cure a layer of the intended dimensions. This is possible with the "Inverse Layer cure model". The inputs and outputs of the Inverse Layer cure model are opposite to those of the Layer cure model. The structure of the Inverse layer cure model is shown in Figure 7.1.

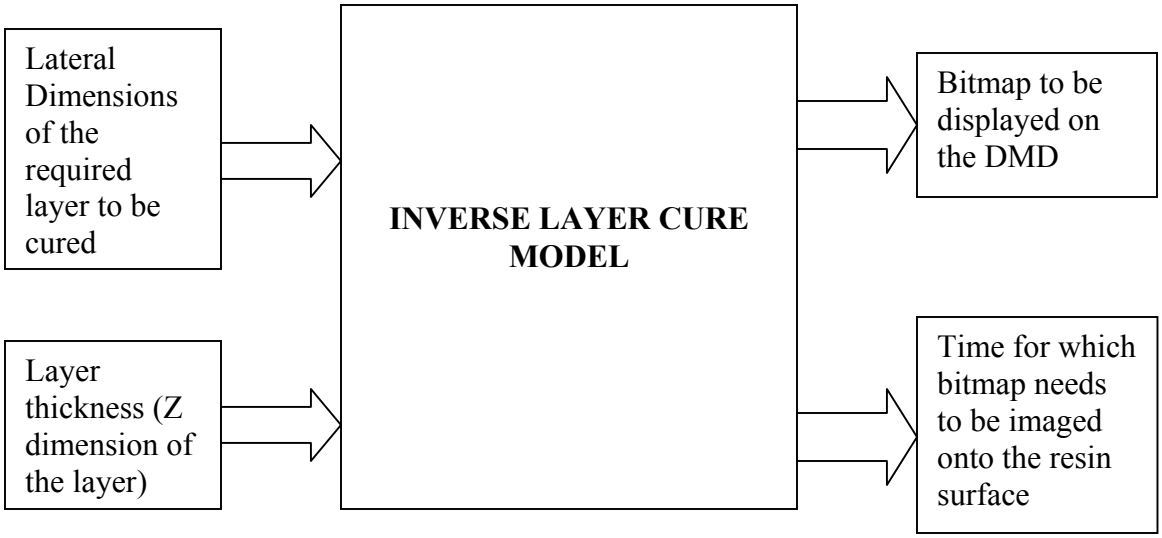

Figure 7. 1 Structure Inverse Layer cure model

In Section 7.1, the detailed structure of the Inverse Layer cure model is explained. In Section 7.2, the Pixel-micromirror mapping model is formulated. In Section 7.3, a case study, showcasing the application of the Inverse Layer cure model is presented.

7.1 FORMULATION OF THE INVERSE LAYER CURE MODEL

The detailed structure of the Inverse Layer cure model is shown in Figure 7.2. The inputs to the Inverse Layer cure model are lateral dimensions of a layer and layer thickness. Using a Pixel mapping model, the bitmap to be displayed on the DMD in order to form an aerial image of the dimensions equal to that of the desired layer is generated. The Pixel mapping model discretizes the intended layer into pixels, and then, maps these pixels onto the pixels of the bitmap to be displayed on the DMD. The Pixel mapping model is explained in Section 7.2. This bitmap is then run through the Irradiance model (formulated in Section 6.3) to obtain the irradiance across the aerial image that will be formed when the bitmap is imaged onto the resin surface. The irradiance at the point receiving the minimum irradiance is computed. From the resin characteristics (experimentally determined in Section 6.2), the time of exposure required for the entire exposed area to cure down to a depth of one layer thickness is computed. Thus, the outputs of the Inverse layer cure model are the bitmap to be displayed on the DMD and the time of exposure.

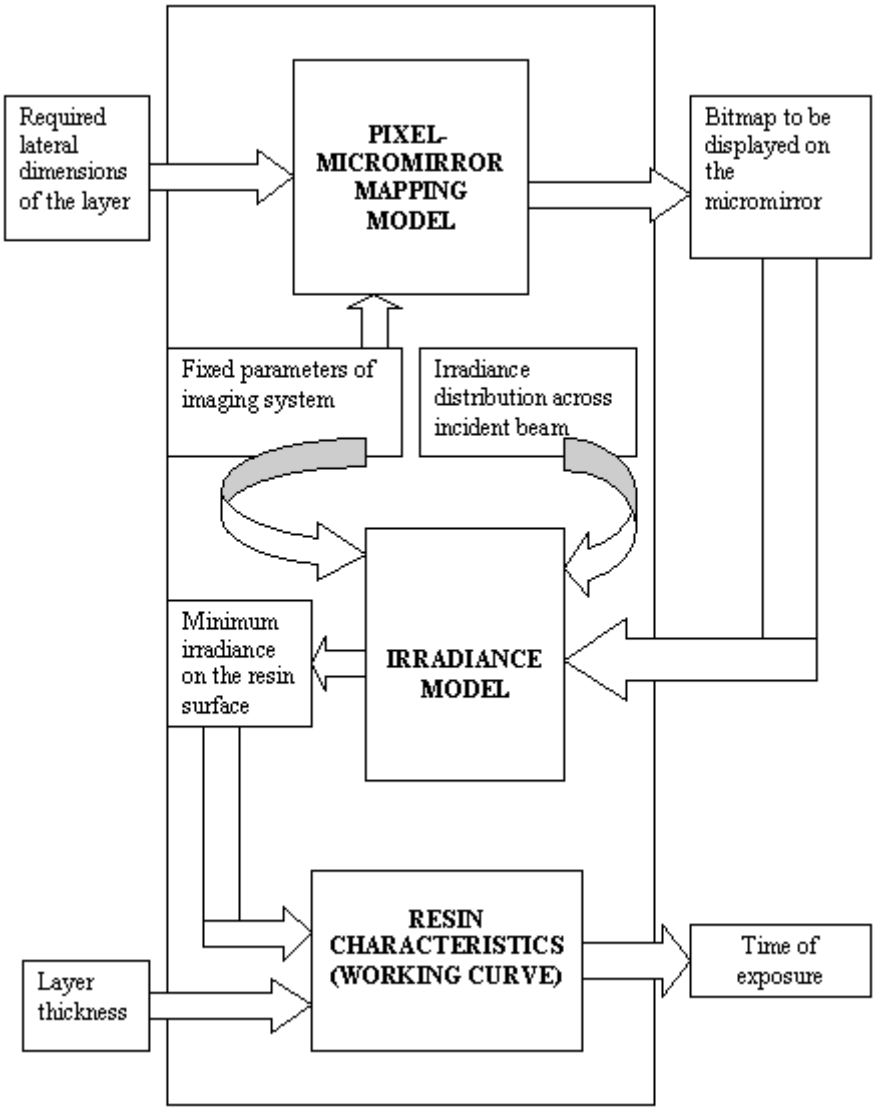

Figure 7. 2 Detailed structure of Inverse Layer cure model

7.1.1 Pixel mapping model

The Pixel mapping model is formulated to generate the bitmap to be displayed on the DMD in terms of the dimensions of the intended layer. The most important part of this model is the "Pixel-micromirror mapping database." This database relates the location of a micromirror on the DMD with the location of the pixel cured by it on the layer. Rays are traced from every micromirror on the DMD and the locations of their points of intersection with the resin surface are computed. The procedure of ray tracing is the one adopted while formulating the Irradiance model. The location of every point on the resin surface is documented against the location of the micromirror on the DMD irradiating it.

The Pixel mapping model is executed in the following steps:

Step 1: Mesh the intended layer with points

The intended layer is meshed with points. The denser these points, the better the representation of the layer.

Step 2: Snap the points on this mesh to the closest pixel on the resin in the Pixel-micromirror mapping database

The Pixel micromirror mapping database relates the micromirrors on the DMD with the points on the resin surface. Every mesh point is snapped to the closest resin point from the Pixel micromirror-mapping database

Step 3: From the Pixel-micromirror mapping database, determine the locations of the micromirrors on the DMD to be turned "ON"

Since the Pixel mapping database creates a one-to-one correspondence between the micromirrors on the DMD and the points on the resin surface, it can be applied in reverse to look up the micromirrors corresponding to the points on the resin surface.

Step 4: Generate the bitmap so that the micromirrors (obtained in Step 3) are turned "ON"

When a monochrome bitmap is supplied to the DMD, every pixel on the bitmap controls one and only one micromirror on the DMD. If a bitmap pixel is white, the corresponding micromirror is switched "ON". If the bitmap pixel is black, the corresponding micromirror is switched "OFF". From the locations of the micromirrors on the DMD that are to be turned "ON", the required monochrome bitmap is generated.

Generating the Pixel-micromirror mapping database

The Pixel-micromirror mapping database is generated by tracing rays from the midpoint of every micromirror on the DMD onto the resin surface. Since the active area of the mask that can be imaged by the imaging lens is only 450x450 pixels, rays are traced from the micromirrors in this area only. The location of the pixels irradiated by the various micromirrors on the DMD is pictorially shown in Figure 7.3. It may be mentioned in passing that the kind of aberration noticed here is "Positive Distortion." Refer Section 6.1.

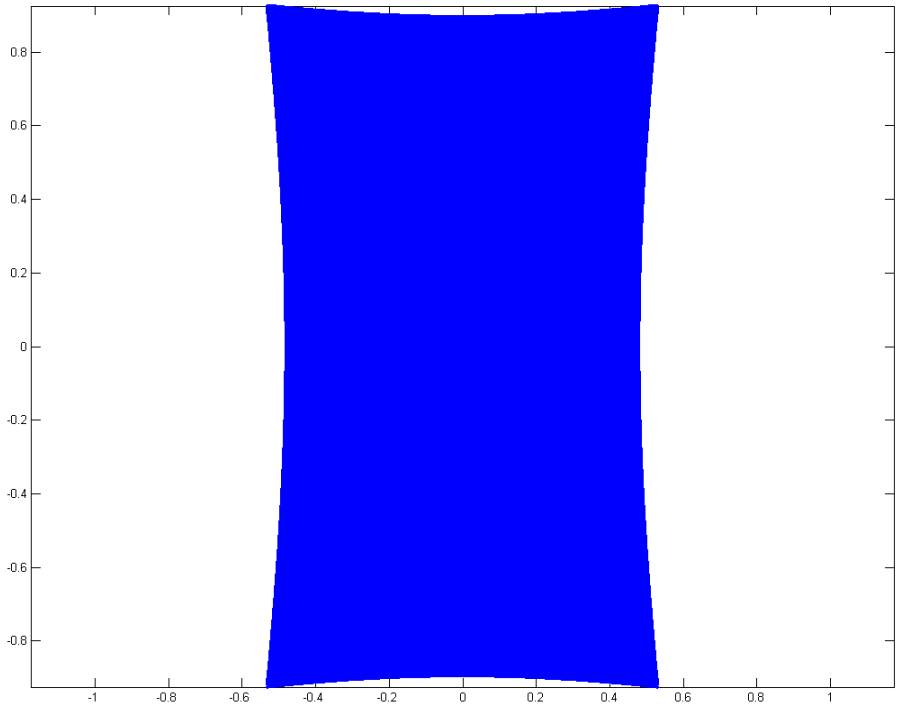

Figure 7. 3 Layer pixels in the Pixel-micromirror mapping database

7.2 CASE STUDY: CURING OF A SOLID CIRCLE

Problem statement: A solid circular layer of diameter 1 mm and of thickness 30µm is to be cured in DSM SOMOS 10120 resin by displaying a bitmap on the MPµSLA system. Generate the bitmap and compute the time for which it should be imaged onto the resin surface.

Solution

The problem will be solved in five steps:

1. Meshing the circle with data points

2. Snap the data-points to the resin points on the database
3. Generate the bitmap to be displayed
4. Use the Irradiance model to determine the minimum irradiance on the circle
5. Determine the time of exposure using the Cure model

Step 1: Mesh the circle with data points

The finer we mesh the circle with data-points, the better will be its representation. At the same time a finer spacing will increase the computation time. A spacing of 2µm is found to be computationally feasible. The meshed 1mm diameter circle is shown in Figure 7.4. In all, 196822 points are meshing the circle.

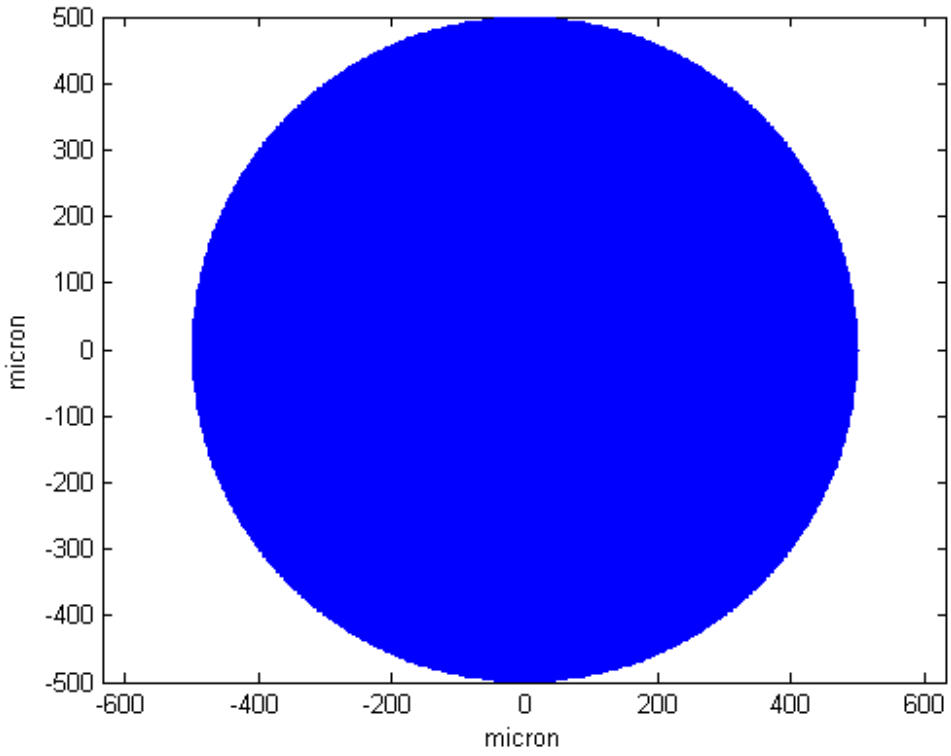

Figure 7. 4 Intended layer meshed with points

Step 2: Snap the data-points to the points in the database

The points are snapped to closest points on the database. The number of points in the database is 203401. The numbers of points meshing the circle are 196822. These points are snapped by executing an algorithm that could efficiently search the database and snap the points meshing the circle. Upon snapping, the circle is as shown in Figure 7.5.

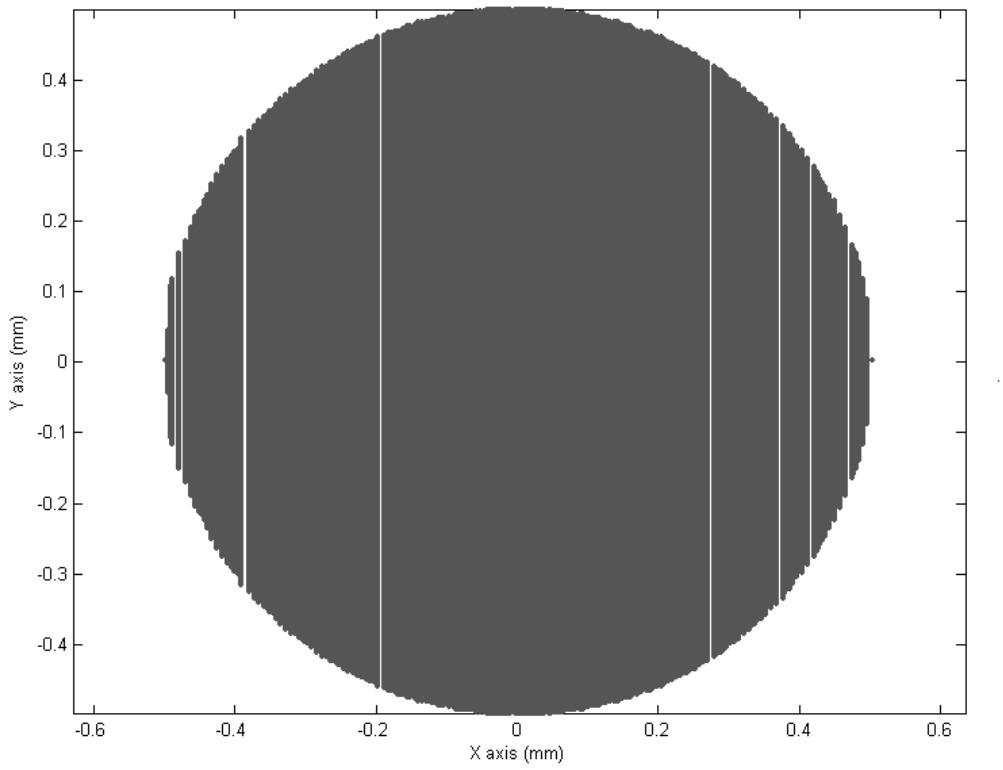

Figure 7. 5 Layer after snapping points to the closest resin points on the database

Due to the snapping of layer points, some errors are introduced. These are responsible for the white lines across the layer. These lines can be eliminated by increasing the density of the points meshing the disc.

Step 3: Generate the bitmap to be displayed

In Step 2, we have generated the pixels that are to be irradiated on the resin. From the Pixel-micromirror mapping database, the micromirrors that need to be turned "ON" in order to irradiate the pixels are noted. These are the pixels that are "white" in the bitmap to be input to the DMD. The bitmap is generated. The bitmap is shown in Figure 7.6. The elliptical bitmap shown in Figure 7.6 consists of black lines across it. These lines are produced because the cured layer is meshed only with a finite number of points. If the meshing density is increased, a whiter bitmap will be obtained.

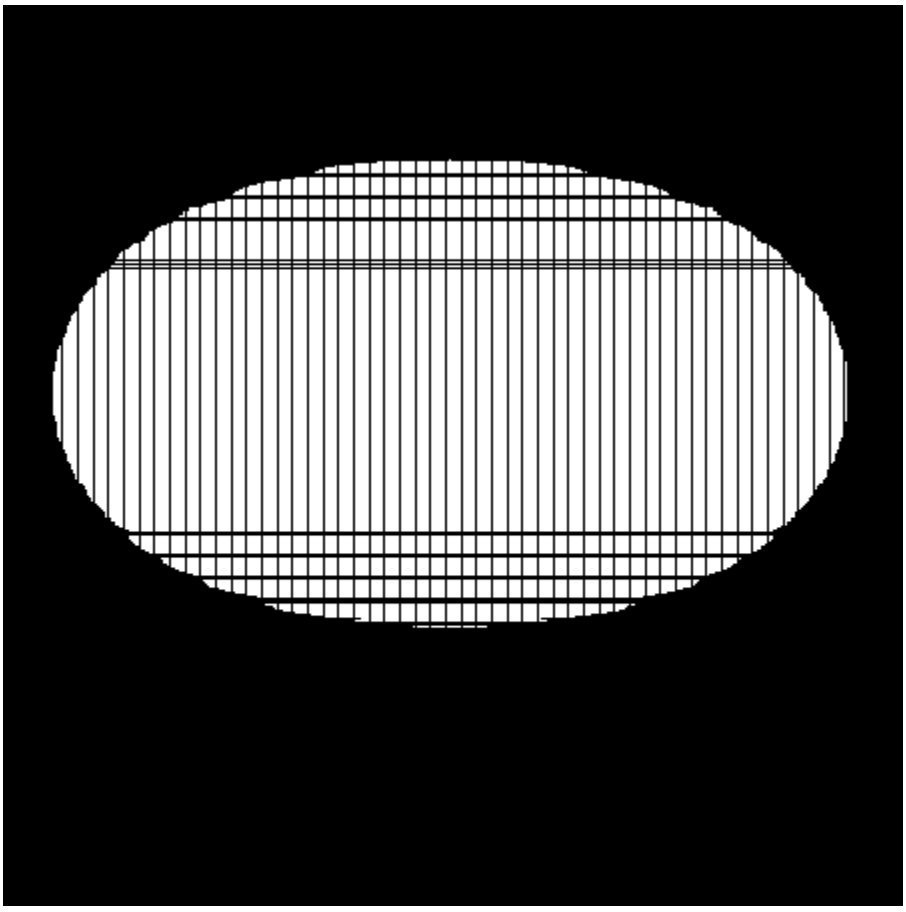

Figure 7. 6 Bitmap to be displayed on the DMD

Step 4 Use the Irradiance model to determine the minimum irradiance on the circle

By running the bitmap generated in Step 3 through the Irradiance model, the minimum irradiance across the image is determined. It is observed that the edges of the aerial image receive the minimum irradiance, equal to 0.29mW/cm^2.

Step 5 Calculate time of exposure using Beer Lambert's law

Using the equation:

$t_{min} = (E_c/minH(pr_i))\, e^{(LT/Dp)}$

the time of exposure is calculated to be 56s.

The code written to execute Steps 1 to 5 is documented in Appendix E.

Solution: The required layer can be cured by displaying the bitmap shown in Figure 7.6 on the DMD and imaging it onto the resin surface for 56s.

Curing of the disc shaped layer

By imaging the bitmap generated in Step 4 onto the resin surface for 43s, single layer parts were cured. The picture of one of them is shown in Figure 7.7. It is seen that the layers are indeed circular in shape. The disc appears distorted. The maximum diameter is measured to be 1mm. The minimum diameter is measured to be 975µm. The following are the reasons for this distortion:

As explained in Chapter 5, the micromirrors of the DMD in their "ON" state make and angle of 10° with the chip on which they are mounted. The DMD chip is mounted at an angle of 10° with two axes due to which the bitmap displayed across the DMD is, in fact, slightly distorted. Such distortion was also observed in Chapter 6 where the Layer cure model was formulated. In order to eliminate this distortion, the Layer cure

model should be calibrated. The Inverse Layer cure model using the database generated by the calibrated Layer cure model will allow us to cure layers accurately.

Figure 7. 7 Experimental layer cured on the system

Summary

The Inverse Layer cure model returns the values of process parameters used to cure a layer of the required dimensions. Thus, this model is the Process planning method which we set out to develop. The accuracy of the Inverse Layer cure model is within 25μm. It can be seen that there is some amount of distortion produced in the layer. Calibration can greatly improve the performance.

CHAPTER 8

CLOSURE AND CONTRIBUTIONS

In this chapter, the research questions posed in Chapter 1 are answered by testing the proposed hypotheses [Section 8.1]. The contributions of this research to the field of Mask projection Micro Stereolithography are presented in Section 8.2. The scope and limitations of the work presented in this thesis are discussed in Section 8.3. Future research directions are proposed in Section 8.4.

8.1 ANSWERING THE RESEARCH QUESTIONS

In this section, the research questions posed in Chapter 4 are revisited and the proposed hypotheses tested.

The purpose of this research is to develop a process planning method for MPμSLA to obtain dimensionally accurate parts. Any micropart fabricated using the MPμSLA process would consist of a number of layers cured one over the other. The first step of curing dimensionally accurate parts is to be able to cure dimensionally accurate layers. The research focus in this work is limited to obtaining dimensionally accurate layers. The research objective stated in Chapter 4 is restated here:

"To develop a process planning method to cure dimensionally accurate layers using the MPμSLA process"

This objective is broken down into research questions and hypotheses are proposed for each of them. The proposed hypotheses are tested in this section.

Research Question 1: How can lateral dimensions of a layer cured using an MPμSLA system be modeled in terms of the process parameters?

Hypothesis 1: The lateral dimensions of a cured layer can be modeled by modeling the layer curing process (Layer cure model) in two steps:

- Modeling the irradiance received by the resin surface in terms of the process parameters by following the ray tracing procedures
- Empirically modeling the curing process that occurs in a resin upon receiving irradiation

Testing the hypothesis: In Chapter 6, the Irradiance model is formulated which computes the irradiance received at every point on the resin surface in terms of the process parameters. A ray tracing procedure has been adopted to solve the Irradiance model. The resin has been characterized and the Cure model has been formulated in the same chapter. The Cure model computes the lateral dimensions of a cured layer in terms of the irradiance received by the resin surface and the resin parameters. These two models are combined to formulate the Layer cure model. The Layer cure model has been validated in Chapter 6. Thus, the hypothesis has been tested and has been found to be valid.

Research Question 2: How can a process planning method be formulated for the MPμSLA process in order to cure dimensionally accurate layers?

Hypothesis 2: A process planning method can be formulated for the MPμSLA process by inverting the Layer cure model (refer Hypothesis 1). The inverse of the Layer cure

model would allow us to determine the values of process parameters required to cure a layer of the required dimensions.

Testing the hypothesis: In Chapter 7, the Inverse Layer cure model was formulated. This model maps the pixels on a cured layer onto the micromirrors on the DMD used to cure those pixels. This mapping is used to determine the micromirrors that need to be turned "ON" and thereby, generate the bitmap to be supplied to the DMD. The bitmap is run through the Irradiance model and then, Beer Lambert's law is used to compute the minimum time of exposure. The process planning methodology has been presented in the form of the following six steps in Chapter 7:

1. Generate a database that relates the location of every micromirror on the DMD with the location of every pixel cured by it on the resin
2. Mesh the intended layer with pixels
3. Snap the pixels to the layer pixels in the database generated in Step 1
4. Using the database generated in Steps 1, determine the micromirrors that shall be turned "ON" on the DMD and thus, bitmap to be fed to the DMD
5. Run the bitmap through the Irradiance model (formulated in Chapter 6) to obtain the irradiance received by the point on the resin receiving the minimum irradiance
6. Determine the time of exposure so that the entire exposed area on the resin cures down to a depth of one layer thickness or more

This process planning method has been tested in a case study presented in Chapter 7. Thus, by formulating the Layer cure model in Chapter 6 and obtaining its inverse to formulate the process planning method for curing dimensionally accurate layers, Hypothesis 2 has been validated.

Research Question 3: How can the theoretical limit on lateral resolution on the MPμSLA system be determined?

Hypothesis 3: The theoretical limiting resolution of the MPμSLA system can be determined by using the process planning method developed as a response to the Research Question 1 to compute the process variable values used to obtain the best possible lateral resolution

Testing the hypothesis: In Chapter 6, the limiting lateral positive resolution of the system has been computed to be 2.1μm. The Layer cure model has been found to be valid for even small feature sizes and so, the limiting resolution computed using it can be assumed to be correct.

However, this hypothesis might not be valid for all the MPμSLA systems. For systems with sophisticated imaging systems, the aberration effects would become negligible and diffraction effects will be predominant. So, for other systems, it is better to take into account the diffraction effects while computing the theoretical limit on resolution.

8.2 CONTRIBUTIONS

Process planning literature available for the conventional laser scanning Stereolithography allows a manufacturer to build prototypes with the required properties. This literature can't be directly extended to Mask Projection micro Stereolithography because the nature of irradiation of the resin surface and curing characteristics of a resin are considerably different in both the cases. The irradiation of the resin surface in the case of MPμSLA is a much more complex process than that achieved by laser scanning. While

the laser beam has a Gaussian irradiance profile, which remains constant regardless of the cross section it is scanning, in case of MPμSLA, the irradiation distribution changes with the change in the pattern imaged.

The primary contributions of this work are in the realm of analyzing the MPμSLA process and explaining it in mathematical terms. The following are the contributions of the thesis to the field of MPμSLA:

1. It has been shown that the method of ray tracing can be satisfactorily used to model the irradiation of the resin surface.
2. The effects of the various process parameters on the layer dimensions have been quantified. This model can be extended to parts consisting of a number of layers. This will enable a manufacturer to obtain dimensionally accurate parts.
3. The analytical model will enable the designer of an MPμSLA system to assign optimum values to the process parameters fixed by the system's design.
4. The DSM SOMOS 10120 resin has been characterized and it has been shown that its behavior under an MPμSLA system is different from that under a scanning Stereolithography system.

8.3 SCOPE AND LIMITATIONS OF THIS RESEARCH

This research had the objective of formulating a process planning method for Mask projection micro Stereolithography. The system that has been developed is a very simple embodiment of the MPμSLA principle. The process planning method has been developed for the layer curing process using this system. This method can be leveraged across to most of the MPμSLA systems. In case of systems with very sophisticated

imaging systems, the aberrations will be negligible and the diffraction effects will dominate. In this case, the ray tracing might be insufficient to model the image formation process because the shape of the aerial image as well as the irradiance across it will be dictated by the diffraction occurring at the lenses and at the mask. So, the scope of this work is limited strictly to MPμSLA systems for which the diffraction effects are negligible.

A limitation of this research is that a commercial resin (DSM SOMOS 10120) was used and characterized. The chemical composition of this resin is kept secret by DSM for commercial reasons and there is some uncertainty as regards the curing reactions that occur in the resin. As a result, the discrepancy observed in the working curve plotted using the MPμSLA system cannot be chemically explained.

In the Irradiance model, the alignment of all the optical components of the system is assumed to be perfect. Since the system is assembled manually, we expect some misalignments in the system. The effects of these misalignments have not been captured by the analytical model. As a result, there is still some discrepancy in the layer dimensions computed by the Layer cure model and the dimensions of the layer actually cured using the system. This would require calibration of the Layer cure model.

8.4 FUTURE WORK

The following directions for future work have been identified:

Quantification of print through and overcure errors

When a layer is cured using the MPμSLA system, its thickness is equal to the depth where the exposure falls to the threshold exposure E_c. The resin below this cured

layer, though not receiving exposure equal to E_c, receives some exposure nevertheless. As more and more layers get cured, this point in the resin receives more and more exposure and finally, undergoes curing when the total exposure received by it equals or exceeds E_c. This results in unwanted curing and the error introduced is called as the print-through error.

Overcure error occurs when a single layer forms an overhang on any surface. The irradiation distribution across a typical aerial image formed by imaging a bitmap on the resin surface is such that the central part of the image gets overexposed. As a result, the central portion of any layer will get cured to a depth larger than the intended layer thickness. The resulting error in the Z dimension of the micropart is referred to as the overcure error.

Print through and overcure errors were not a concern in this thesis because the research objective was only to cure dimensionally accurate layers. If we want to manufacture dimensionally accurate 3D parts, there errors will have to be minimized. Just like in conventionally Stereolithography, the print through errors can be minimized by a method called “Layer compensation”, where a few bottom layers are deliberately skipped to compensate for the unwanted curing that occurs due to print through. Overcure errors can be eliminated by decreasing the time for which the bitmap is imaged onto the resin surface.

As a future work, the process planning method formulated in this thesis can be extended to compute the compensations required to control the print through and overcure errors.

Calibration of the Layer cure model

In Chapter 6, the Layer cure model has been validated. It has been observed that there is a slight discrepancy between the analytical solution and the experimental solution. This discrepancy is because of certain misalignments that might exist in the optical system. These distortions can be eliminated by calibrating the Layer cure model.

Modifications in the design of the MPμSLA system

The current MPμSLA system was designed with the purpose of formulating a process planning method for any general system. So, it was a very simple embodiment of the MPμSLA principle. Now that we have validated the process planning method, it is possible to modify the optical setup of the system, more specifically the imaging setup of the system to improve the resolution obtained.

Another improvement in the system's design can be by incorporating an XY stage. Currently, the ratio:

$$\frac{\text{Positive lateral resolution of the system}}{\text{Maximum area that can be cured by the system}}$$

for the MPμSLA system is 1e-6. The smaller this ratio the better. For the SLA Viper system, this ratio is 6.2e-9. This ratio is an important measure of the applicability of any manufacturing system. For example, it is not possible to fabricate assemblies consisting of too many parts using the MPμSLA system because while on one hand the number of components in the assembly is limited by the maximum area that can be cured, the miniaturization of the components of the assembly is limited by the system's resolution.

The ratio can be improved by incorporating an XY stage in the system to move the cured micropart underneath the imaging system. This will increase the maximum area of that can be cured while keeping the resolution same.

APPENDIX A

DRAWINGS AND BILL OF MATERIALS OF THE MASK PROJECTION MICRO STEREOLITHOGRAPHY SYSTEM

The Front view, the Top view and the Bill of materials of the Mask Projection Micro Stereolithography system are presented on subsequent pages.

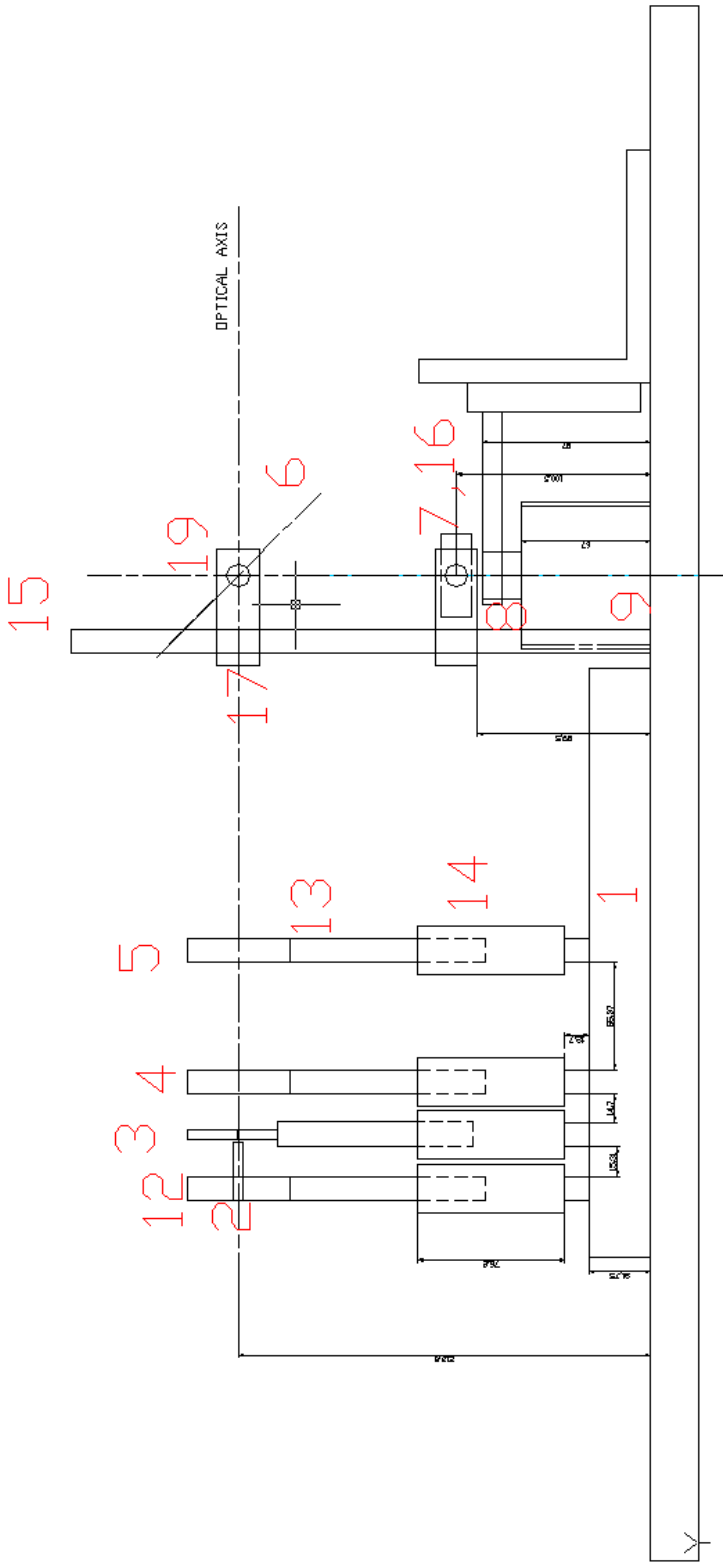

Figure A. 1 Front View of the MPμSLA system

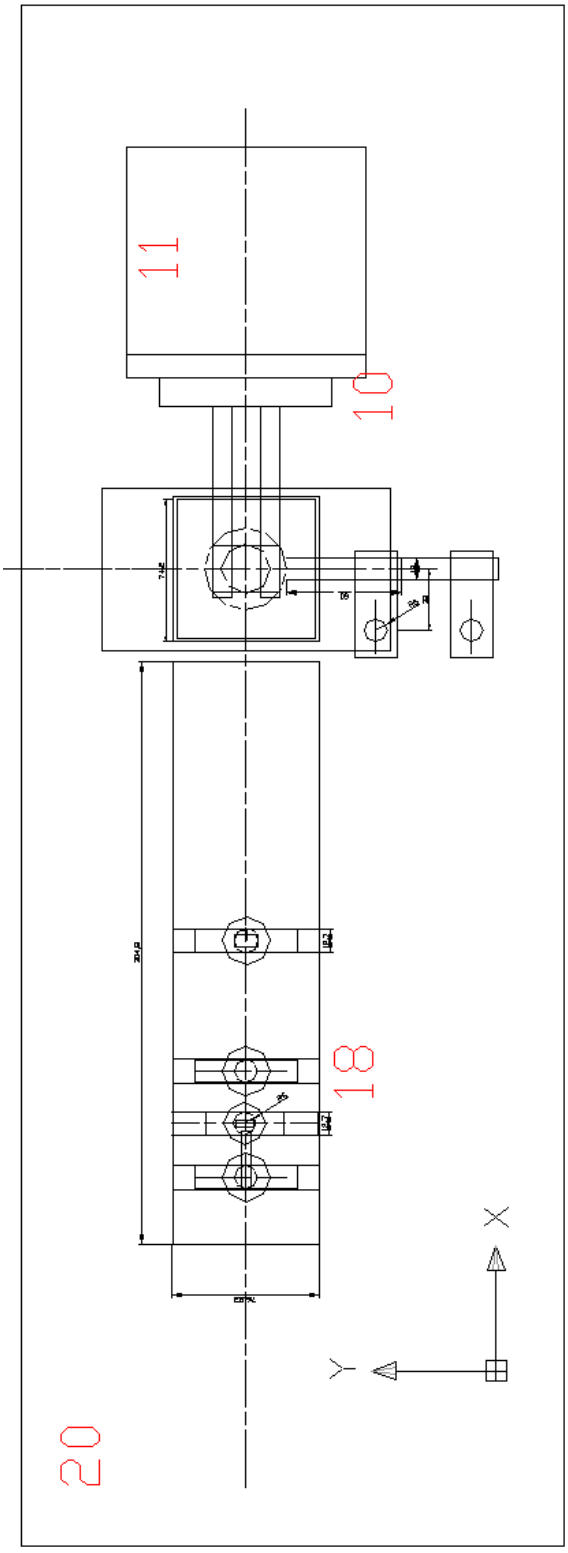

Figure A. 2 Top view of the MPμSLA system

Table A. 1 Bill of Materials for the MPμSLA system

BILL OF MATERIALS						
Component #	Component	Manufacturer	Stock #	#	Cost per component ($)	Total cost
1	Dovetail optical rail	Edmund Optics	H54-401	1	99.7	99.7
2	UV lamp	Edmund Optics	NT56-767	1	2000	2000
3	Iris diphragm	Edmund Optics	H53-914	1	48.3	48.3
4	Collimating lens	Edmund Optics	H45-082	1	23.9	23.9
5	Filter	Edmund Optics	H43-051	1	68.9	68.9
6	Digital Micromirror Device	PSI	DMD1100	1	8000	8000
7	Imaging lens	Edmund Optics	H46-292	1	103.8	103.8
8	Platform			1		0
9	Vat			1		0
10	Translation stage	Newport	UMR8.25	1	233	233
	Micrometer	Newport	DM-17-25	1	373	373
11	Right angle bracket	Edmund Optics	H55-378	1	82.5	82.5
12	Three screw mount	Edmund Optics	H03-668	3	61.8	185.4
13	Mounting post (english)	Edmund Optics	H36-499	6	9.5	57
14	Post holder	Edmund Optics	H03-647	4	14.3	57.2
15	Mounting post (metric)	Edmund Optics	H54-942	2	13.2	26.4
16	Optical mount	Edmund Optics	H56-762	1	72.6	72.6
17	Metric cross clamp	Edmund Optics	H54-969	2	38.5	77
18	Micro Vice	Oriel	20846	1		0
19	Dovetail carrier	Edmund Optics	H54-403	4	49.5	198
20	Optical breadboard	Oriel	20846	1	1650	1650
Miscellaneous components and purchases						
	Socket head screws (M)	Edmund Optics	H55-194	1	12.5	12.5
		Edmund Optics	H55-195	1	11.4	11.4
	Socket head screws (E)	Edmund Optics	H55-177	1	11.4	11.4
		Edmund Optics	H55-178	1	10.4	10.4
	Allen Wrenches	Edmund Optics	H55-200	1	7	7
	Goggles	Edmund Optics	H55-162	4	62.95	251.8
					TOTAL COST ($)	**13661.2**

(not inclusive of taxes and shipping charges)

APPENDIX B

CHARACTERIZING THE RESIN

In this appendix, the microscope-pictures of the polymer threads cured in order to plot the working curve of the DSM SOMOS 10120 water clear resin are documented. This appendix is referenced in Chapter 6.

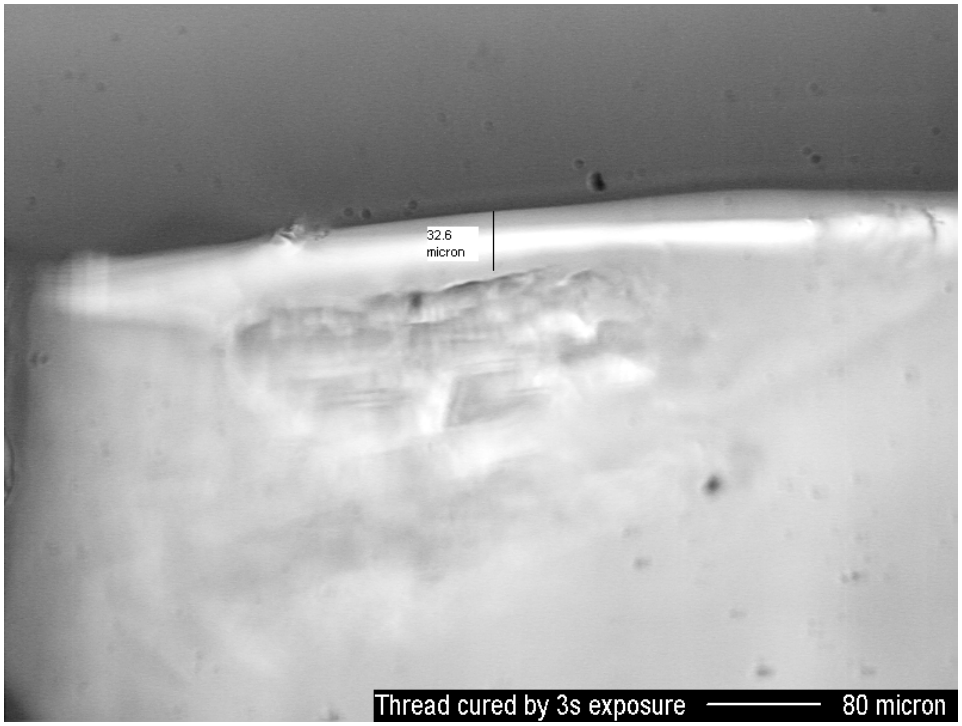

Figure B. 1 Polymer thread cured by 3s exposure

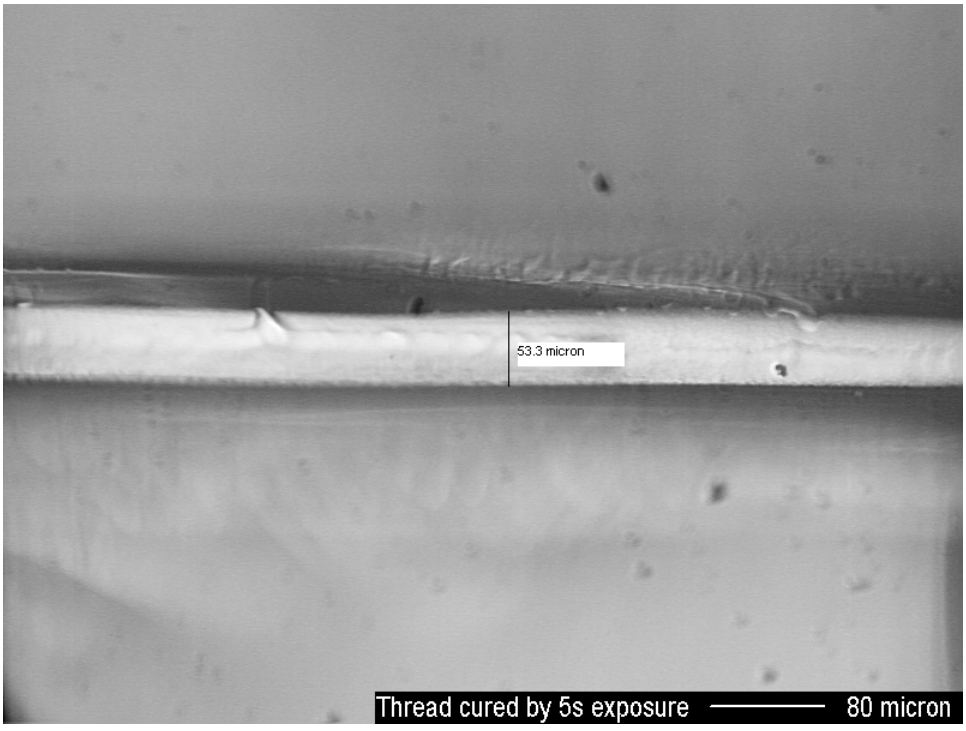

Figure B. 2 Polymer thread cured by 5s exposure

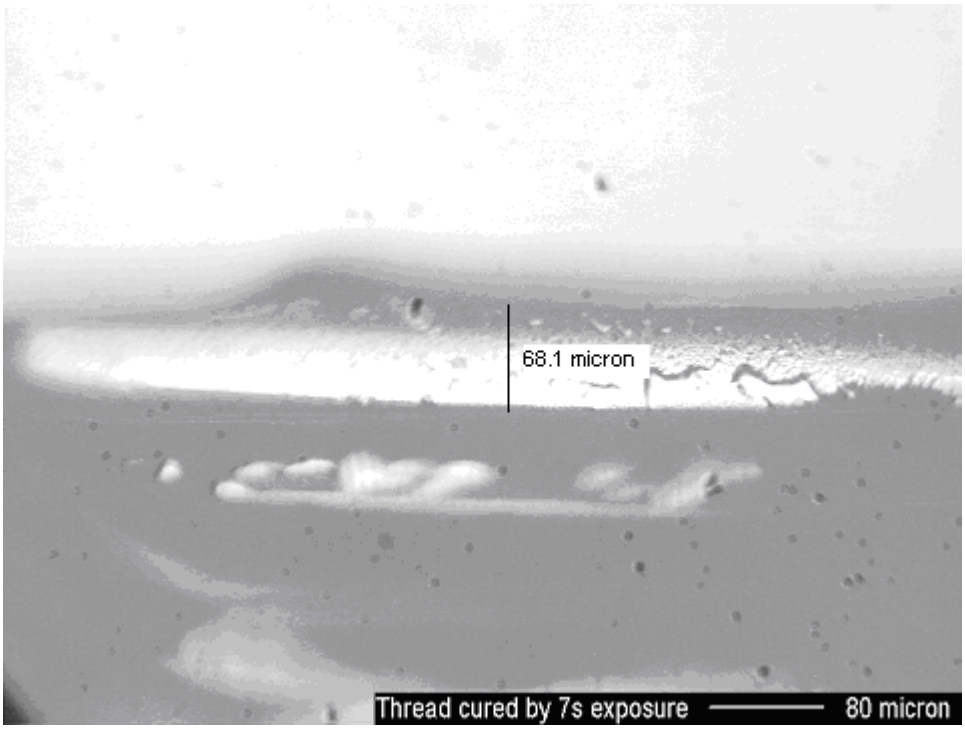

Figure B. 3 Polymer thread cured by 7s exposure

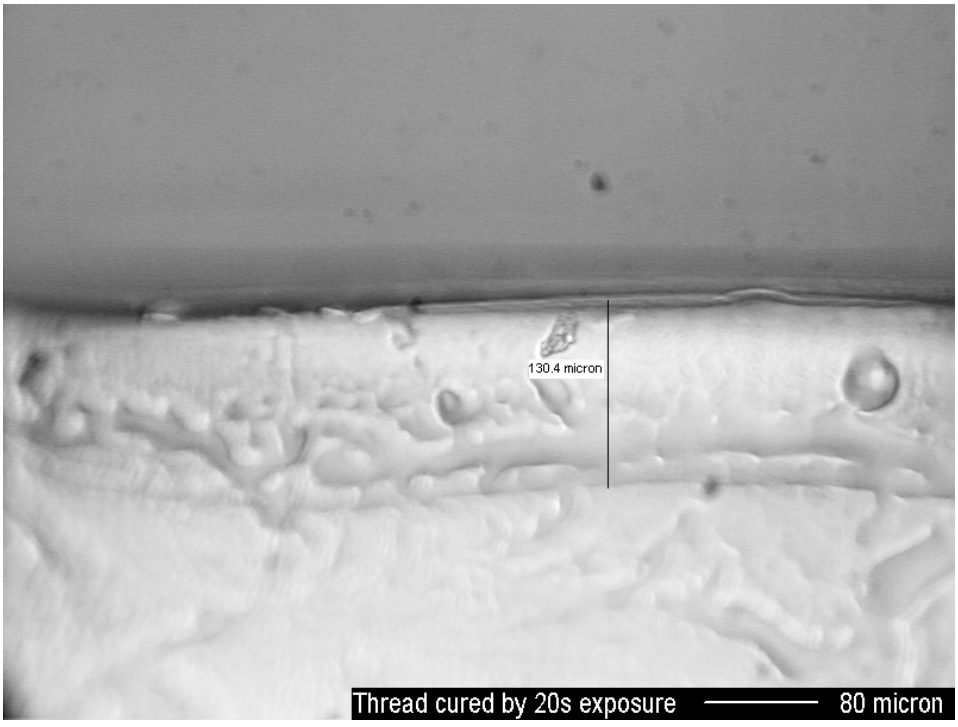

Figure B. 4 Polymer thread cured by 20s exposure

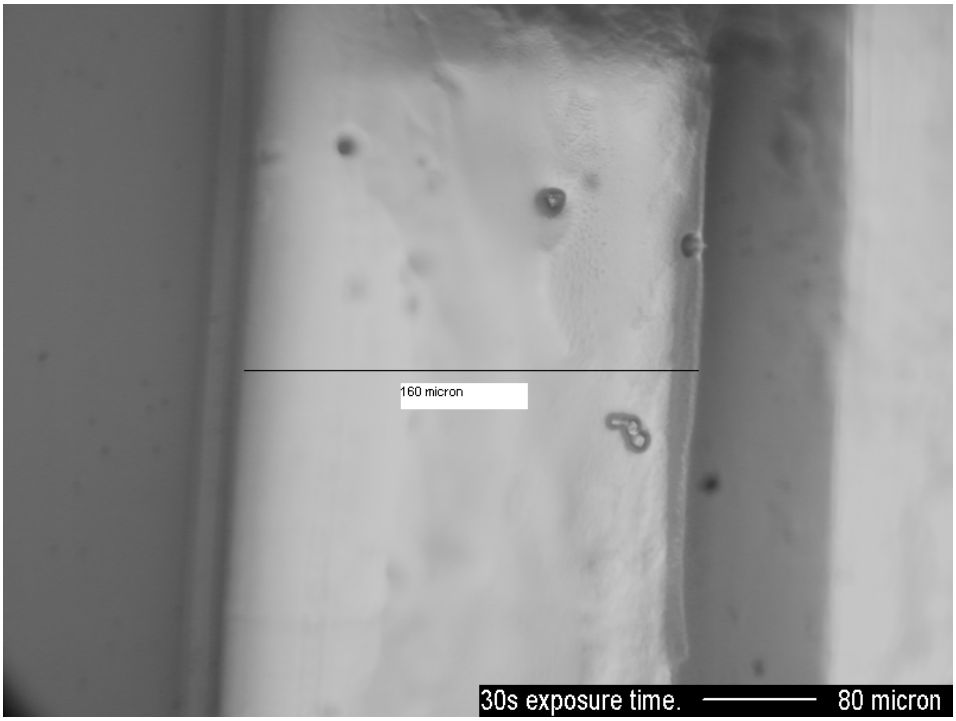

Figure B. 5 Polymer thread cured by 30s exposure

APPENDIX C

CODE FOR EXECUTING LAYER CURE MODEL

In this section, the Matlab code used to execute the layer cure model described in Chapter 6 is presented.

```
%Matlab script written to model the aerial image and the irradiance
%distribution across the image for arrow shaped bitmap

%Script written by Ameya on 8th July 2004


clear all;
%Inputing the Imaging system parameters:
c(1) = 0; % c is the curvature of surface
c(2) = 0.046664;
c(3) = -0.046664;
c(4) = 0;
t(2) = 10.9; %t is the distance
t(3) = 32.95-5.45;
objectdistance = 113;
N(1) = 1; %N is the refractive index
N(2) = 1.45848;
N(3) = 1;
DMDangley = 7.052*3.142/180;
DMDanglez = 52.052*3.142/180; %This is the angle at which the DMD is mounted to the horizontal


%**************************************************************************
raycount = 1;
%Getting the extents of the bitmap
bitmap_ysize = 200;
bitmap_zsize = 100;
%Specifying the offsets
y_offset = -100;
z_offset = 0;
bitmap_ymin = (y_offset - bitmap_ysize/2)*13.7/1000*cos(DMDangley);
bitmap_ymax = (y_offset + bitmap_ysize/2)*13.7/1000*cos(DMDangley);
bitmap_zmin = (z_offset - bitmap_zsize/2)*13.7/1000*cos(DMDanglez);
bitmap_zmax = (z_offset + bitmap_zsize/2)*13.7/1000*cos(DMDanglez);

%**************************************************************************

%Meshing the bitmap in a meshy x meshz grid.
meshy = 125 %Mesh spacing = 200/80 = 2.5 micromirrors
meshz = (meshy/2*sin(45*3.142/180))
temp_stepy = bitmap_ysize*13.7*cos(DMDangley)/1000/meshy;
temp_stepz = bitmap_zsize*13.7*cos(DMDanglez)/1000/meshz;
tempcount = 1;
for tempy = (bitmap_ymin:temp_stepy:bitmap_ymax);
    bitmap_y(tempcount) = tempy;
    tempcount = tempcount + 1;
end
clear tempcount;
tempcount = 1;
for tempz = (bitmap_zmin:temp_stepz:bitmap_zmax);
   bitmap_z(tempcount) = tempz;
   tempcount = tempcount + 1;
end
clear temp_stepy, temp_stepz, tempy, tempz;
```

```
%The mesh has been stored as bitmap_y and bitmap_z



%**************************************************************************

%Selecting the point on the bitmap grid and calculating the object distance
%for it
for count_ybitmap = (1:1:meshy + 1);
   for count_zbitmap = (1:1:meshz + 1);
      startpoint_y = bitmap_y(count_ybitmap);
      startpoint_z = bitmap_z(count_zbitmap);
      %Now, the distance of the pattern-point from the center of the beam
      %is calculated. This distance is stored as p and then the weight of
      %the rays emitting from this point are calcuated as the column
      %matrix w
      p = sqrt(startpoint_y^2*sin(DMDangley) + (startpoint_z*sin(DMDanglez))^2);
      t(1) = objectdistance - 5.45 - startpoint_z*tan(DMDanglez) - startpoint_y*tan(DMDangley);

%**************************************************************************


            pupilpoint_y = startpoint_y;
            pupilpoint_z = startpoint_z;
            length = sqrt((pupilpoint_y-startpoint_y)^2 + (pupilpoint_z-startpoint_z)^2 + 100^2);
            X(1) = 100/length;
            Y(1) = (pupilpoint_y-startpoint_y)/length;
            Z(1) = (pupilpoint_z-startpoint_z)/length;

%**************************************************************************

 %Tracing the ray through the lens
            x(1) = 0;
            y(1) = startpoint_y;
            z(1) = startpoint_z;
            for (i = 2:1:3)
               %Transfer equations
               e(i) = t(i-1)*X(i-1) - (x(i-1)*X(i-1) + y(i-1)*Y(i-1) + z(i-1)*Z(i-1));
               Mx(i) = x(i-1) + e(i)*X(i-1) - t(i-1);
               Msquare(i) = x(i-1)^2 + y(i-1)^2 + z(i-1)^2 - e(i)^2 + t(i-1)^2 - 2*t(i-1)*x(i-1);
               E(i) = sqrt(X(i-1)^2 - c(i)*(c(i)*Msquare(i) - 2*Mx(i)));
               L(i) = e(i) + (c(i)*Msquare(i) - 2*Mx(i))/(X(i-1)+E(i));
               x(i) = x(i-1) + L(i)*X(i-1) - t(i-1);
               y(i) = y(i-1) + L(i)*Y(i-1);
               z(i) = z(i-1) + L(i)*Z(i-1);

               %Refarction equations
                Edash(i) = sqrt(1- ((N(i-1)/N(i))^2) * (1-E(i)^2));
               g(i) = Edash(i) - ((N(i-1)/N(i)))*E(i);
               X(i) = (N(i-1)/N(i))*X(i-1) - g(i)*c(i)*x(i) + g(i);
               Y(i) = (N(i-1)/N(i))*Y(i-1) - g(i)*c(i)*y(i);
               Z(i) = (N(i-1)/N(i))*Z(i-1) - g(i)*c(i)*z(i);

            end
```

```
            %Transfer equations from last lens surface to image plane
          for i = 4;
            e(i) = t(i-1)*X(i-1) - (x(i-1)*X(i-1) + y(i-1)*Y(i-1) + z(i-1)*Z(i-1));
            Mx(i) = x(i-1) + e(i)*X(i-1) - t(i-1);
            Msquare(i) = x(i-1)^2 + y(i-1)^2 + z(i-1)^2 - e(i)^2 + t(i-1)^2 - 2*t(i-1)*x(i-1);
            E(i) = sqrt(X(i-1)^2 - c(i)*(c(i)*Msquare(i) - 2*Mx(i)));
            L(i) = e(i) + (c(i)*Msquare(i) - 2*Mx(i))/(X(i-1)+E(i));
            x(i) = x(i-1) + L(i)*X(i-1) - t(i-1);
            y(i) = y(i-1) + L(i)*Y(i-1);
            z(i) = z(i-1) + L(i)*Z(i-1);
          end
%*************************************************************************
%Recording the position of the ray on the image plane
            xpos(raycount) = x(i);
            ypos(raycount) = y(i);
            zpos(raycount) = z(i);
            w(raycount) = 1 - 0.00086*p - 0.00883*p*p;
            raycount = raycount + 1;
%The points of intersection with the image plane are recorded as xpos, ypos,
%zpos;
%*************************************************************************

   end
end
%Here ends the loops selecting the point on the bitmap.

%*************************************************************************
%*************************************************************************
%Now starts the code to plot the traingle of the arrow. The triangle is
%400 pixels base and 200 pixels height.

triangle_raycount = 1;
%Getting the extents of the bitmap
triangle_ysize = 200;
triangle_zsize = 400;
%Specifying the offsets
y_offset = 100;
z_offset = 0;
triangle_ymin = (y_offset - triangle_ysize/2)*13.7/1000;
triangle_ymax = (y_offset + triangle_ysize/2)*13.7/1000;
triangle_zmin = (z_offset - triangle_zsize/2)*13.7/1000;
triangle_zmax = (z_offset + triangle_zsize/2)*13.7/1000;

%*************************************************************************
%Meshing the tirangle
temp_stepy = triangle_ysize*13.7/1000/meshy;
temp_stepz = 0.0137*(200/meshy)*sin(45*3.142/180);
tempcount = 1;
for tempy = (triangle_ymin:temp_stepy:triangle_ymax)
   for tempz = (triangle_zmin+tempy:temp_stepz:triangle_zmax-tempy)
      triangle_bitmap_y(tempcount) = tempy*cos(DMDangley);
      triangle_bitmap_z(tempcount) = tempz*cos(DMDanglez);
   tempcount = tempcount + 1;
```

```
   end
end
clear temp_stepy, temp_stepz, tempy, tempz;
triangle_size = size(triangle_bitmap_y);
%The mesh has been stored as bitmap_y and bitmap_z

%*************************************************************************

%Now, the points on the triangular part of bitmap are selected and rays are
%traced

%Selecting the point on the bitmap grid and calculating the object distance
%for it
for count_triangle = (1:1:max(triangle_size))
      startpoint_y = triangle_bitmap_y(count_triangle);
      startpoint_z = triangle_bitmap_z(count_triangle);
      %Now, the distance of the pattern-point from the center of the beam
      %is calculated. This distance is stored as p and then the weight of
      %the rays emitting from this point are calcuated as the column
      %matrix w
      p = sqrt(startpoint_y^2*sin(DMDangley) + (startpoint_z*sin(DMDanglez))^2);
      t(1) = objectdistance - 5.45 - startpoint_z*tan(DMDanglez) - startpoint_y*tan(DMDangley);

%*************************************************************************

            pupilpoint_y = startpoint_y;
            pupilpoint_z = startpoint_z;
            length = sqrt((pupilpoint_y-startpoint_y)^2 + (pupilpoint_z-startpoint_z)^2 + 100^2);
            X(1) = 100/length;
            Y(1) = (pupilpoint_y-startpoint_y)/length;
            Z(1) = (pupilpoint_z-startpoint_z)/length;

%*************************************************************************

 %Tracing the ray through the lens
            x(1) = 0;
            y(1) = startpoint_y;
            z(1) = startpoint_z;
            for (i = 2:1:3)
               %Transfer equations
               e(i) = t(i-1)*X(i-1) - (x(i-1)*X(i-1) + y(i-1)*Y(i-1) + z(i-1)*Z(i-1));
               Mx(i) = x(i-1) + e(i)*X(i-1) - t(i-1);
               Msquare(i) = x(i-1)^2 + y(i-1)^2 + z(i-1)^2 - e(i)^2 + t(i-1)^2 - 2*t(i-1)*x(i-1);
               E(i) = sqrt(X(i-1)^2 - c(i)*(c(i)*Msquare(i) - 2*Mx(i)));
               L(i) = e(i) + (c(i)*Msquare(i) - 2*Mx(i))/(X(i-1)+E(i));
               x(i) = x(i-1) + L(i)*X(i-1) - t(i-1);
               y(i) = y(i-1) + L(i)*Y(i-1);
               z(i) = z(i-1) + L(i)*Z(i-1);

               %Refarction equations
                Edash(i) = sqrt(1- ((N(i-1)/N(i))^2) * (1-E(i)^2));
               g(i) = Edash(i) - ((N(i-1)/N(i)))*E(i);
               X(i) = (N(i-1)/N(i))*X(i-1) - g(i)*c(i)*x(i) + g(i);
               Y(i) = (N(i-1)/N(i))*Y(i-1) - g(i)*c(i)*y(i);
```

```
            Z(i) = (N(i-1)/N(i))*Z(i-1) - g(i)*c(i)*z(i);

         end

            %Transfer equations from last lens surface to image plane
         for i = 4;
            e(i) = t(i-1)*X(i-1) - (x(i-1)*X(i-1) + y(i-1)*Y(i-1) + z(i-1)*Z(i-1));
            Mx(i) = x(i-1) + e(i)*X(i-1) - t(i-1);
            Msquare(i) = x(i-1)^2 + y(i-1)^2 + z(i-1)^2 - e(i)^2 + t(i-1)^2 - 2*t(i-1)*x(i-1);
            E(i) = sqrt(X(i-1)^2 - c(i)*(c(i)*Msquare(i) - 2*Mx(i)));
            L(i) = e(i) + (c(i)*Msquare(i) - 2*Mx(i))/(X(i-1)+E(i));
            x(i) = x(i-1) + L(i)*X(i-1) - t(i-1);
            y(i) = y(i-1) + L(i)*Y(i-1);
            z(i) = z(i-1) + L(i)*Z(i-1);
         end
%*************************************************************************
%Recording the position of the ray on the image plane
            triangle_xpos(triangle_raycount) = x(i);
            triangle_ypos(triangle_raycount) = y(i);
            triangle_zpos(triangle_raycount) = z(i);
            triangle_w(triangle_raycount) = 1-0.00086*p-0.00883*p*p;
            triangle_raycount = triangle_raycount + 1;
%The points of intersection with the image plane are recorded as xpos, ypos,
%zpos;
%*************************************************************************

   end

%Here ends the loops selecting the point on the bitmap.
%*************************************************************************
%Plotting the points on the image plane


ypos = -1 * ypos;

triangle_ypos = -1 * triangle_ypos;

plot(zpos,ypos,'.');
hold on;
plot(triangle_zpos, triangle_ypos, '.');
axis equal;

%*************************************************************************
%Measuring the irradiance
%Dividing the resin surface area into a 100x100 grid
%Resin surface considered square from -1 to +1 along both directions
%Creating the grid
x = 25;
temp = 1;
for ygrid = (-1:2/x:1);
   ylocation(temp) = ygrid;
   temp = temp + 1
end
clear temp;
```

```
temp = 1;
for zgrid = (-1:2/x:1);
   zlocation(temp) = ygrid;
   temp = temp + 1;
end
clear temp;

%Select the ray under consideration. Divide its ypos by 0.9. Round it
%off. From the rounded off, determine the value of ylocaton it lies in.
%Same for zpos
%Initializing number_of_rays = 0;
for ytemp = (1:1:(x+1))
   for ztemp = (1:1:(x+1))
      number_of_rays(ytemp, ztemp) = 0;
   end
end
clear ytemp, ztemp;

num_of_rays1 = (meshy+1)*double(int8((meshz+1)))
for temp = (1:1:num_of_rays1)
   y_ray = ypos(temp);
   z_ray = zpos(temp);
   ynumber = y_ray+1;
   znumber = z_ray+1;
   ynumber1 = int8(1 + ynumber/(2/x));
   znumber1 = int8(1 + znumber/(2/x));
   number_of_rays(ynumber1, znumber1) = number_of_rays(ynumber1,znumber1) + w(temp);
end

clear temp;

num_of_rays2 = max(triangle_size)
for temp = (1:1:num_of_rays2)
   y_ray = triangle_ypos(temp);
   z_ray = triangle_zpos(temp);
   ynumber = y_ray+1;
   znumber = z_ray+1;
   ynumber1 = int8(1 + ynumber/(2/x));
   znumber1 = int8(1 + znumber/(2/x));
   number_of_rays(ynumber1, znumber1) = number_of_rays(ynumber1,znumber1) + triangle_w(temp);
end

%now, converting the number_of_rays into irradiance
%for (ytemp = 1:1:(x+1))
 %   for (ztemp = 1:1:(x+1))
  %      irradiance(ytemp,ztemp) = number_of_rays(ytemp,ztemp)*5*x*x*x*0.5/1027/25
  % end
  %end

%Totalling the number of weights.
clear temp;
sigmaw = 0;
for temp = 1:1:raycount-1;
   sigmaw = sigmaw + w(temp);
```

```
end
clear temp;
for temp = 1:1:triangle_raycount-1;
    sigmaw = sigmaw + triangle_w(temp);
end

  irradiance= 5*number_of_rays*x*x/(sigmaw);
```

APPENDIX D

VALIDATING THE LAYER CURE MODEL

In this appendix, the microscope pictures of the 15 arrow shaped layers cured in resin to validate the Layer cure model are presented. This appendix is referenced in Chapter 6.

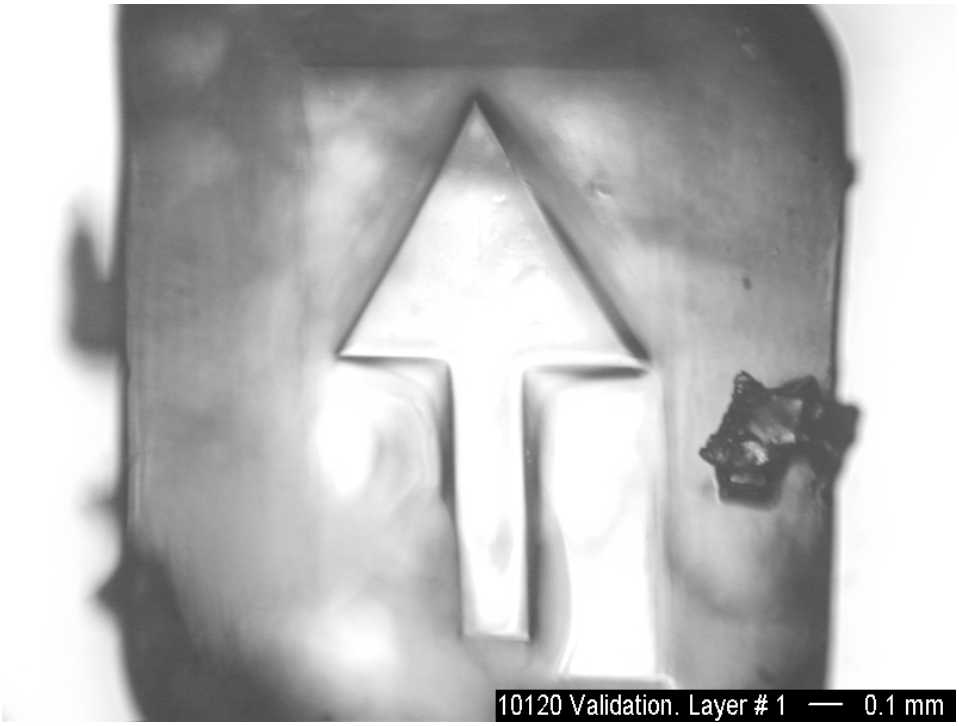

Figure D. 1 Validation layer 1

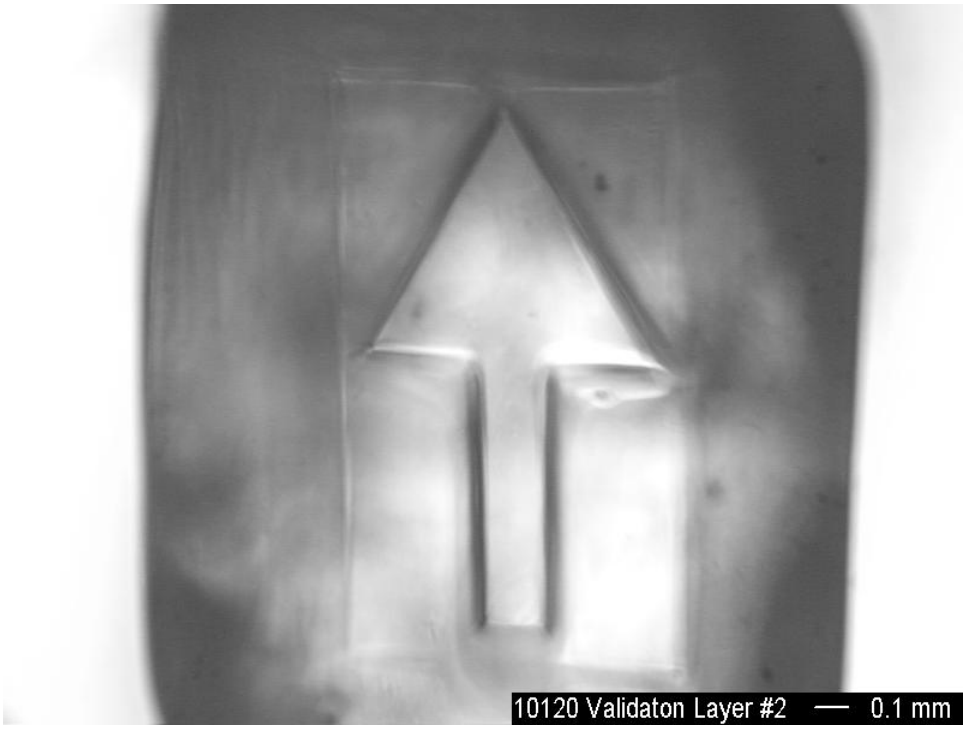

Figure D. 2 Validation layer 2

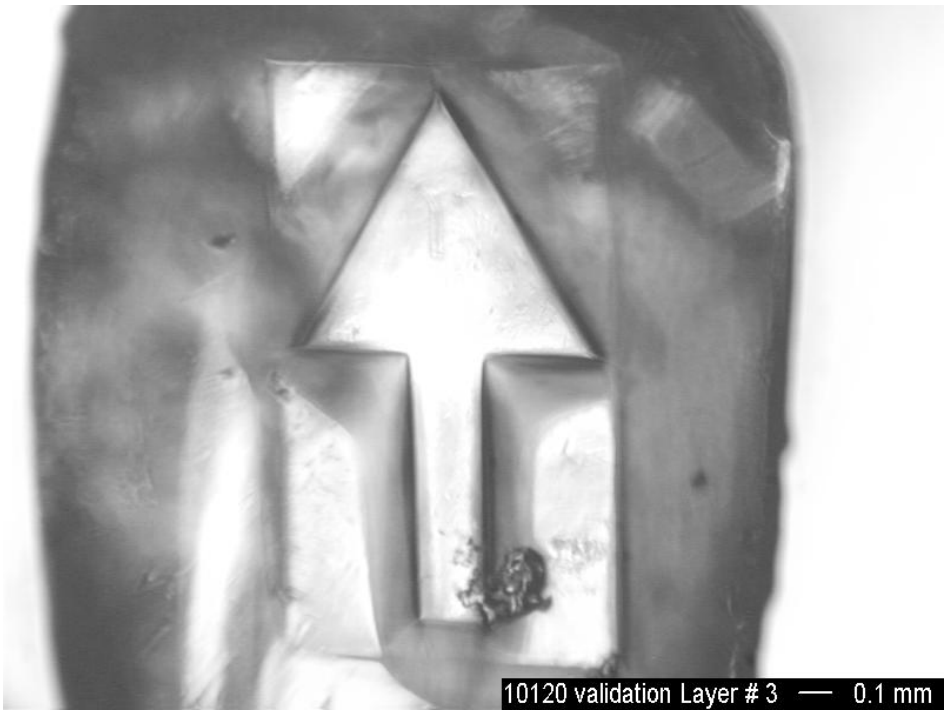

Figure D. 3 Validation layer 3

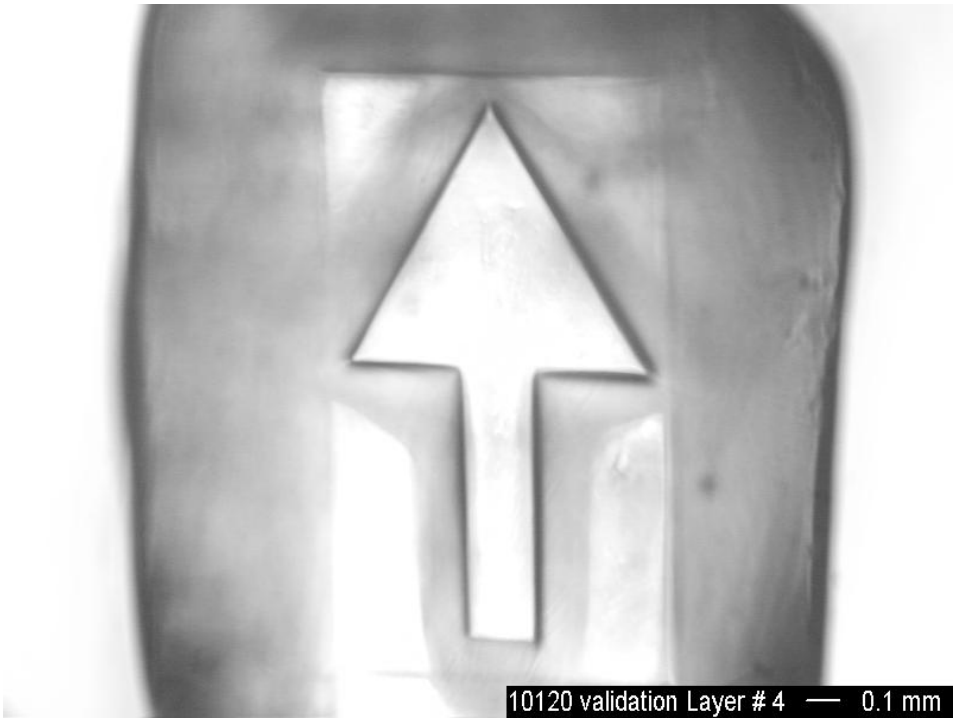

Figure D. 4 Validation layer 4

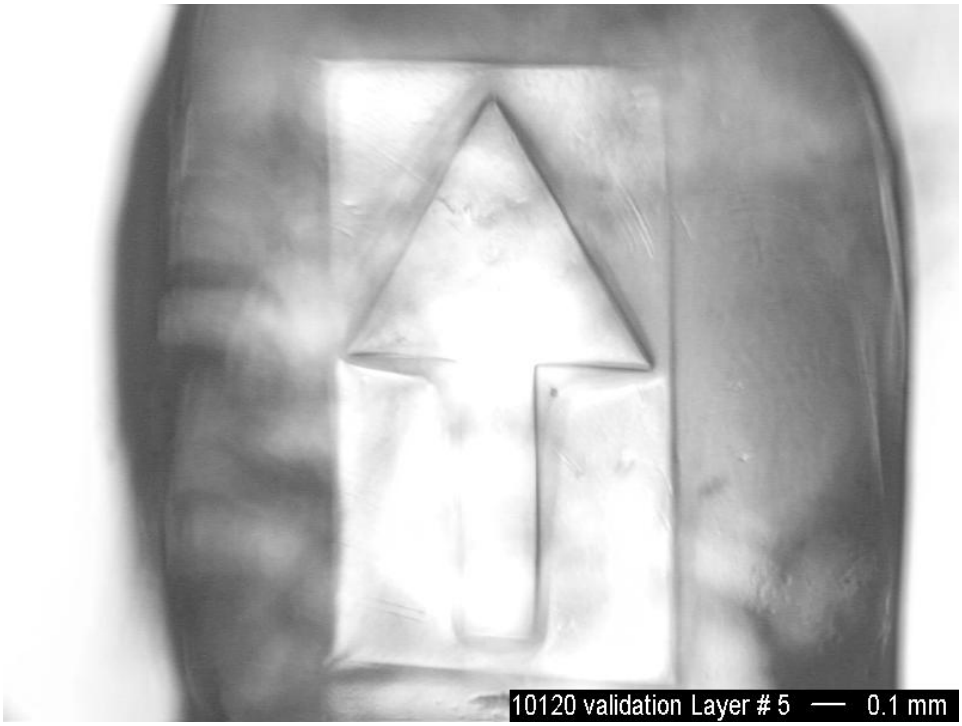

Figure D. 5 Validation layer 5

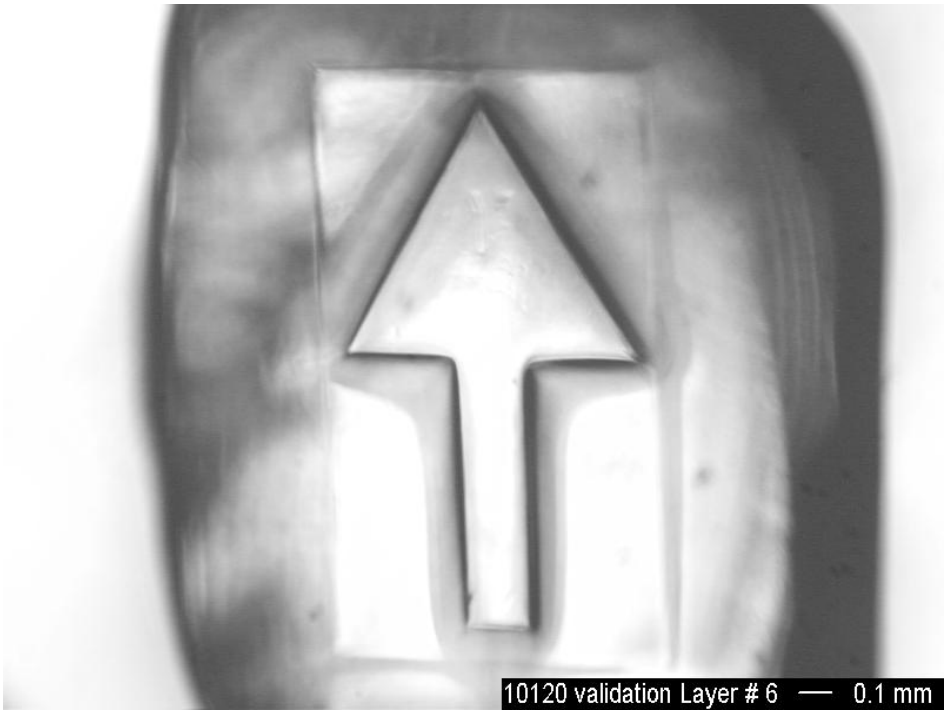

Figure D. 6 Validation layer 6

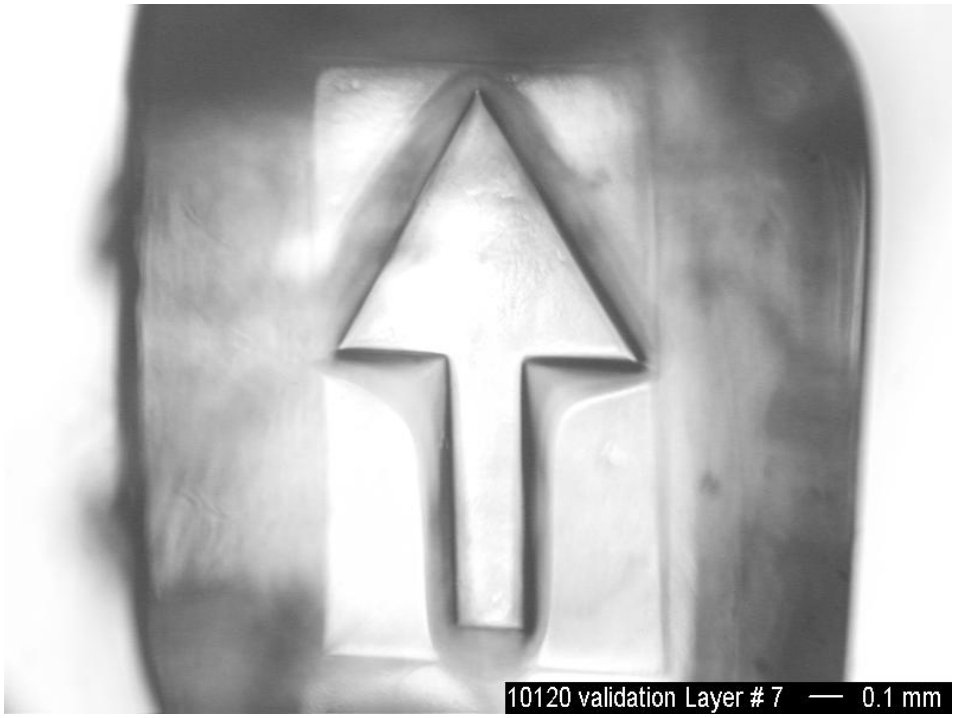

Figure D. 7 Validation layer 7

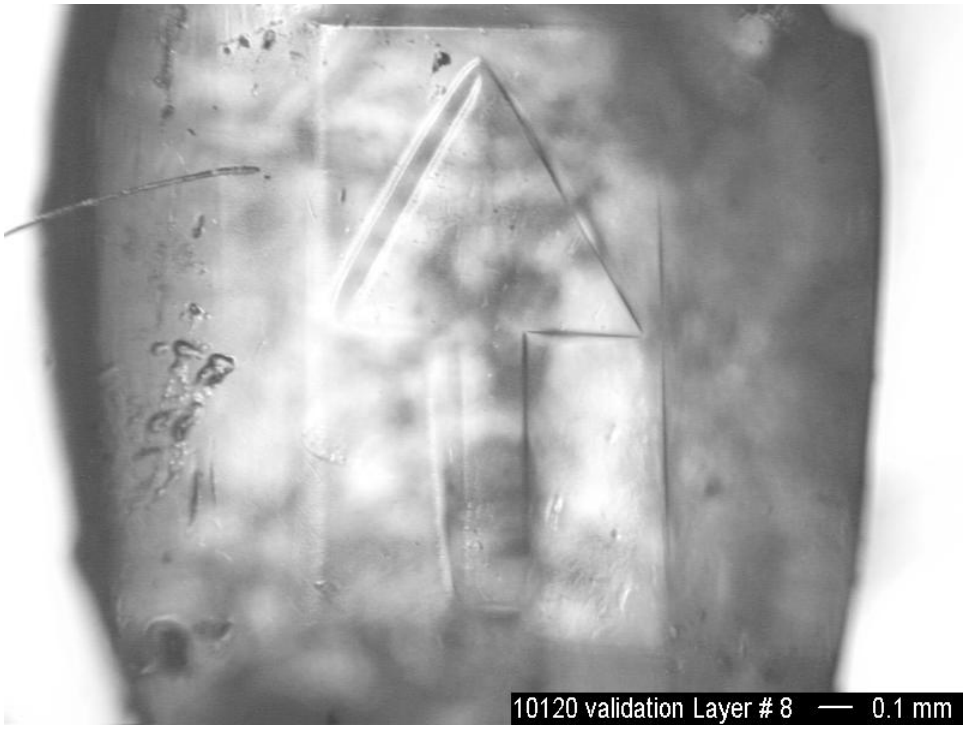

Figure D. 8 Validation layer 8

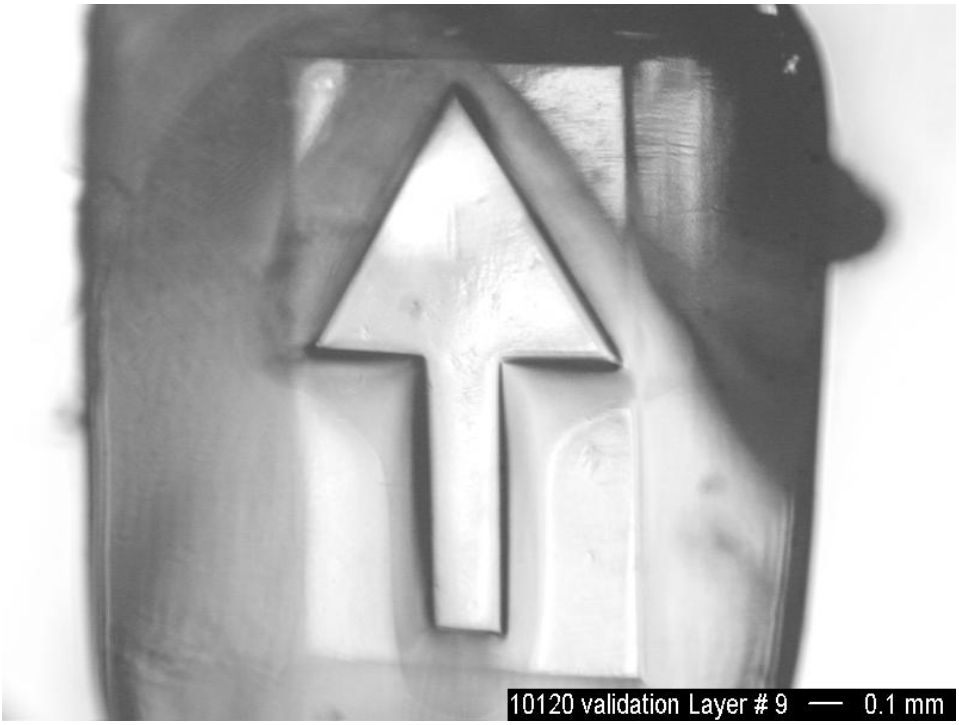

Figure D. 9 Validation layer 9

Figure D. 10 Validation layer 10

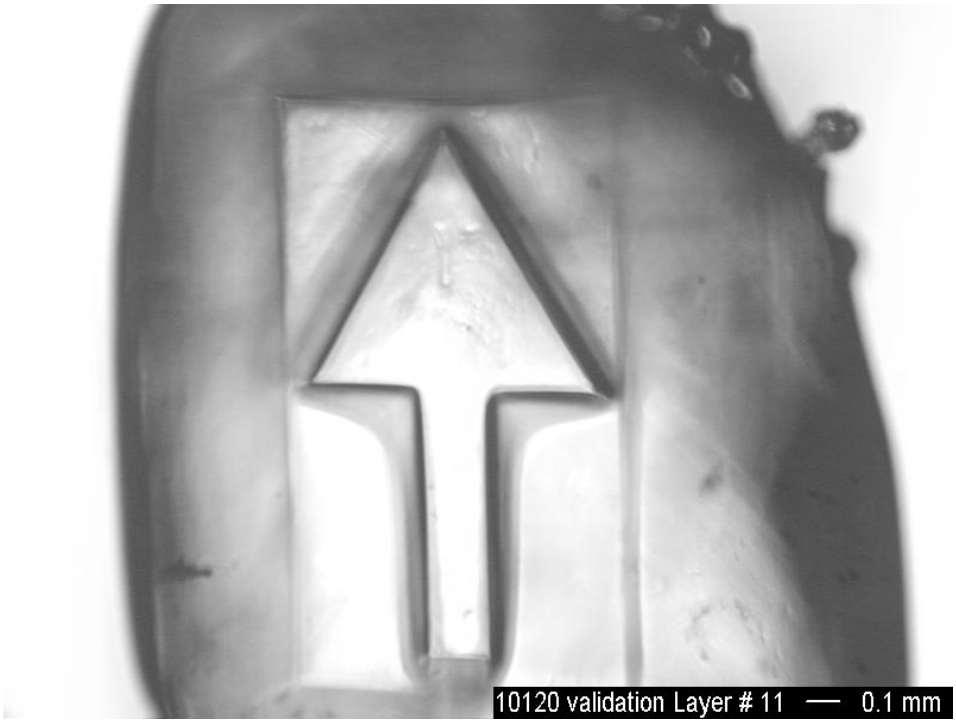

Figure D. 11 Validation layer 11

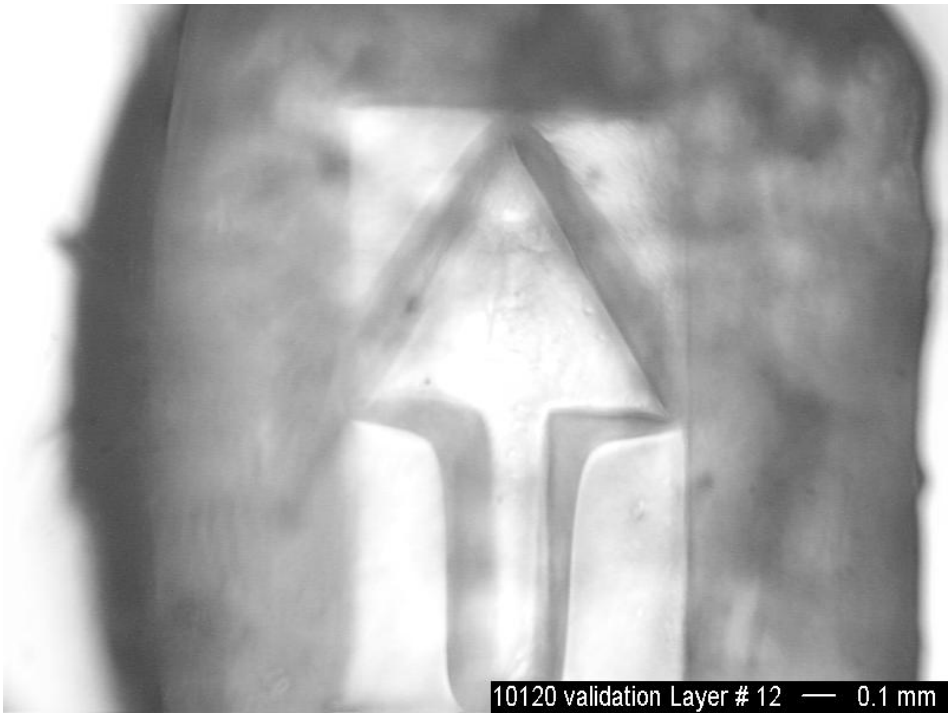

Figure D. 12 Validation layer 12

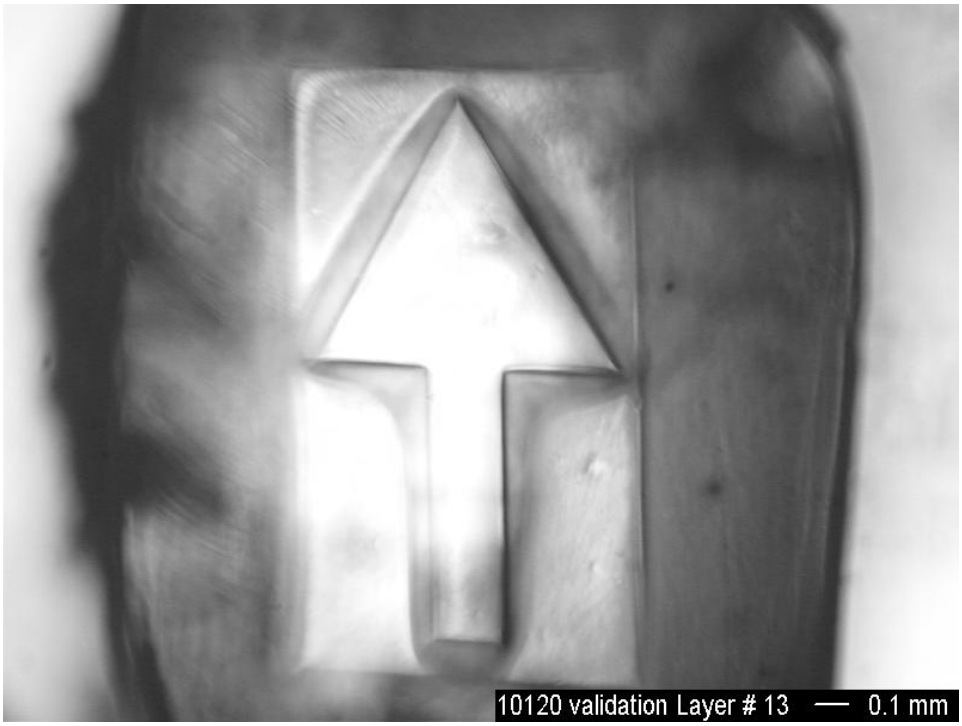

Figure D. 13 Validation layer 13

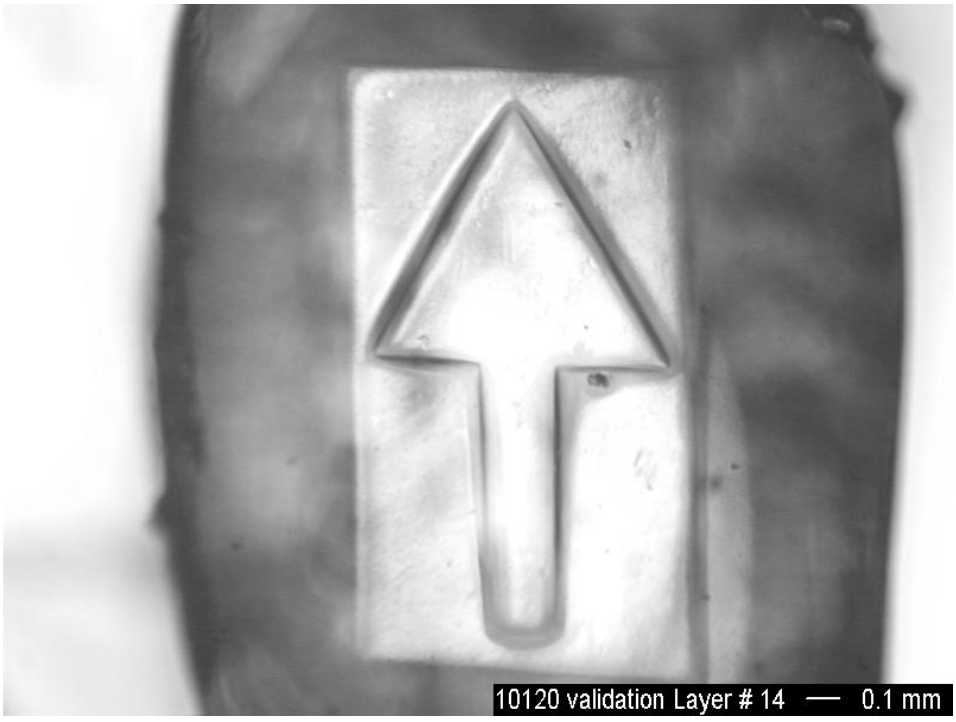

Figure D. 14 Validation layer 14

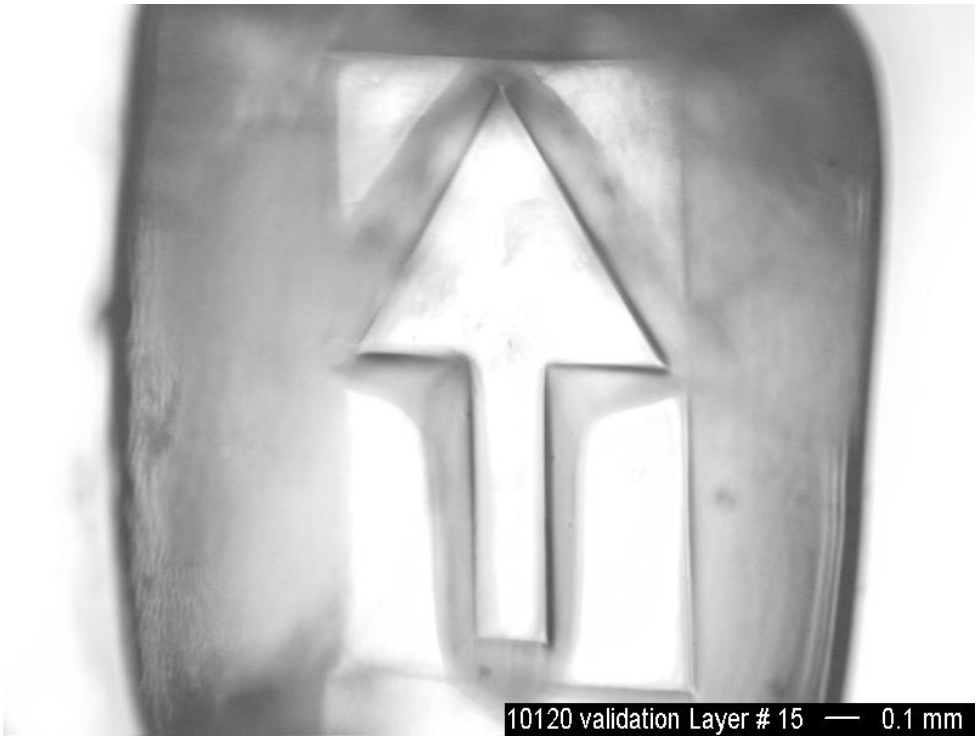

Figure D. 15 Validation layer 15

APPENDIX E

CODE FOR INVERSE LAYER CURE MODEL

In this appendix, the code used to execute the inverse layer cure model as explained in Chapter 7 is presented. This code achieves the following:

1. Generates the Pixel-micromirror mapping database
2. Mesh the 1mm diameter disc with pixels
3. Map the pixels onto the micromirrors. Generate the required bitmap
4. Run the bitmap through the Irradiance model. Compute the irradiance received by the point on the aerial image receiving the minimum irradiance

%Code plotted for generating the Pixel-micromirror mapping database

```
clear all;
%Inputing the Imaging system parameters:
c(1) = 0; % c is the curvature of surface
c(2) = 0.046664;
c(3) = -0.046664;
c(4) = 0;
t(2) = 10.9; %t is the distance
t(3) = 33.45-5.45;
objectdistance = 113;
N(1) = 1; %N is the refractive index
N(2) = 1.45848;
N(3) = 1;
DMDangley = 7.052*3.142/180;
DMDanglez = 52.052*3.142/180;


%************************************************************************
raycount = 1;
%Getting the extents of the bitmap
bitmap_ysize = 450;
bitmap_zsize = 450;
%Specifying the offsets
y_offset = 0;
z_offset = 0;
bitmap_ymin = -225*13.7/1000*cos(DMDangley);
bitmap_ymax = 225*13.7/1000*cos(DMDangley);
bitmap_zmin = -225*13.7/1000*cos(DMDanglez);
bitmap_zmax = 225*13.7/1000*cos(DMDanglez);

%************************************************************************

%Meshing the bitmap in a 10x10 grid.
temp_stepy = 13.7/1000;
temp_stepz = 13.7*cos(45*3.142/180)/1000;
tempcount = 1;
for tempy = (bitmap_ymin:temp_stepy:bitmap_ymax);
    bitmap_y(tempcount) = tempy;
    tempcount = tempcount + 1;
end
clear tempcount;
tempcount = 1;
for tempz = (bitmap_zmin:temp_stepz:bitmap_zmax);
   bitmap_z(tempcount) = tempz;
   tempcount = tempcount + 1;
end
clear temp_stepy, temp_stepz, tempy, tempz;
%The mesh has been stored as bitmap_y and bitmap_z

%************************************************************************

%Selecting the point on the bitmap grid and calculating the object distance
%for it
```

```
for count_ybitmap = (1:1:447);
   for count_zbitmap = (1:1:392);
      startpoint_y = bitmap_y(count_ybitmap);
      startpoint_z = bitmap_z(count_zbitmap);
      t(1) = objectdistance - 5.45 - startpoint_z*tan(DMDanglez) - startpoint_y*tan(DMDangley);

%*************************************************************************

            pupilpoint_y = startpoint_y;
            pupilpoint_z = startpoint_z;
            length = sqrt((pupilpoint_y-startpoint_y)^2 + (pupilpoint_z-startpoint_z)^2 + 100^2);
            X(1) = 100/length;
            Y(1) = (pupilpoint_y-startpoint_y)/length;
            Z(1) = (pupilpoint_z-startpoint_z)/length;

%*************************************************************************

 %Tracing the ray through the lens
            x(1) = 0;
            y(1) = startpoint_y;
            z(1) = startpoint_z;
            for (i = 2:1:3)
               %Transfer equations
               e(i) = t(i-1)*X(i-1) - (x(i-1)*X(i-1) + y(i-1)*Y(i-1) + z(i-1)*Z(i-1));
               Mx(i) = x(i-1) + e(i)*X(i-1) - t(i-1);
               Msquare(i) = x(i-1)^2 + y(i-1)^2 + z(i-1)^2 - e(i)^2 + t(i-1)^2 - 2*t(i-1)*x(i-1);
               E(i) = sqrt(X(i-1)^2 - c(i)*(c(i)*Msquare(i) - 2*Mx(i)));
               L(i) = e(i) + (c(i)*Msquare(i) - 2*Mx(i))/(X(i-1)+E(i));
               x(i) = x(i-1) + L(i)*X(i-1) - t(i-1);
               y(i) = y(i-1) + L(i)*Y(i-1);
               z(i) = z(i-1) + L(i)*Z(i-1);

               %Refarction equations
                Edash(i) = sqrt(1- ((N(i-1)/N(i))^2) * (1-E(i)^2));
               g(i) = Edash(i) - ((N(i-1)/N(i)))*E(i);
               X(i) = (N(i-1)/N(i))*X(i-1) - g(i)*c(i)*x(i) + g(i);
               Y(i) = (N(i-1)/N(i))*Y(i-1) - g(i)*c(i)*y(i);
               Z(i) = (N(i-1)/N(i))*Z(i-1) - g(i)*c(i)*z(i);

            end

               %Transfer equations from last lens surface to image plane
            for i = 4;
               e(i) = t(i-1)*X(i-1) - (x(i-1)*X(i-1) + y(i-1)*Y(i-1) + z(i-1)*Z(i-1));
               Mx(i) = x(i-1) + e(i)*X(i-1) - t(i-1);
               Msquare(i) = x(i-1)^2 + y(i-1)^2 + z(i-1)^2 - e(i)^2 + t(i-1)^2 - 2*t(i-1)*x(i-1);
               E(i) = sqrt(X(i-1)^2 - c(i)*(c(i)*Msquare(i) - 2*Mx(i)));
               L(i) = e(i) + (c(i)*Msquare(i) - 2*Mx(i))/(X(i-1)+E(i));
               x(i) = x(i-1) + L(i)*X(i-1) - t(i-1);
               y(i) = y(i-1) + L(i)*Y(i-1);
               z(i) = z(i-1) + L(i)*Z(i-1);
            end
%*************************************************************************
%Recording the position of the ray on the image plane
```

```
            xpos(raycount) = x(i);
            ypos(raycount) = y(i);
            zpos(raycount) = z(i);
            raycount = raycount + 1
%The points of intersection with the image plane are recorded as xpos, ypos,
%zpos;
%*************************************************************************

   end
end
%Here ends the loops selecting the point on the bitmap.

%*************************************************************************
plot(zpos,ypos,'.');
hold on;
axis equal;
```

%Here ends the code for generating the Pixel-micromirror mapping database

%**
%**

%The second step of the Inverse Layer cure model code is now presented
%This code achieves the following:
%1. Meshes a 1mm diameter disc with pixels
%2. Maps the pixels onto the micromirrors on the DMD
%3. Generates the bitmap to be displayed on the DMD

```
%The mesh point spacing is taken to be 2 micron

clear all;
mesh_density = 2; %Density of 2 micron
diameter = 1000; %1000 micron dismeter circle
%The mesh points will have coordinates circle_y and circle_z.
%circle_county and circle_countz will be increased from 0 in steps of 10 micron.
%It will be checked if the circle_rad is greater than 500 micron.
%If YES, the loop will be terminated
for temp = 1;
  for circle_county = -500:mesh_density:500;
    circle_y(temp) = circle_county;
    circle_countz = 0;
    circle_rad = sqrt(circle_county^2 + circle_countz^2);
    while (circle_rad <= 500)
      circle_y(temp) = circle_county;
      circle_z(temp) = circle_countz;
      temp = temp + 1;
      circle_y(temp) = circle_county;
      circle_z(temp) = (-1) * circle_countz;
      temp = temp + 1;
      circle_countz = circle_countz + mesh_density;
      circle_rad = sqrt(circle_county^2 + circle_countz^2);
```

```
     end
   end
end
%plot(circle_z, circle_y, '.');
%axis equal;



%Now, we will snap the points to the points on the pixel_mapping_database
%We will increase ypos in steps of 426 and see when the circle_y snaps to ypos.
%Then, we will go individually through the zpos and see the z pos which works
%The first one that snaps is chosen

circle_y = circle_y/1000;
circle_z = circle_z/1000;
load D:\Ameya\pixel_mapping_database.mat;
clear temp;
i = 1;
for circle_count = 1:1:196822
    tempy = 1;
    while (abs(circle_y(circle_count)-ypos(tempy))>0.005)
      tempy = tempy + 426;
   end
    tempz = 1;
    while (abs(circle_z(circle_count)-zpos(tempz))>0.002)
      tempz = tempz + 1
    end
    snapy(i) = ypos(tempy);
    snapz(i) = zpos(tempz);
    tempory = int16((tempy + 451)/451);
    tempory = double(tempory)
    tempmaty(i) = bitmap_y(tempory);
    tempmatz(i) = bitmap_z(tempz)/cos(DMDangle);
    i = i+1;
 end
%Now we generate the bitmap matrix, lets call it the micromirror matrix,
%which can be given to imwrite to create the output bitmap

for j = 1:1:(i-1)
   micromirrory = (tempmaty(j)/0.0137) + 225;
   micromirrory = int16(micromirrory);
   micromirrorz = (tempmatz(j)/0.0137) + 225;
   micromirrorz = int16(micromirrorz);
   micromirror(micromirrory,micromirrorz) = 1;
end
imwrite(micromirror, 'D:\Ameya\Ameya', 'bmp');%The generated file is stored as Ameya.bmp

%Here ends the code to generate the required bitmap
```

%Matlab code written to run the bitmap Ameya.bmp
%through the irradiance model

```
clear all;
```

```
%Matlab code to run the bitmap file generated through the Irradiance model
Ameya = imread('D:\Ameya\Ameya', 'bmp')
%We see which elements of the matrix Ameya are 255
%Then, we find their location in mm
%Then, we trace rays from all these points
%We find the position of these rays as z pos, ypos

%Selecting points on the matrix
tempcount = 1;
for ycount = 1:1:450
   for zcount = 1:1:450
      if (Ameya(ycount, zcount) == 255)
         ymirror(tempcount) = (ycount-225)*0.0137;
         zmirror(tempcount) = (zcount-225)*0.0137;
         tempcount = tempcount + 1;
      end
   end
end

%Now, we trace rays from all these points
% A loop goes from 1 to tempcount-1. startpointy and startpointz
%are selected.

%Inputing the Imaging system parameters:
c(1) = 0; % c is the curvature of surface
c(2) = 0.046664;
c(3) = -0.046664;
c(4) = 0;
t(2) = 10.9; %t is the distance
t(3) = 33.45-5.45; %oiginal disttance was 34.2
objectdistance = 113; %The original distance was 113
angle = 0.01; %This is the angle at which rays leave every point on the pattern %Original angle was 0.15
N(1) = 1; %N is the refractive index
N(2) = 1.45848;
N(3) = 1;
DMDangley = 7.052*3.142/180;
DMDanglez = 52.052*3.142/180; %This is the angle at which the DMD is mounted to the horizontal

%**************************************************************************

raycount = 1;

for tempcount1 = 1:1:(tempcount-1);
      startpoint_y = ymirror(tempcount1)*cos(DMDangley);
      startpoint_z = zmirror(tempcount1)*cos(DMDanglez);
      %Now, the distance of the pattern-point from the center of the beam
      %is calculated. This distance is stored as p and then the weight of
      %the rays emitting from this point are calcuated as the column
      %matrix w
      p = sqrt(startpoint_y^2*sin(DMDangley) + (startpoint_z*sin(DMDanglez))^2);
      t(1) = objectdistance - 5.45 - startpoint_z*tan(DMDanglez) - startpoint_y*tan(DMDangley);


%**************************************************************************
```

```
            pupilpoint_y = startpoint_y;
            pupilpoint_z = startpoint_z;
            length = sqrt((pupilpoint_y-startpoint_y)^2 + (pupilpoint_z-startpoint_z)^2 + 100^2);
            X(1) = 100/length;
            Y(1) = (pupilpoint_y-startpoint_y)/length;
            Z(1) = (pupilpoint_z-startpoint_z)/length;

%*************************************************************************

 %Tracing the ray through the lens
            x(1) = 0;
            y(1) = startpoint_y;
            z(1) = startpoint_z;
            for (i = 2:1:3)
               %Transfer equations
               e(i) = t(i-1)*X(i-1) - (x(i-1)*X(i-1) + y(i-1)*Y(i-1) + z(i-1)*Z(i-1));
               Mx(i) = x(i-1) + e(i)*X(i-1) - t(i-1);
               Msquare(i) = x(i-1)^2 + y(i-1)^2 + z(i-1)^2 - e(i)^2 + t(i-1)^2 - 2*t(i-1)*x(i-1);
               E(i) = sqrt(X(i-1)^2 - c(i)*(c(i)*Msquare(i) - 2*Mx(i)));
               L(i) = e(i) + (c(i)*Msquare(i) - 2*Mx(i))/(X(i-1)+E(i));
               x(i) = x(i-1) + L(i)*X(i-1) - t(i-1);
               y(i) = y(i-1) + L(i)*Y(i-1);
               z(i) = z(i-1) + L(i)*Z(i-1);

               %Refarction equations
                Edash(i) = sqrt(1- ((N(i-1)/N(i))^2) * (1-E(i)^2));
               g(i) = Edash(i) - ((N(i-1)/N(i)))*E(i);
               X(i) = (N(i-1)/N(i))*X(i-1) - g(i)*c(i)*x(i) + g(i);
               Y(i) = (N(i-1)/N(i))*Y(i-1) - g(i)*c(i)*y(i);
               Z(i) = (N(i-1)/N(i))*Z(i-1) - g(i)*c(i)*z(i);

            end

               %Transfer equations from last lens surface to image plane
            for i = 4;
               e(i) = t(i-1)*X(i-1) - (x(i-1)*X(i-1) + y(i-1)*Y(i-1) + z(i-1)*Z(i-1));
               Mx(i) = x(i-1) + e(i)*X(i-1) - t(i-1);
               Msquare(i) = x(i-1)^2 + y(i-1)^2 + z(i-1)^2 - e(i)^2 + t(i-1)^2 - 2*t(i-1)*x(i-1);
               E(i) = sqrt(X(i-1)^2 - c(i)*(c(i)*Msquare(i) - 2*Mx(i)));
               L(i) = e(i) + (c(i)*Msquare(i) - 2*Mx(i))/(X(i-1)+E(i));
               x(i) = x(i-1) + L(i)*X(i-1) - t(i-1);
               y(i) = y(i-1) + L(i)*Y(i-1);
               z(i) = z(i-1) + L(i)*Z(i-1);
            end
%*************************************************************************
%Recording the position of the ray on the image plane
            xpos(raycount) = x(i);
            ypos(raycount) = y(i);
            zpos(raycount) = z(i);
            w(raycount) = 1 - 0.00086*p - 0.00883*p*p;
            raycount = raycount + 1;
%The points of intersection with the image plane are recorded as xpos, ypos,
%zpos;
```

```
%*************************************************************************

   end
end
%Here ends the loops selecting the point on the bitmap.


%Now, the irradiance is calculated by counting the rey density on the resin grid

%Creating the grid
x = 10;
temp = 1;
for ygrid = (-0.5:1/x:0.5);
   ylocation(temp) = ygrid;
   temp = temp + 1
end
clear temp;
temp = 1;
for zgrid = (-0.5:1/x:0.5);
   zlocation(temp) = zgrid;
   temp = temp + 1;
end
clear temp;

%Select the ray under consideration. Divide its ypos by 0.9. Round it
%off. From the rounded off, determine the value of ylocaton it lies in.
%Same for zpos
%Initializing number_of_rays = 0;
for ytemp = (1:1:(x+1))
   for ztemp = (1:1:(x+1))
      number_of_rays(ytemp, ztemp) = 0;
   end
end
clear ytemp, ztemp;

num_of_rays = 60404
for temp = (1:1:num_of_rays)
   y_ray = ypos(temp);
   z_ray = zpos(temp);
   ynumber = y_ray + 0.5;
   znumber = z_ray + 0.5;
   ynumber1 = int8(1 + ynumber/(1/x));
   znumber1 = int8(1 + znumber/(1/x));
   number_of_rays(ynumber1, znumber1) = number_of_rays(ynumber1,znumber1) + w(temp);
end

clear temp;

sigmaw = 0;
for temp = 1:1:raycount-1;
   sigmaw = sigmaw + w(temp);
end
clear temp;
irradiance= 5*number_of_rays*x*x/(sigmaw);
```

REFERENCES

Beluze L., Bertsch A., Renaud P., 1999, "Microstereolithography: a new process to build complex 3D objects", SPIE Symposium on design, test and microfabrication of MEMS/MOEMS, Vol. 3680, pp. 808-17.

Bertsch A., Zissi S., Jezequel J., Corbel S., Andre J., 1997, "Microstereolithography using liquid crystal display as dynamic mask-generator", Microsystems Technologies, pp.42-47.

Bertsch A., Jezequel J. Y., Andre J.C., 1997, "Study of spatial resolution of a new 3D microfabrication process: the microstereolithography using a dynamic mask-generator technique", Journal of Photochemistry and Photobiology A: Chemistry 107, pp. 275-281.

Bertsch A., Bernhard P., Vogt C., Renaud P., 2000, "Rapid prototyping of small size objects", Rapid Prototyping Journal, Vol. 6, Number 4, pp. 259-266.

Bertsch A., Bernhard P., Renaud P., 2001, "Microstereolithography: Concepts and applications", IEEE pp. 289-298.

Bertsch A., Jiguet S., Renaud P., 2004, "Microfabrication of ceramic components by microstereolithography", Journal of Micromechanics and Microengineering, pp.197-203

Chatwin C., Farsari M., Huang S., Heywood M., Young R., Bitch P., Claret-Tournier F., Richardson J., 1999, "Characterisation of epoxy resins for microstereolithographic rapid prototyping", International Journal of Advanced Manufacturing technologies, Vol. 15, pp.281-6.

Chatwin C., Farsari M., Huang S., Heywood M., Birch P., Young R., Richardson J., 1998, "UV microstereolithography system that uses spatial light modulator technology", Applied Optics, Vol. 37, pp.7514-22.

Dudley D., Duncan W., Slaughter J., 2003, "Emerging Digital Micromirror Device (DMD) applications", SPIE proceedings, Vol. 4985.

Edmund Industrial Optics 2003, "Optical and optical instruments Catalog".

Farsari M., Huang S., Birch P., Claret-Tournier F., Young R., Budgett D., Bradfield C., Chatwin C., 1999, "Microfabrication by use of spatial light modulator in the ultraviolet: experimental results", Optics Letters, Vol. 24, No. 8, pp. 549-50.

Farsari M., Claret-Tournier F., Huang S., Chatwin C., Budgett D., Birch P., Young R., Richardson J., 2000, "A novel high-accuracy microstereolithography method employing an adaptive electro-optic mask", Journal of Material Processing Technology 107, pp. 167-172.

Fujimasa I., 1996, “Micromachines: A new era in Mechanical Engineering”, Oxford University Press.

Gardner J., Varadan V., Awadelkarim O., 2001, “Microsensors MEMS and Smart Devices”, John Wiley and Sons.

Hadipoespito G., Yang Y., Choi H., Ning G., Li X., 2003, “Digital Micromirror device based microstereolithography for micro structures of transparent photopolymer and nanocomposites”, Proceedings of the Solid Freeform Fabrication Symposium, Austin Texas, pp. 13-24.

Ikuta K., Hirowatari K., 1993, “Real three dimensional micro fabrication using Stereolithography and metal molding”, Proceedings IEEE MEMS, pp.42-47.

Jacobs P., 1996, “Rapid Prototyping and Manufacturing Fundamentals of StereoLithography”, Society of Manufacturing Engineers.

Kalpakjian S, 1992, “Manufacturing Engineering and Technology, second edition”, Addison Wesley Publishing Company Inc., Menlo Park, California.

Monneret S., Loubere V., Corbel S., 1999, “Microstereolithography using dynamic mask generator and a non-coherent visible light source”, Proc. SPIE, Vol.3680, pp.553-561.

Monneret S., Provin C., Le Gall H., 2001, “Micro-scale rapid prototyping by stereolithography”, 8th IEEE international conference on emerging technologies and factory automation (ETFA 2001), Vol. 2, pp. 299-304.

Nakamoto T, Yamaguchi K., 1996, “Consideration on the producing of high aspect ratio microparts using UV sensitive photopolymer”, Proceedings 7th International Symposium on Micromachine Human Sciences, pp.53-58.

Nakamoto T., Yamaguchi K., Abraha P., Mishima K., 1996, “Manufacturing of htree-dimensional micro-parts by UV laser induced polymerization”, Journal of Micromachining and Microengineering, pp.204-253.

Nayar S. K., Branzoi V., Boult T. E., 2004, “Programmable imaging using digital micromirror array”, Computer Vision and Pattern Recognition, 2004. CVPR 2004. Proceedings of the 2004 IEEE Computer Society Conference on, Vol.1, 27 June - 2 July 2004, Pages: 436- 443.

www.newport.com

Oriel instruments, 2003, “The Book of Photon Tools”.

Pahl G., Beitz W., 1996, “Engineering Design: A Systematic Approach”, Springer Verlag.

Schenck H., 1979, “Theories of Engineering Experimentation, third edition”, Hemisphere Publishing Corporation.

Sheats J., Smith B., 1998, “Microlithography Science and Technology”, Marcel Dekker, Inc.

Smith W., 1990, “Modern optical engineering: the design of optical systems”, McGraw Hill.